INFLUENCE OF THERMALLY RADIATIVE STAGNATION POINT FLOW OF CASSON NANOFLUID WITH MAGNETIC FIELD

By

MUHAMMAD AHSAN IFTIKHAR

NATIONAL UNIVERSITY OF MODERN LANGUAGES
ISLAMABAD

January 2023

Influence of Thermally Radiative Stagnation point flow of Casson Nanofluid with Magnetic Field

By

MUHAMMAD AHSAN IFTIKHAR

MS Math, National University of Modern Languages, Islamabad, 2023

A THESIS SUBMITTED IN PARTIAL FULFILMENT OF

THE REQUIREMENTS FOR THE DEGREE OF

MASTER OF SCIENCE

In **Mathematics**

To

FACULTY OF ENGINEERING & COMPUTER SCIENCE

NATIONAL UNIVERSITY OF MODERN LANGUAGES ISLAMABAD

© Muhammad Ahsan Iftikhar, 2023

THESIS AND DEFENSE APPROVAL FORM

The undersigned certify that they have read the following thesis, examined the defense, are satisfied with overall exam performance, and recommend the thesis to the Faculty of Engineering and Computer Sciences for acceptance.

Thesis Title: Influence of Thermally Radiative Stagnation point flow of Casson Nanofluid with Magnetic Field

Submitted By: Muhammad Ahsan Iftikhar **Registration #:** 11 MS/Math/S20

Master of Science in Mathematics (MS MATH)
Title of the Degree

Mathematics
Name of Discipline

Dr. Hadia Tariq
Name of Research Supervisor

Signature of Research Supervisor

Dr. Muhammad Noman Malik
Name of Dean (FE&CS)

Signature of Dean (FE&CS)

Brig. Syed Nadir Ali
Name of Pro-Rector Resources/ Director General

Signature of Pro-Rector Resources/ DG

January 17th, 2023

AUTHOR'S DECLARATION

I Muhammad Ahsan Iftikhar

Son of Muhammad Iftikhar Nazir

Registration #11 MS/Math /S20

Discipline Mathematics

Candidate of **Master of Science in Math (MS Math)** at the National University of Modern Languages do hereby declare that the thesis **Influence of Thermally Radiative Stagnation point flow of Casson Nanofluid with Magnetic Field** submitted by me in partial fulfillment of MS Math degree, is my original work, and has not been submitted or published earlier. I also solemnly declare that it shall not, in future, be submitted by me for obtaining any other degree from this or any other university or institution. I also understand that if evidence of plagiarism is found in my thesis/dissertation at any stage, even after the award of a degree, the work may be cancelled and the degree revoked.

Signature of Candidate

M Ahsan Iftikhar
Name of Candidate

17th January 2023
Date

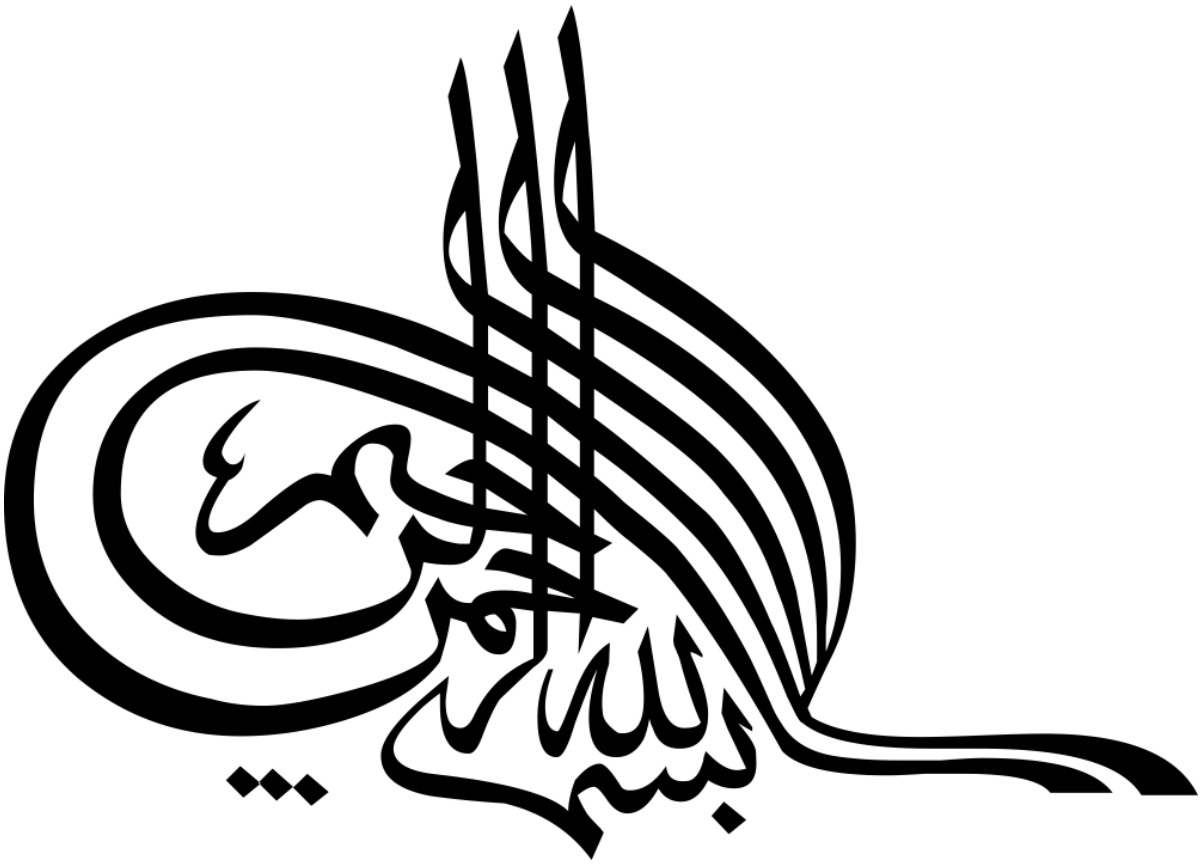
بسم الله الرحمن الرحيم

ABSTRECT

Title: Influence of Thermally Radiative Stagnation point flow of Casson Nanofluid with Magnetic Field

The primary goal of this thesis is to investigate the influence of thermally radiative stagnation point flow of Casson nanofluid with magnetic field. A mathematical model design for physical flow of fluid is in the form of partial differential equation and it converts partial differential equations (PDEs) into ordinary differential equation (ODEs) by using suitable transformations and employing shooting method to obtain the possible numerical results. For computational work, MATLAB has been used. The graphs show how various parameters affect the non-dimensional velocity, temperature and concentration profiles. Tables also display and examine the numerical values of the Heat generation coefficient, Thermal Grashoff number, Concentration number, Schmidt number, Prandtl number, Eckert number, Nusselt number and Sherwood number.

TABLE OF CONTENTS

List of TABLES

LIST OF FIGURES

LIST OF ABBREVIATIONS

2D	Two-dimensional
3D	Three-dimensional
BVP	Boundary value problem
IVP	Initial value problem
MHD	Magnetohydrodynamics
ODEs	Ordinary differential equations
PDEs	Partial differential equations

LIST OF SYMBOLS

u	Velocity in x-direction
v	Velocity in y-direction
M	Magnetic parameter
N	Exponential parameter
N^*	Buoyancy force ratio
T	Temperature
C	Concentration
T_0	Temperature constant
T_s	Sheet temperature
C_0	Concentration constant
ξ	Similarity variable
f	Dimensionless velocity
θ	Dimensionless Temperature
ϕ	Dimensionless Concentration
Nu_x	Nusselt Number
Sh_x	Sherwood Number
Re_x	Reynolds Number
Pr	Prandtl Number
Ec	Eckert Number
Sc	Schmidt Number
G_r	Thermal Grashof Number
G_c	Concentration Grashof Number
R	Radiation Parameter
γ, k_c	Chemical Reaction Parameter
Q_T	Thermal Heat generation parameter
Q_E	Space based exponential Heat generation parameter
S	Suction/injection parameter
ρ	Fluid Density
ν	Kinematic Viscosity
μ	Fluid Viscosity

k	Thermal Conductivity
k_0	Chemical reaction constant
k_1	Chemical reaction rate
k^*	Absorption coefficient
C_p	Specific Heat
m	Mass
D_m	Mass diffusion Coefficient
q_m	Mass flux
B_0	Magnetic Flux Density
β	Concentration expansion coefficient
σ	Electrical conductivity
σ^*	Boltzmann constant
w	Condition at the surface
T_w	Temperature at surface wall
C_w	Concentration at surface wall
q_w	Wall heat flux
τ_w	Wall shear stress
∞	Condition at the free stream
T_∞	Ambient temperature
C_∞	Ambient concentration
λ	Mixed convection variable
k^*_p	Porosity parameter
Nb	Brownian motion parameter
Nt	thermophoresis parameter
Sc	Schmidt number
p_c	critical parameter
c_f	skin friction coefficient
$\lambda_1 and\ \lambda_2$	Linear and Non-linear coefficient of thermal expansion
$\lambda_3 and\ \lambda_4$	Linear and Non-linear coefficient of concentration
β_1	Nonlinear temperature variable
E	Electric field
B	Magnetic field

J	Current density
, ρ_v	Volume charge density
μ_0	Permeability of free space
ϵ_0	Permittivity for fixed space
β_2	Nonlinear convection variable
m	Order of chemical reaction

ACKNOWLEDGMENT

First and foremost, I want to thank and praise the Almighty **Allah** for making this study feasible and successful. Without the sincere encouragement provided by numerous sources, this project could not have been completed, and for that, I would want to convey my heartfelt appreciation. However, there were important people who helped me succeed, and I will never forget their contributions. In particular, my research supervisor, **Dr. Hadia Tariq** and co-supervisor, **Dr. Sajid Shah**, went above and beyond to help me during my research journey.

Additionally, I want to thank the Department of **Mathematics** for their ongoing support and assistance in helping me overcome my research-related obstacles. I want to express my gratitude to everyone who I did not include but who made a big contribution anyway.

DEDICATION

I dedicate this sincere effort to my dear ***Parents***, ***Brothers*** *and my* ***Professors***, *whose sacrifices and contributions to my life are truly priceless and whose thoughtful consideration of my academic career, made me consolidated and motivated me as I am at this grade right now.*

CHAPTER 1

INTRODUCTION

A substance that continuously deforms after applying shear stress or an external force on it is called Fluid. Fluid can be found as liquids, gases, or plasma (Cengel et al. 2013). It is a material that has a vanishing shear modulus, or to put it another way, it is a material that cannot withstand any applied shear stress. Since fluid is a need for daily life and plays a crucial role in many natural processes, scientists from around the globe are striving to delve into a variety of fluid flow-related facts. In the subfield of fluid dynamics known as fluid dynamics, we investigate fluid flow while simultaneously examining its underlying causes and how the fluid flow is influenced by forces. It offers ways to comprehend how the blood circulates as well as how the stars, seas, currents, and tectonic plates have evolved (B. Xia, et al., 2002). Fluid fluxes are used in a variety of applications, including wind turbines, oil pipelines, rocket engines and air conditioning systems (R. Banerjee, et al., 2002). Newtonian flow properties are exhibited by most low molecular weight materials, such as organic and inorganic liquids, low molecular weight inorganic salt solutions, molten metals, molten salts, and gases, at constant temperature and pressure. The dynamic viscosity, which is the constant of proportionality, is the measure of a fluid's resistance to shear stress at constant temperature and pressure and is proportional to the rate of shear. This type of fluid is known as Newtonian fluid (R. P. Chhabra, 2010). Non-Newtonian fluids act like solids and stay semi-solid or excessively viscous. Newton's viscosity law does not apply to this type of fluid. (Huilgol, 1968) made some remarkable research on second order fluid. (K. R. Rajagopal, 1984) explored the exact result for a Non-Newtonian fluid flowing over an infinite porous plate. The investigation of MHD Casson fluid flow through a vertical porous plate under the impact of heat diffusion and chemical reaction was contributed by (Kodi & Raghunath et al., 2022). In a article by (Afify, 2004), the author discussed various phenomena that occur in the flow of a viscous, electrically conducting fluid in the presence of a magnetic field. These phenomena include the magnetic effect, chemical reactions, convection, and the behavior of the fluid when it is subjected to a stretching surface and is incompressible.

1.1 Casson fluid

The Casson fluid, first described by (Casson, 1959), is a type of fluid that exhibits shear thinning behavior. Examples of materials that exhibit this behavior include jelly, honey, soup, and concentrated fruit juices. Both at extremely high and extremely low shear rates, the Casson model is more realistic. Both biomechanics and the manufacturing of polymers benefit greatly from its use. The Casson fluid constitutive equation has been shown to fit adequately in silicon suspensions, water-soluble bentonite suspensions and lithographic varnishes. It explains the nonlinear connection between stress and strain rate and has been shown to be very beneficial for printing inks. Some researchers have done extraordinary work on Casson fluid. In recent years, there have been several studies on the behavior of Casson fluids in various settings. (K. Anantha Kumar, 2020) investigated the impact of heat radiation on the flow of an MHD Casson fluid across an exponentially increasing curved sheet. (M. Hamid, 2019) studied heat transfer in a partially heated trapezoidal cavity using a Casson fluid. (Thumma, 2020) used a simplified differential quadrature method to study the behavior of an unstable 3D MHD radiating dissipative Casson fluid that is carrying small particles.

1.2 Magnetohydrodynamics (MHD)

Magnetohydrodynamics (MHD) is the analysis of fluid motion in the presence of a magnetic field. It is particularly concerned with the movement of electrically conductive fluids such as plasmas, liquid metals, and salt water or electrolytes in magnetic fields. MHD was first defined by Maxwell in terms of charge density, sources, and current density. Set of Maxwell equations define as:

$$\nabla . E = \frac{\rho_v}{\epsilon_0} \qquad \text{(Gauss' s Law of Electricity)}$$

$$\nabla . B = 0 \qquad \text{(Gauss's Law of Magnetism)}$$

$$\nabla \times E = -\frac{\partial B}{\partial t} \qquad \text{(Faraday's Law)}$$

$$\nabla \times B = \mu_0 J + \mu_0 \epsilon_0 \frac{\partial E}{\partial t} \qquad \text{(Ampere's Law)}$$

The applications of MHD are wide-ranging and include fields such as geophysics, astrophysics, and engineering. In recent years, there have been several studies on MHD flows

of various types of fluids in different settings. For example, (S. K. Asha & G. Sunitha, 2019) discussed research on MHD peristaltic blood circulation of Powell Eyring nanofluid through an uneven conduit. (JU Abubakar & AD Adeoye, 2020) studied MHD permeable tapered stenosed artery subject to radiation effect. (AS Idowu & BO Falodun, 2020) investigated Soret–Dufour, thermophoresis, heat and mass transmission of Casson nanofluid over an inclined plate. (L. Khan, M. Raza, N. Mir, & R. Ellahi, 2019) studied MHD nanofluid peristaltic flow in an asymmetric channel with various nanoparticle morphologies. (Y. El-Masry, 2019) used iteration approaches on the flow of Powell Eyring fluid to solve the MHD variation on free convective heat transfer analysis over the wavy channel. This research has demonstrated that the magnetic field effect provides an opposing force that reduces the frictional force of MHD conducting fluid. (Afridi, 2018) reported entropy production reduction in frictional and Joule heating induced MHD boundary layer flow across a stretched, smearing sheet.

1.3 Stagnation points

A stagnation point is a point in a fluid flow where the local velocity of the fluid is zero. These points can occur on the surfaces of objects in the flow field, where the fluid comes to rest due to the presence of the object. Recently, there have been several studies on the behavior of different types of fluids in the vicinity of stagnation points. For example, (Khan, M. Riaz, Kejia Pan, Arif Ullah Khan, & S. Nadeem, 2020) analyzed dual solutions for SiO2-Al2O3/water hybrid nanofluid mixed convection flow approaching the stagnation point across a curved surface. (Ijaz Khan, 2020) conducted numerical simulations to investigate the impact of binary chemical reactions and activation energy on the nonlinear thermal radiative stagnation point flow of Walters'-B nanofluid. (Warke, 2022) made a numerical investigation of the stagnation point flow of radiative magneto micropolar liquid past a heated porous stretching sheet. (Mustafa, 2012) studied the movement of a Casson fluid in the region of a stagnation point in the direction of a stretched sheet.

1.4 Nanofluid

Nanofluid is a mixture of conventional low thermal conductivity fluid and nanoparticles with a size smaller than 100 nm. (Choi, 1998) introduced the term "nanofluid," which defined a new kind of fluid. Nanofluids are suspensions of microscopic particles (nano size) in a base fluid. Carbon nanotubes, carbides, metals and oxides are the most often employed nanoparticles in nanofluids. These fluids are created to have higher thermal conductivity than other basic fluids. The use of nanoparticles of gold, copper, silver and other metals inside base fluid will increase thermal conductivity of nanofluid. (Buongiorno J. , 2006) investigated the mechanism underlying the rise in the thermal conductivity of nanofluids. He observed that the fluid's thermal conductivity changes because of the Brownian motion and the thermophoresis effect. In the information technology and heavy vehicle industries, nanofluid can also be utilized as a coolant. Overall, nanofluid is a boon in a variety of industrial, biomedical, and technical domains.

1.5 Porous Medium

When a solid or group of solids has enough free space within or around them for a fluid to travel through or around them, the solid is said to have a porous medium. A porous media can be conceptually described in a variety of ways. One idea is a solid that is continuous yet has holes in it. Consolidated refers to such a medium, and the pores may be impermeable or permeable (Shamey, 2014). Porous medium has one of the main property, porosity ε.

$$\varepsilon = \frac{Total\ volume - solid\ volume}{Total\ volume}.$$

In recent studies, researchers have investigated the behavior of Casson fluids in various settings, utilizing magnetohydrodynamics (MHD) to analyze the flow. For example, (G. Mahanta a. S., 2015) investigated a 3D Casson fluid flow across a porous, linearly extending sheet using MHD, adding a convective boundary condition at the surface where the fluid's thermal conductivity varies linearly with temperature. (Khalid, 2015) also examined the unsteady MHD free flow of a Casson fluid across an oscillating vertical plate with constant wall temperature, considering that the fluid was moving through a porous medium. (Ullah, 2017) studied the impact of the slip condition on the non-Newtonian fluid's free convective flow across

a nonlinearly stretched sheet filled with porous medium with Newtonian heating. (Swain, 2018) investigated Williamson nanofluid flows across porous media in an MHD boundary layer under convective boundary conditions.

1.6 Thesis Contributions

In this thesis, a detailed review of work by (S. M. Ibrahim, 2020) has been included. Some important parameters, heat and mass transfer of a radiative MHD Casson fluid across an exponentially permeable stretching sheet with nonlinear chemical reaction and other effects such as nonlinear mixed convection, magnetic, suction/ injection and stagnation point are discussed. In this, we converted PDEs into ODEs by using suitable transformations and employed shooting method to obtain the possible numerical results. For computational work we used MATLAB. Obtained results will be displayed graphically as well as in tabular form.

1.7 Thesis Organization

This thesis is further divided into the following chapters, which are as follows:

Chapter 2 comprises the related literature review.

Chapter 3 covers fundamental description, rules and ideas which are important in realizing forthcoming work. On the concluding page of this chapter, the mathematical model and shooting method are also mentioned.

Chapter 4 provides a review work of (S. M. Ibrahim, 2020).

Chapter 5 is the extended work of (S. M. Ibrahim, 2020). In this, we converted PDEs into ODEs by using suitable transformations and have used shooting method.

Chapter 6 contains the conclusions drawn in chapter 5.

In the end, the Reference list contains all the references utilized in this research.

CHAPTER 2

LITERATURE REVIEW

Fluid mechanics is a topic that has grown rapidly in the engineering world, and this is reflected in the use of cooling systems and lubricants in machinery. The first mathematical model representing the fluid motion resulting from Newton's second law for viscous fluid substances was developed by Navier and Stokes (Pletcher, Tannehill, & Anderson, 2012). Then, Prandtl particularly simplified the nonlinear term on the Navier-Stokes equation system for the boundary layer problem (Prandtl, 1904). Several more variables that affected the flow characteristics were then taken into consideration when these theoretical investigations were being developed.

Casson fluid, due to its unique rheological properties, is a widely utilized non-Newtonian fluid (S. Nadeem, 2014). Researchers have studied its behavior in various scenarios, such as the Casson fluid flow in three dimensions past a porous linearly stretching sheet in the presence of a convective boundary condition (G. Mahanta S. S., 2015) and the heat transfer and Casson fluid flow forward through an exponentially highly permeable stretching surface (S. Pramanik, 2014). Many industries make use of the suction and injection processes, such as in the design of thrust bearings, radial diffusers, and thermal oil recovery. Studies presented by (W.M.Rohsenow, 1998) and (Pantokratoras, 1991) have investigated on the impact of suction or injection on boundary layer flow and heat transfer and the effect of radiation on the stagnation-point flow of a micropolar fluid across a nonlinearly expanding surface with suction/injection effects was presented by (Jayachandra Babum, 2015). The behavior of a non-compressible micropolar fluid across a sheet stretched in its own plane has also been examined by (R. Nazar, N. Amin, D. Filip, & I. Pop, 2004). The influence of a magnetic field on the unstable natural convection flow of a micropolar fluid sandwiched between two vertical walls was presented by (H. Kataria & H. Patel, 1996).

(A. Mishra & M. Kumar, 2020) investigated the impact of thermal radiation, viscous-Joule heating and heat generation over an implanted stretching layer with MHD nanofluid flow caused by suction/blowing in the permeable material. (Vinita, Poply, Goyal, & Sharma, 2020) investigated the effect of magnetohydrodynamic slip flow with radiation influence on a nonlinear extending channel in the presence of external velocity. (Vaidyaa, et al., 2020) studied the flow of fluid with different properties (thickness and thermal conductivity) through the permeable medium. (Yazdi, Moradi, & Dinarvand, 2014) demonstrated the 2D mixed convection MHD boundary layer stagnation point flow in the presence of heat radiation using a vertical plate loaded with nanofluid. Kumar (K. A. Kumar, 2019) used a nonlinear surface to investigate the impact of heat transport in MHD Casson nanofluid. (F. Aman, 2013) examined the flow of a 2D incompressible viscous fluid in the presence of an external magnetic field using a decreasing surface. (U. Khan, 2018) conducted a study on the impact of a magnetic field on heat transfer in the flow of nanofluids between two parallel plates. The research aimed to understand how the magnetic field influences the thermal characteristics of the nanofluid flow and how it affects the heat transfer process. He discovered that the form factor has no effect on fluid velocity. It was also determined that nanoparticles with a larger form factor will raise the temperature while decreasing heat transfer. Using Lie group analysis, the heat and mass transport characteristics of an inviscid Newtonian fluid with temperature-dependent viscosity and constant thermal over a vertical stretching / shrinking sheet with changing flow conditions were investigated by (Sivagnana Prabhu KK, 2009).

Thermophoresis refers to the movement of tiny particles suspended in a fluid or gas due to temperature differences. The particles will tend to move towards the area of lower temperature. This phenomenon can be observed in various systems such as lighting fixtures, where carbon particles produced by combustion will be drawn towards the cooler glass globe and deposit there, as explained by (L. Talbot, 1980). Thermophoresis has a wide range of applications in various fields, including lighting systems, air conditioning systems, biotechnology, combustion and propulsion and materials science. In lighting systems, the blackening of the glass globe is caused by the thermophoresis of carbon particles emitted during combustion being drawn towards the cooler area of the globe. In air conditioning systems, thermophoresis can be used to filter out particles and microorganisms. In biotechnology, it can be used to manipulate cells and particles in microfluidic devices. In combustion and propulsion,

thermophoresis can be used to control the dispersion of fuel droplets and prevent soot formation. In materials science, it can be used to manipulate and sort particles based on their size and charge. The ability to control the movement of particles through temperature gradients makes thermophoresis a versatile tool with potential applications in a wide range of fields. (Sandeep, 2016) explored the diffusion system for the Casson fluid flow based on an abrupt pressure gradient at a stagnation point, as well as the loss of heat energy at the lowest thermodynamic temperature. The space-dependent heat is modified so that the internal thermal source of energy can meet temperatures both near and far from the surface.

In recent years, researchers have been studying the behavior of magnetohydrodynamic (MHD) fluids at stagnation points, particularly in the presence of porous materials and heat sources. For example, (Jena, 2017) examined the flow of an MHD fluid at a stagnation point through a porous material with a heat source. (Bhattacharyya, 2012) analyzed the heat transfer and flow at a stagnation point across a sheet that decreases exponentially and found that the range of velocity ratios where a similarity solution exists is wider than when the sheet decreases linearly. Additionally, the study found that dual solutions can exist even when the shrinking rate is less than the straining rate, and that heat addition or absorption may be possible under certain conditions. (Zainal, 2020) used MHD and mixed convection stagnation point flow to examine the movement of a hybrid nanofluid across a perpendicular flat plate with a convective boundary condition.

Thermal stratification is a phenomenon caused by the structure of layers or strata in a fluid flow regime. According to heat transfer analysis, the impact of boundary layer fluxes and temperature stratification is significant. Temperature stratification can occur because of temperature changes or the combination of differing densities of fluids. There are various practical uses of thermal stratification, such as in thermal energy storage systems (such as solar ponds), atmospheric density stratification, and the manufacturing of sheeting materials. Due to these uses, many researchers and scientists have found that the boundary layer movement of Newtonian fluids is not as well-suited as the flow of non-Newtonian fluids. The flow variability of non-Newtonian fluids in nature makes it difficult to achieve a complete physical description using a single relationship between shear rate and stress. As a result, there are several models

available in the literature to describe the unique rheological properties of non-Newtonian fluids. (Powell, 1944) proposed a unique fluid model known as the Powell-Eyring fluid model. This model has some advantages over non-Newtonian models as it is developed from atomic theory of gases rather than experimental relationships and it converts to a Newtonian mode at low and high shear rates. Even though the mathematics of the model is more complex, the benefits of this fluid model outweigh the complexity. The Eyring-Powell model can be used to describe the flows of modern industrial products such as ethylene glycol and powdered graphite. Different geophysical, natural and industrial issues, such as moisture and temperature distribution over agricultural pitches, environmental contamination, subsurface energy transit, etc., are greatly influenced by heat diffusion through the Eyring-Powell fluid. (Yoon, 1987) wrote a remark on Eyring-Powell fluid flow and determined that for zero shear rate viscosity, Eyring-Powell is truly sensitive to slight fluctuations and moderately responsive for infinite shear rate viscosity.

(F. Shahzad, 2019) studied flow of nanofluid through horizontal sheet in the presence of an external magnetic field utilizing Joule heating effect. (Naramgari, 2016) analyzed a stretched surface's impact on MHD nanofluid caused by heat radiation. (Abolbashari, 2015) investigated the use of slip velocity and surface boundary conditions to transfer heat and energy in a constant laminar Casson nanofluid flow. (S. S. Ghadikolaei, 2018) examined the MHD flow of a Casson nanofluid over a porous non-linear sheet and evaluated several physical characteristics such as chemical reactions, thermal radiation, suction, Joule heating, heat generation and absorption. The unstable nanofluid flows in presence of heat radiation were investigated using a stretching surface by (Das, 2014). (Ibrahim, 2013) studied the boundary layer flow of a non-Newtonian nanofluid utilizing the slip boundary condition, thermal radiation and magnetic field effect. (M. R. Krishnamurthy, 2016) explored the numerical analysis of Williamson nanofluid flow through a permeable surface, as well as the influence of chemical parameters in the presence of nanoparticles.

(Abbas, 2020) observed a sliding plate with various slip coefficients is impinged upon by a 3D axisymmetric stagnation flow of a hybrid nanofluid in two orthogonal directions. The impacts of a non-uniform heat source/sink as well as viscous dissipation were investigated. The

flow change from the classical Hiemenz (1911) and Homann (1936) solutions for the 2D and axisymmetric stagnation-point boundary layers to the local Brinkman equation (1947) solution in the stagnation zone of a cylinder or sphere was examined by (Q. Wu, 2005) When increasing concentrations of fibers are introduced equally to the medium surrounding these blunt structures, the viscous resistance of the fibers dissipates the fluid's inertia. In a study conducted by(Layek GC, 2007), the authors measured mass and energy transfer for an incompressible viscous fluid's boundary layer stagnation point flow towards a heated porous stretching sheet embedded in a porous medium. The fluid flow was subject to suction and blowing with internal heat generation or absorption.

The simultaneous occurrence of heat and mass transfer in a fluid requires a thorough understanding of the interplay between fluxes and driving potentials in both theoretical and experimental studies. Researchers have discovered that energy fluxes can be generated not only by temperature gradients but also by concentration gradients. This led (Alam MS, 2006) to investigate the effects of Dufour and Soret on the unsteady flow of MHD, free convection and mass transfer through a vertical porous plate in a porous medium, with a particular focus on fluids with low and medium molecular weight. The Darcy's flow model depicts a linear relationship between flow rate and pressure drop in a porous medium, any deviation from this is referred to as non-Darcy flow.

The ability to control heat exchange and fluid flow near various types of obstacles using magnetic fields has stimulated increased interest in studying boundary layer flows under the influence of an external magnetic field. However, it is also important to consider the effect of ohmic heating in order to fully understand the impact of the magnetic field on thermal transport in the boundary layer. Research has been conducted on the impact of ohmic heating on the MHD free convective heat transfer of Newtonian fluids, the influence of ohmic heating on mixed convection boundary layer flow of a micropolar fluid from a rotating cone with a power law change in surface temperature, and the effect of ohmic heating on combined heat and mass transfer in MHD 3D flow over a stretched surface for a viscous incompressible fluid with temperature-dependent viscosity and thermal conductivity.

Many industrial processes are carried out at extreme temperatures, making radiation heat transfer an important consideration in the design of associated equipment. Nuclear power plants, gas turbines, and various propulsion technologies used in aircraft, missiles, satellites, and space vehicles are all examples of this. Many industrial processes involving flow and mass transfer over a flat surface, such as the manufacture of polymers, ceramics, or glassware, may entail chemical reactions that result in the formation or absorption of diffusing species. This can have a substantial impact on the flow and, as a result, the quality and attributes of the finished product. The order of a chemical reaction determines whether it is heterogeneous or homogeneous. A reaction is of n^{th} order if its rate is proportionate to the n^{th} power of concentration. (Das, U. N, Deka, R. K, & Soundalgekar, V. M , 1994) conducted a study on the effect of a homogeneous first-order chemical reaction on the flow through an infinite vertical plate with impulsively begun uniform heat flux and mass transfer. They considered the heat generated during the dissipation process, which is an essential factor in the design of many devices. Viscous dissipation, which is the ability of a velocity to do work against viscous forces, and Joule heating, which occurs when an electric current passes through a conductor, are both critical in the operation of various devices that operate at high deceleration or high rotating speeds. (O.A. Plumb, 1981) was the first to investigate the influence of horizontal crossflow and radioactivity on natural convection from a vertically hot wall in a saturated porous medium. Additionally, several attempts have been made to analyze the effect of a transverse magnetic field on boundary layer flow behavior with specific industrial applications in mind, such as polymer processing technology.

The study of hydromagnetic flows with mass and temperature transfer in porous media has gained increasing attention in recent years due to their relevance in various technical fields such as boundary layer flow, magnetic levitation, casting, filtration of liquid metals, temperature control of nuclear reactors, fusion control, and measures to prevent scaling in heat exchangers. Additionally, research on irregular hydromagnetic flows is important from a practical standpoint as fluid transients can occur during the startup of many industrial processes and devices such as MHD power sources, MHD hydraulic systems, MHD accelerators, MHD flow meters, and controlled thermonuclear power plants. (M. A. Hossain & A. C. Mandal, 1985) investigated the flow of an unstable magnetohydrodynamic natural convection thermal and mass transfer fluid along a flat plate in a fluid-saturated porous material. Many fluid flow

problems of physical importance involve a large temperature difference between the ambient fluid and the surface of the solid, such as chemical reactions in fluids that are exothermic or endothermic, heat evacuation from nuclear fuel debris, buried disposal of radioactive waste, food storage, and dissociating fluids in fixed bed reactors. Therefore, it is important to take into consideration temperature-dependent heat sources and sinks, which can have a significant impact on heat transfer characteristics.

Natural convection is a method of heat transfer that occurs because of density variations in a fluid caused by temperature differences. The fluid movement caused by these density variations, known as buoyancy forces, causes warmer fluid to rise and cooler fluid to sink, creating a circulating flow pattern known as a natural convection loop. The rate of natural convection can be affected by factors such as the properties of the fluid, the geometry of the system, and the temperature difference between the fluid and its surrounding surfaces. This phenomenon can occur in both liquids and gases and is commonly found in various industrial and natural settings such as electronic device cooling, heat exchangers, and air movement in a room. (R. Muthucumarswamy, 2000) conducted a study on the transient free convection flow of an incompressible thick fluid over a vertical surface that is impulsively started and considering a first-order homogeneous chemical reaction. MHD flows across a porous material in the existence of a chemical process is another typical pattern in the chemical sector. When a liquid that conducts electricity flows through a porous medium under magnetohydrodynamic conditions, the pressure drop and the amount of liquid retained in the medium, such as a packed pebble bed in a blanket for fission-fusion hybrid reactors, will be higher than when non-conducting fluids are used, in order to maintain a constant flow rate. Another usage for external magnetic fields is in the formation of crystals, where it has been effectively used to eliminate non uniform composition and inhibit unstable flow while also improving the quality of the crystal. (K. D. Singh, 2010) examined how chemical reactions affect the unsteady flow of heat and mass transfer through a surface that is embedded in a porous medium and fully immersed in a permeable material, with heat production or absorption, under magnetohydrodynamic conditions. Similarly, (Makinde, 2010) investigated how an nth-order homogeneous chemical interaction between the fluid and the diffusing species affects the MHD mixed convection flow of an optically thin radiated fluid through a vertical porous plate that is submerged in a permeable material.

Homogeneous or heterogeneous processes can be used to model chemical reactions. A homogeneous reaction occurs uniformly throughout a phase, while a heterogeneous reaction is limited to a specific area or within the boundaries of a phase. (Soundalgekar, 1977) studied the movement of a viscous fluid through an infinite vertical plate with an infinite heat flux and an impulsively initiated chemical reaction. The Laplace transform method was used to obtain the solution and the effects of cooling or heating the plate on the flow field were analyzed using the Grashof number. One of the remarkable effects to be introduced is joule heating, which allows excellent control over the direction of magnetohydrodynamic fluid motion. Joule heating, also known as Ohmic heating, is the process of converting electrical into thermal energy, which generates heat through reactance in the medium. The Joule heating effect is also widely and effectively used in many electrical, digital and electronic devices. The most beneficial application of Joule heating is carrying an electric potency to manage losses in terms of minimizing current. Several studies have been conducted to study the flow of different types of magnetohydrodynamic fluids and the impact of Joule heating on them. (Chakraborty, 2013) looked into the impact of variable viscosity and Joule heating on the stream of an electromagnetohydrodynamic fluid connected to a continuous heat flux.

Bioconvection of nanofluids is an intriguing field of research with a wide range of applications, including microfluidic devices, pharmaceutical production, gas bearings, sediment transport, modeling, fuel and lubricant development, enhanced oil recovery, hydrodynamic systems, and polymer fabrication. This phenomenon occurs due to the spontaneous upward swimming motion of microorganisms that are denser than water. Bioconvection is a method that produces non stability by causing tiny density motile bacteria to float near the surface of a liquid. Gyrotactic microorganisms, such as algae, tend to congregate on the surface of a liquid due to their tendency to swim towards the top. This can lead to a thicker surface layer and an unstable surface. Depending on the specific conditions, these microorganisms can be further classified as gyrotactic, oxytactic, or chemotactic. The movement of nanomaterials is driven by Brownian motion or thermophoresis. Understanding the behavior of these motile microorganisms in the context of nanofluids is particularly fascinating, as it has implications for a variety of fields, including microbiology and health. The accumulation of microorganisms in a liquid can result in the formation of a thick layer of bacteria on the surface of the liquid. Because of their low density relative to water, these microorganisms tend to congregate at the

top of the liquid. Bioconvection is a term used to describe the natural movement of swimming microorganisms in a liquid. This phenomenon is like Rayleigh-Benard convection, but it is driven by the absorption and swimming of microorganisms. Biochemical nano-liquids are liquids, which can be either water-based or non-water-based, that contain gyrotactic motile bacteria and metal-derived nanoparticles. Different researchers have investigated different aspects of the bioconvection phenomenon. For instance, (Platt, 1961) first introduced the term "bioconvection" to describe the process of development in the movement of swimming motile microorganisms. This phenomenon is analogous to Rayleigh-Benard convection, but it is caused by the absorption and swimming of microorganisms. (Kuznetsov, 2011) studied the concept of isothermal convection using two different types of motile bacteria, gyrotactic and oxytactic. (Abdelmalek, 2021) examined the bioconvection of nanoparticles in the flow of micropolar fluids over a stretched surface.

Activation energy refers to the minimum amount of energy required for a substance to undergo a chemical reaction or change. The concept of activation energy was first introduced by Svante Arrhenius in 1889. It can be thought of as the amount of energy needed to overcome the potential barriers or obstacles that exist between the initial reactants and the final products. Activation energy plays an important role in a variety of fields such as industrial engineering, oil storage and production, geothermal energy, fluid mechanics, oil emulsification, and food production. In a study conducted by (Bestman, 1990), the boundary layer flow of heat and mass transfer on the surface of a dividing boundary was analyzed using a mathematical model based on the Arrhenius activation energy concept for a two-component reacting system. The study specifically focused on how the boundary layer flow affected heat and mass transfer on the surface of the boundary divider and how the Arrhenius activation energy concept could be used to better understand these processes. In this investigation, he used an irritant technique to give an empirical approach to the topic. (Elayarani, 2021) investigated the alteration in mass and thermal properties of a Carreau base fluid containing microorganisms across a slandering surface.

Micropolar nano fluids are a type of non-Newtonian fluid that exhibit particular microscopic and nano phenomena. These effects model the structure of micromotions as well

as the Brownian movements of fluid particles. Micropolar nanofluids are being developed to study the behavior of many industrial and biological products. (Ahmadi, 1976), studied the self-similar solution of micropolar fluid on a semi-infinite plate. Nanofluids have many practical applications such as in medicine, hybrid engines, fuel cells, microelectronics and more recently in the field of nanotechnology due to their unique properties which make them suitable for a wide range of applications. The (Buongiorno J. , 2006) method for nanofluids more realistically measures the spread of nanoparticles across the fluid flow. Researchers have extensively used this model to explore the heat conduction enhancement of ordinary fluids. Nanofluid research has grown dramatically in the last two decades, particularly in the creation of highly effective coolants and improved heat transfer technologies.

In a study conducted by (Watanabe, 1990), the flow of a non-similar boundary layer on a trough with constant suction or injection was investigated. The difference-differential method was utilized to derive the standard boundary layer equations and transform them into dimensionless stream function equations. These equations were then transformed into integral equations with the boundary conditions. The numerical solutions were obtained through iterative numerical quadrature, and the results for velocity and temperature distributions, as well as the coefficients of skin friction and heat transfer, were presented for a variety of pressure gradient and suction/injection parameter values. The study found that it is possible to significantly alter flow field and rate of heat transmission from the surface by the process of suction or injection, like mass transfer cooling. (Erickson, 1966) pioneered suction or injection through a stretching sheet. It was introduced a porous medium compressor with an interconnected heat exchanger. Unlike a catalytic combustor, this burner uses flames to burn inside a porous medium. Combustion in porous media has been shown to be a promising approach for developing burners with high power densities, wide power dynamic ranges, and minimal emissions, as studied by (TRIMIS, 1996). The paper describes the test rig and operating principle of the combustor and provides results and specifications for the burner. Additionally, the paper discusses the mechanisms of heat transfer and the possible fields of application for this technology.

A heat exchanger's operation, the melting of ice on an airport runway using resistance heating, the heating of a frying pan on an electric range, the use of an absorber plate to dissipate heat from an electronic bundle, the heating of an item on a hot plate, the operation of a heat exchanger and many other industrial activities that involve heating or cooling all involve the transfer of heat by conduction. High thermal conductivity materials (such as a heat sink material) are required for effective heat transfer by conduction. Good thermal contact must also exist between the two interfaces (such as a heat sink's surface and a printed circuit board's surface) through which heat transfer takes place. A good thermal contact necessitates the use of a thermal interface substance, such as a thermal grease, that is thin (tiny in thickness) between the contact surface, conforms to the topographical of the mating surface, and preferably has a high thermal conductivity. In a study conducted by (Raju, 2016) , the use of the finite element method was explored to simulate unsteady MHD free convection flows past a vertically inclined porous plate, considering thermal diffusion and diffusion thermally effects. The study focused on the importance of viscous dissipation temperature difference in the free convective flow of fluids when the flow field is low in temperature, extreme in size, or has a high gravitational field. This is important in many fields, such as in polymer processing flows where significant temperature rises are observed, as well as in the conversion of certain types of mechanical, nuclear, electrical or hydro processes to thermal energy in the medium. (Hayat, 2008) investigated mass transfer in a steady two-dimensional boundary layer flow of MHD of a potential to lift Maxwell fluid via a porous shrinking sheet in the absence of a chemical reaction. The study used a HAM method to obtain formulas for the velocity and concentration distributions.

(Mahapatra, 2001) carried out a study that looked at the continuous 2D flow of a non-compressible fluid that conducts electricity approaching a extending surface in the presence of a uniform transverse magnetic field, and also determined the temperature in this flow when the stretch surface is kept at a constant temperature. (Mahapatra, T. R & Gupta, A. S., 2003) examined the flow of an incompressible fluid over a flat deformable surface at an axisymmetric stagnation point when the surface is extended asymmetrically in its own plane with a velocity that is proportional to the distance from the stagnation-point. (Roy, 2007) investigated unsteady mixed convection streams over a vertical cone with suction or injection and discovered that the buoyancy force causes an overshoot in velocity profiles near the wall for lower Prandtl numbers

but not for higher Prandtl numbers, and that the magnitude of the overshoot increases with the buoyancy parameter but decreases with time.

(Gebhart, 1962) observed that when an induced kinetic energy exceeds the amount of heat transfer, the effect of viscous dissipation in natural convection becomes more prominent. It happens when the equivalent body force or the convection region is large. The study focused on vertical surfaces under isothermal and uniform-flux surface conditions. Viscous dissipation has been observed to have a significant impact in natural convection in a variety of systems that are subjected to large decelerations or operate at high rotational speeds. Additionally, significant viscous dissipation effects may be present in greater gravitational fields and in processes that occur on a large scale, such as on larger planets, large amounts of gas in space, and geological features in fluids within various bodies. These types of processes have been studied in the past, particularly in spinning cavities. Lighthill in 1953 conducted research into the possibility of cooling turbine blades through the fluid flow of an internal coolant, resulting in an analysis that outlined flow patterns and projected heat-transfer characteristics. Viscous dissipation or the local production of thermal energy via the framework of viscous stresses, is a common occurrence in both viscous flow of clear fluids and fluid flow within porous media. In comparison to other thermal influences on fluid motion (Examples include buoyancy forces induced by heated or cooled blocks, as well as localized heat sources or sinks), the impact of heat emitted by viscous dissipation ranges from negligible to significant, as studied by (Magyari, 2005).

CHAPTER 3

FUNDAMENTAL CONCEPTS AND BASIC LAWS

Some books on the basic and physical principles of fluid have been written by (Fox, 2006), (GENICK BAR-MEIR, 2013), (Kothandaraman, 2006), (Y. A. Cengel, 2010), (White, 2006), (Kunes, 2012), (Smits, 2000), (Papanastasiou, 2021), (J. Kunes, 2012) and (Lwis, 2004). In this chapter, certain definitions from the books indicated above that include essential rules and notions for solving nonlinear differential equations that will be utilized in the next chapters, have been mentioned.

3.1 Basic Definitions

In this section, a few basic definitions, laws and terminologies have been presented that are beneficial for further discussion.

3.1.1 Fluid

A fluid is a type of material that deforms continually under shear stress, with the amount of stress being constant. Thus, fluids have two types of liquid and gas in physical forms in which substance exists.

3.1.2 Fluid Mechanics

Fluid mechanics is a branch of mechanics that studies the condition of fluids at rest and in motion.

3.1.3 Fluid Dynamics

Fluid Dynamics is a subfield of fluid mechanics that describes the properties of fluid as it moves from one site to another.

3.1.4 Fluid Statics

Fluid statics is a subfield of fluid mechanics that investigates the behavior of fluids in a stationary or resting posture.

3.2 Physical Properties of the Fluid

In this section, we have defined physical properties of fluid. Every fluid has own properties according to nature and physical appearance.

3.2.1 Pressure

Pressure is defined as force applied across a unit area $\left(P = \frac{F}{A}\right)$. It is a vector quantity having SI unit pascal (Pa). Pascal is newton per square meter $\left(\frac{N}{m^2}, \frac{kg}{m \cdot s^2}\right)$, where P, F & A represents pressure, force and area respectively.

3.2.2 Density

Density is described as mass per unit volume $\left(\rho = \frac{m}{v}\right)$, where ρ is symbol for density, m is mass, and v is volume occupied by the substance.

3.2.3 Temperature

Temperature is a physical property of matter that quantifies the hotness or coolness of a body. The temperature of an object, usually measured in Fahrenheit, kelvin and Celsius. It is denoted by T. Thermodynamic temperature is a measurement of the kinetic energy in a substance's molecules or atoms.

3.2.4 Viscosity

Viscosity is defined as a fluid's resistance to progressive deformation caused by tensile or shear stress. In other notations, a fluid viscosity is that characteristic which measures the amount of resistance to the shear stress. It is denoted by μ and mathematically one can write as:

$$\left(\text{Viscosity } = \mu = \frac{\text{shear stress}}{\text{rate of shear strain}}\right).$$

3.2.5 Kinematic Viscosity

Kinematic viscosity is a measure of a fluid's resistance to flow and is defined as the ratio of a fluid's dynamic viscosity to its density $\left(\upsilon = \frac{\mu}{\rho}\right)$, where μ and ρ denote dynamic viscosity and density respectively. The dimension of kinematic viscosity is $\left(\frac{L^2}{T}\right)$.

3.2.6 Stress

Stress is a pressure on fluid defined as force acted upon a material per unit of its area and is denoted by τ. The mathematical form is $\left(\tau = \frac{F}{A}\right)$, where F denotes the force and A shows the area.

3.2.7 Shear Stress

Shear stress is a form of stress in which the force vector is oriented perpendicular to the surface or cross-section of the material.

3.2.8 Normal Stress

Any item or body that experiences stress from an external force perpendicular to its cross-sectional area will eventually return to its original shape and the tension produced by a force acting perpendicularly on a certain area is known as normal stress.

3.2.9 Tensile stress

Tensile stress is generated when a force applied perpendicular to the object's sectional area, causing it to stretch from its initial shape. The mathematical form is $\left(\sigma = \frac{F}{A}\right)$, where σ is the tensile stress, F is the force acting and A is the cross-sectional area.

3.2.10 Compressive stress

When a force operates perpendicular to an object's surface area, compressing it to distort its shape, the resulting stress is known as compressive stress. The mathematical form is $\left(\sigma = \frac{F}{A}\right)$,where F is force acting, σ is compressive stress and A is the cross-section area.

3.2.11 Newton's Law of Viscosity

The shear stress is directly and linearly related to the velocity gradient in this respect. Mathematically, it can be written as:

$$\tau_{xy} \propto \left(\frac{\partial u}{\partial y}\right),$$

$$\tau_{xy} = \mu \left(\frac{\partial u}{\partial y}\right).$$

In the above expression, τ_{xy} is the shear stress applied to the velocity component 'u' of fluid and μ is the viscosity proportionality constant.

3.3 Types of Fluid Flow

3.3.1 Flow

It is the deformation of a material in the presence of various forces. The motion of a fluid influenced by many unbalanced forces is referred to as fluid flow. It is primarily a branch of fluid mechanics and fluid flow dealing with fluid dynamics. The fluid continues to travel until it is subjected to additional imbalanced forces.

3.3.2 Compressible and Incompressible Flows

Flow that has minimal density variations is called incompressible, otherwise it is considered compressible. The flow of gases is the most typical example of compressible flow, whereas the movement of liquids is often described as incompressible. Mathematically,

$$\frac{D\rho}{Dt} = 0,$$

where ρ expresses fluid density and $\frac{D}{Dt}$ is derivative of the material given by

$$\frac{D}{Dt} = \frac{\partial}{\partial t} + \boldsymbol{V} \cdot \nabla,$$

where $\boldsymbol{V}$ is the velocity of flow and ∇ is the differential operator. The equation for ∇ in the Cartesian coordinate system is given.

$$\nabla = \frac{\partial}{\partial x}\hat{\imath} + \frac{\partial}{\partial y}\hat{\jmath} + \frac{\partial}{\partial z}\hat{z}.$$

3.3.3 Uniform and Non-uniform Flows

The flow is said to be uniform if the direction and magnitude of the velocity are same at every place and for the non-uniform flow at any given instant is that in which the velocity is not equal at each point.

3.3.4 Steady and Unsteady Flows

Steady flow is defined as the flow in which the fluid's characteristics do not vary over the time at a single spot,

$$\frac{\partial \lambda_w}{\partial t} = 0,$$

where λ_w is any fluid property.

Unsteady flow is one in which the fluid characteristics change over time, i.e.

$$\frac{\partial \lambda_w}{\partial t} \neq 0.$$

3.3.5 Laminar and Turbulent Flows

A flow can be either laminar, if fluid particles travel in smooth layers, but turbulent fluid particles rapidly mix as they flow due to random 3D velocity differences.

3.4 Types of Fluids

3.4.1 Ideal Fluid

An ideal fluid is incompressible and has zero viscosity, which means that shear stress is always equal to zero regardless of the fluid's velocity.

3.4.2 Real Fluid

A compressible fluid which experiences some resistance during the flow is characterized as a real or viscid fluid.

3.4.3 Newtonian and Non-Newtonian Fluids

A Newtonian fluid is one that complies with Newton's viscosity law. Non-Newtonian fluids are very viscous liquids that behave like solids and remain solid or semi-solid. Mathematical form of Newtonian fluids:

$$\tau_{xy} = \mu\left(\frac{\partial u}{\partial y}\right),$$

where μ = dynamic viscosity, τ_{xy} shear stress $= \frac{F}{A}$ and $\frac{\partial u}{\partial y}$ = rate of shear deformation. The most common examples of Newtonian fluid are water, alcohol, glycerol. Non-Newtonian fluids are those that do not satisfy Newton's viscosity law. For such fluids,

$$\tau_{xy} = k\left(\frac{\partial u}{\partial y}\right)^{n},$$

where *k* represents flow consistency index and n is the index of flow behavior. For $n = 1$ and $k = \mu$, the above equation decreases to the Newton's law of viscosity. Industrial processes such as papermaking, textile manufacturing, and oil drilling. Non-Newtonian fluids have countless applications in industries such as: Food and pharmaceutical industries where they are used as thickeners, emulsifiers, and lubricants, construction materials such as paint and concrete, industrial cleaning and waste treatment and in the field of civil and mechanical engineering.

3.4.4 Nano Fluid

Nanofluids are a promising technology with a wide range of applications in various fields. They are widely used in the enhancement of heat transfer in various industrial processes such as electronics cooling, and power generation. In biomedical applications, they have been used in drug delivery and imaging. Additionally, they have been used to improve the efficiency of solar thermal energy systems and enhance the thermal performance of engines and machinery. They also have applications in improving the performance of lubricants and cutting fluids in manufacturing and machining processes, enhancing the performance of batteries and fuel cells, and in environmental remediation and water treatment. They have also been used to improve the efficiency of refrigeration and air-conditioning systems and enhance the performance of heat exchangers and heat pipes. With the ongoing research, there are more applications are being developed such as in the field of nanocomposite materials and in the field of nanotechnology.

3.5 Heat Transfer Mechanism and Properties

3.5.1 Heat Transfer

It is the energy transfer due to temperature difference between two surfaces. Heat transfer is normally conducted from a high temperature region to a low temperature region. For example, heat is transferred from stove to the cooking pan.

3.5.2 Mass Transfer

Mass exchange is the total movement of mass from one place to another.

3.5.3 Conduction

Conduction is the process in which heat is transferred through the material between the objects that are in physical contact. For example, frying vegetables in a pan, picking up a hot cup of tea, after a car starts the engine becomes hot and auto mobile radiator.

3.5.4 Convection

Convection is a mechanism in which heat is transferred through fluids (gases or liquids) from a hot place to a cool place. For example, a steaming cup of hot tea demonstrates heat transfer into the air.

3.5.5 Radiation

Thermal radiation is the process by which heat is transported from a body due to its temperature without the use of an intermediary medium. For example, heat from the sun warming the face, heat from a light bulb, and heat from a fire toaster toast bread by using thermal radiation released by its element.

3.6 Some Important Definition

In this portion we discuss some of the important definitions.

3.6.1 Streamlines

A streamline is a path or line that is always parallel to the velocity field. For 2D flows, the streamline slop must be equal to a tangent to the angle formed by the velocity angle with the x-axis.

3.6.2 Stream Function

Stream function is a useful tool for studying fluid dynamics. The stream function is typically used to produce streamlines which are then used to realize the flow pattern around an object. A stream function is defined as one that solves the given equation.

$$u = \frac{\partial \psi}{\partial y},\ v = -\frac{\partial \psi}{\partial x}.$$

3.6.3 Viscous Dissipation

Viscous dissipation denotes the irreversible (in thermodynamic terms) conversion of flow kinetic energy into fluid internal energy.

3.6.4 Thermal Conductivity

Thermal conductivity (k) is a property that describes a material's ability to conduct heat. The mathematical representation of heat conductivity is

$$k = \frac{q\nabla l}{A\nabla t},$$

where q is the amount of heat. Surface area A and ∇l is the effect of a temperature differential ∇t across a distance. A, l and ∇t are assumed to be unit measurements.

3.6.5 Thermal Diffusivity

Thermal diffusivity is the relationship between the heat flowing through the material and the heat per unit of volume stored in the material.
Mathematically

$$\alpha = \frac{k}{\rho c_\rho},$$

where k denotes thermal conductivity, ρ density and c_ρ specific heat.

3.6.6 Mixed Convection

The properties of both forced and natural convection are combined in mixed convection. When density variations induced by temperature changes generate fluid motion, this is referred

to as free or natural convection. When an external force, such as pumping or blowing, causes fluid mobility, this is referred to as forced convection.

3.6.7 Shear Thickening Fluids

Shear thickening fluids are a small-scale category of actual liquids whose velocity increases with increasing shear rate. Dilatant fluids are also known as shear thickening fluids. Corn starch and heat absorption paste are two examples.

3.7 Boundary Layer

Viscous impacts are most prevalent on solid surfaces where the strong contact between the fluid's particle and the solid's molecule results in a motionless surface with practically zero relative velocity. As a result, approaching the wall, the fluid velocity must drop to zero. This is known as a no slip situation. Under some conditions, the fluid and solid surfaces do not move relative to one another at their point of contact. As a result, huge velocity gradients form near to the wall as the flow velocity varies with distance from the wall increasing from zero at the wall to its greatest value some distance away. This area is known as a boundary layer because it is generally narrow (in relation to the average body dimension).

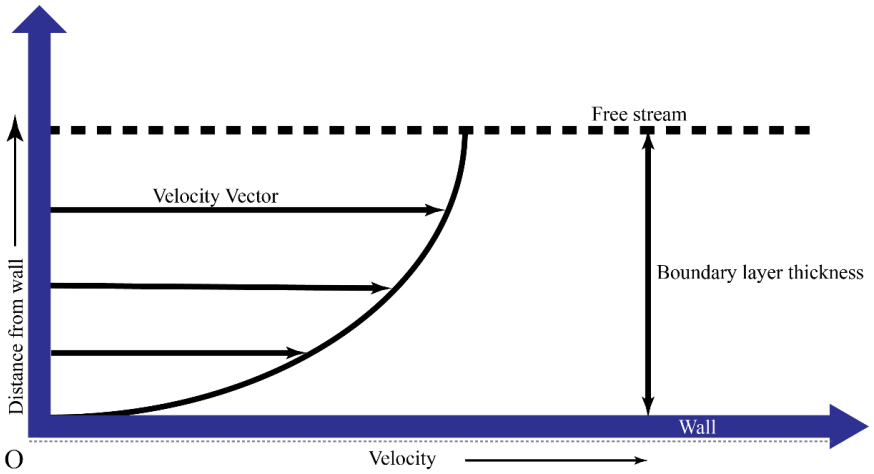

Fig. 3.1: Boundary Layer

3.8 Solution Methodology

To solve higher order nonlinear ordinary differential equations, the shooting method can be applied. To apply this method, we must first convert the higher order ODEs into a first order ODE system. If the missing beginning conditions exist. As an initial value issue, the Runge-Kutta method is employed to numerically integrate the differential equations. Comparing the computed values of the dependent variables at the terminal point to their given value allows us to determine whether the fictitious missing initial condition was correct. Newton's method is used with the new set of beginning conditions to modify boundary conditions that are not met with the requisite accuracy. Until the requisite precision is attained, the procedure is done once again. We analyze the following general second order boundary value problem to describe the shooting approach. Consider

$$y''(x) = f\big(x, y, y'(x)\big), \tag{3.1}$$

in terms of the boundary conditions

$$y(0) = 0,\ y(L) = B. \tag{3.2}$$

Let

$$y = y_1,\ \ {y_1}' = y_2. \tag{3.3}$$

By using the notations (3.3) in (3.1) and (3.2), we get

$$\left.\begin{aligned} {y_1}' &= y_2, \qquad y_1(0) = 0, \\ {y_2}' &= f(x,\, y_1,\, y_2),\ \ y_1(L) = B. \end{aligned}\right\} \tag{3.4}$$

Let the missing initial condition be $y_2(0) = p$, we obtain the following IVP

$$\left.\begin{aligned} {y_1}' &= y_2, \qquad y_1(0) = 0, \\ {y_2}' &= f(x,\, y_1,\, y_2),\ \ y_1(L) = p. \end{aligned}\right\} \tag{3.5}$$

The initial value issue now meets the boundary condition $y_2(L) = B$.

$$y_1(L, p) - B = g(p) = 0. \tag{3.6}$$

The Newton's method for finding an approximate root of (3.6) is expressed as

$$p_{n+1} = p_n - \frac{g(P_n)}{g'(p_n)}, \tag{3.7}$$

or

$$p_{n+1} = p_n - \frac{y_1(L,p_n)-B}{\frac{\partial}{\partial p}(y_1(L,p_n)-B)}. \tag{3.8}$$

Consider the following representations

$$\frac{\partial y_1}{\partial p} = y_3,\ \frac{\partial y_2}{\partial p} = y_4. \tag{3.9}$$

We derive the four ODEs and the initial conditions by differentiating (3.5) regarding p, are

$$\left.\begin{aligned} y_3{}' &= y_4, \quad y_3(0) = 0, \\ y_4{}' &= y_3\frac{\partial f}{\partial y_1} + y_4\frac{\partial f}{\partial y_2}, \quad y_4(0) = 1. \end{aligned}\right\} \tag{3.10}$$

Now, solving the IVP (3.10), we get y_3 at L. This is derivative of y_1 with respect to p to compute at L. Using the value of $y_3(L,p)$ in (3.8), modified value of p can be achieved. New value of p can be utilized to solve the problem (3.10) and the method is repeated until the required precision.

3.9 Laws of Conservation and Basic Equations

Three conservation laws, which can be expressed in integral or differential form are used to model the problems in fluid dynamics. The integral formulations of these laws represent changes in mass, momentum or energy inside the control volume.

3.9.1 Continuity Equation

The equation of continuity represents the mass conservation of fluid entering and leaving the control volume, as well as the resulting mass balance. This equation demonstrates mass conservation.

$$\frac{\partial \rho}{\partial t} + \nabla \cdot (\rho \boldsymbol{V}) = 0. \tag{3.11}$$

where ρ is the density of the fluid, t is time, $\boldsymbol{V}$ is the velocity of the fluid, Equation (3.11) for constant flow can be written as

$$\nabla \cdot (\rho \boldsymbol{V}) = 0. \tag{3.12}$$

In the case of incompressible flow, equation (3.12) becomes

$$\nabla \cdot \boldsymbol{V} = 0. \tag{3.13}$$

3.9.2 Momentum Equation

The term "linear momentum" refers to the sum of a body's mass and velocity. Newton's second law states that the rate of change in momentum of a body is equal to the net force applied to the body, so a body's acceleration is proportional to the net force applied to it and inversely related to its mass. As a result, when no net force acts on a system, its momentum is constant, and such systems' momentum is conserved. This is referred to by the momentum conservation principle. The momentum equation for any fluid is

$$\frac{\partial(\rho V)}{\partial t} + \nabla.[(\rho \boldsymbol{V})V] - \nabla \cdot T - \rho g = 0. \tag{3.14}$$

Since $T = -PI + \tau$, the momentum equation takes the form

$$\rho\left(\frac{\partial \boldsymbol{V}}{\partial t} + \boldsymbol{V}.\nabla \boldsymbol{V}\right) = \nabla \cdot (-PI + \tau) + \rho g. \tag{3.15}$$

The basis vectors of an orthogonal coordinate system are combined using the scalar product, A can be divided into three scalar parts equation (3.15). By setting $g = g\nabla z$, where z is distance in direction of gravity from an arbitrary reference elevation can be also expressed as

$$\rho\left(\frac{\partial \boldsymbol{V}}{\partial t} + \boldsymbol{V}.\nabla \boldsymbol{V}\right) = \nabla + \nabla(\rho g z). \tag{3.16}$$

According to the momentum equation, a particle accelerates after it begins to move due to a net force represented by the pressure, viscous, and gravitational gradients.

3.9.3 Energy Equation

The first law of thermodynamics is a natural rule, commonly known as the concept of energy conservation. It asserts that energy cannot be generated or destroyed throughout a process, it can only change form. In two-dimensional system, energy equation for base fluid can be expressed as in form of T temperature.

$$\boldsymbol{V} \cdot \nabla T = \alpha \nabla^2 T. \qquad (3.17)$$

3.10 Dimensionless Parameters

3.10.1 Prandtl Number

Prandtl number is ratio between the viscous diffusivity and the thermal diffusivity. Mathematically, it can be written as

$$Pr = \frac{\upsilon}{\alpha} = \frac{\mu/\rho}{k/\rho C_P} = \frac{\mu C_p}{k},$$

where α indicates the thermal diffusivity and υ represents the viscous diffusivity. It characterizes the physical properties of a fluid with convective and diffusive transfers.

3.10.2 Eckert Number

Eckert number is the dimensionless number used in the mechanical behavior of materials modeled as a continuous mass rather than as separate particles. It describes ratio between advective transport (heat difference at boundary layer) and heat dissipation potential. Mathematical form of Eckert number is

$$E_c = \frac{u^2}{C_p \nabla T},$$

where u is velocity, C_p is specific heat and ∇T is difference between internal body and wall temperature.

3.10.3 Schmidt Number

It is the ratio of viscosity υ to molecular diffusion D. It is denoted by Sc. Mathematical form is

$$S_C = \frac{\upsilon}{D},$$

where υ is kinematic viscosity and D is the mass diffusivity.

3.10.4 Nusselt Number

Convective to conductive heat transfer to the boundary is measured as the Nusselt number. It is denoted by N_u, mathematically expressed

$$N_u = \frac{hL}{k_f},$$

where h is convective heat transfer, L defines characteristic length and k_f describes thermal conductivity.

3.10.5 Sherwood Number

The ratio of convective mass transfer to diffusion mass transfer is expressed by the Sherwood number, a non-dimensional quantity. Mathematically

$$S_h = \frac{kL}{D_m},$$

where L is characteristics length, k is mass transfer co-efficient and D_m is mass diffusivity.

CHAPTER 4

MODELING OF HEAT AND MASS TRANSFER OF RADIATIVE MHD CASSON WITH CHEMICAL REACTION

4.1 Introduction

In this chapter, we have reviewed (S. M. Ibrahim, 2020) the impact of heat source, chemical reaction, MHD and suction/injection on Casson fluid over an exponentially penetrable stretching sheet. Applicable similarity transformation is used to convert PDEs into ODEs and shooting method has been used to achieve the numerical results. A variety of factors, including magnetic properties, exponential behavior, suction and injection techniques, radiation principles, the Prandtl and Eckert numbers, the heat source factor, the Schmidt number and chemical reaction constants, are presented and illustrated through the use of tables and graphs.

4.2 Mathematical Formulation

The movement of a Casson fluid across a stretched sheet in 2D steady incompressible MHD with stagnation point has been studied. The location of an exponentially stretched sheet is at $y = 0$. The flow of Casson fluid confined to $y > 0$. Magnetic field $B = B_0 e^{\frac{Nx}{L}}$ is applied normally to sheet. In the flow region, no electric field exists. The flow zone is characterized by a relatively weak induced magnetic field, resulting in a relatively low magnetic Reynolds number. Consider chemical reaction $k_1 = k_0 e^{\frac{Nx}{L}}$ and heat source $Q = Q_t e^{\frac{Nx}{L}}$. Due to two opposing pressures, the surface is extended along x- axis, origin is locked in place and sheet produces a thin slit. Constitutive equation for Casson fluid flow that is isotropic and incompressible is:

$$\tau_{ij} = \begin{cases} 2\left(\mu_B + \frac{p_y}{\sqrt{2\pi}}\right) e_{ij}, & \pi > \pi_c, \\ 2\left(\mu_B + \frac{p_y}{\sqrt{2\pi_c}}\right) e_{ij}, & \pi_c > \pi, \end{cases} \tag{4.1}$$

where μ_B is non-Newtonian fluid's plastic dynamic viscosity, p_y is fluid's yield stress, π is the product of the deformation rate component and π_c is a critical parameter for the product in a non-Newtonian model.

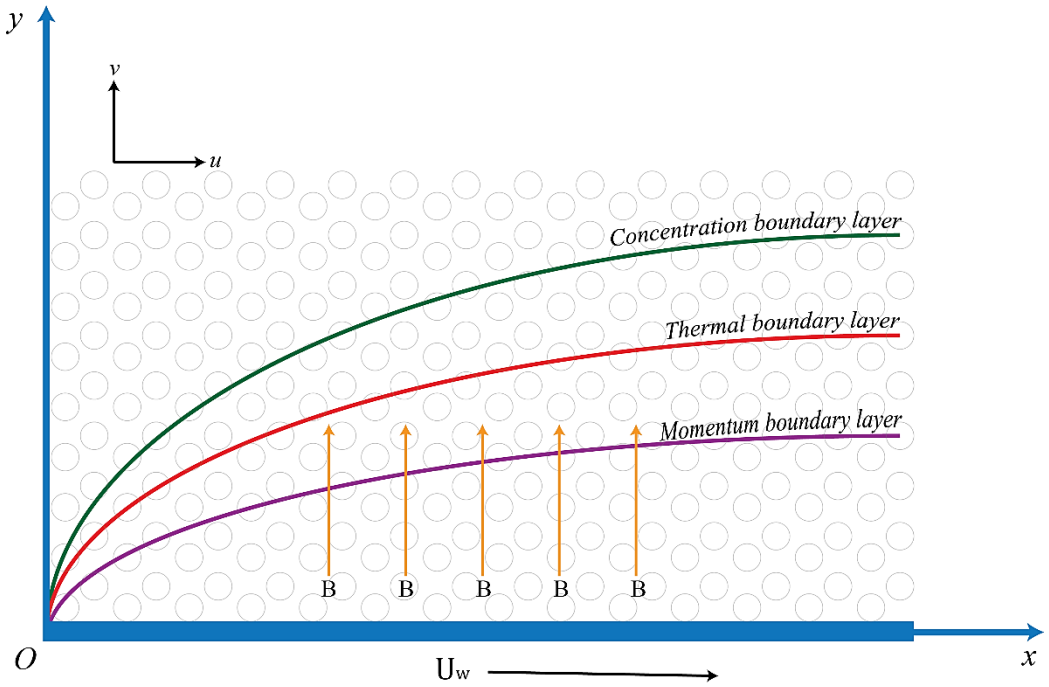

Fig. 4.1: Geometry of physical model.

The governing equations for the flow are as follows.

$$\frac{\partial u}{\partial x} + \frac{\partial v}{\partial y} = 0, \tag{4.2}$$

$$u\frac{\partial u}{\partial x} + v\frac{\partial u}{\partial y} = \nu\left(1 + \frac{1}{\beta}\right)\frac{\partial^2 u}{\partial y^2} + g\beta_T(T - T_\infty) + g\beta_C(C - C_\infty) - \frac{\sigma B^2 u}{\rho}, \tag{4.3}$$

$$u\frac{\partial T}{\partial x} + v\frac{\partial T}{\partial y} = \frac{k}{\rho C_p}\frac{\partial^2 T}{\partial y^2} + \frac{\nu}{C_p}\left(1 + \frac{1}{\beta}\right)\left(\frac{\partial u}{\partial y}\right)^2 - \frac{1}{\rho C_p}\frac{\partial q_r}{\partial y} - \frac{1}{\rho C_p}Q_t(T - T_\infty), \tag{4.4}$$

$$u\frac{\partial C}{\partial x} + v\frac{\partial C}{\partial y} = D_m\frac{\partial^2 C}{\partial y^2} - k_1(C - C_\infty), \tag{4.5}$$

with boundary conditions

$$u = U,\ v = -V(x),\ T = T_w,\ C = C_w,\ at\ y = 0, \tag{4.6}$$

$$u \to 0,\ T \to T_\infty,\ C = C_\infty,\ at\ y \to \infty. \tag{4.7}$$

Similarity transformations to be used are

$$\left.\begin{array}{lll} u=U_0 e^{\frac{Nx}{l}} f'(\xi), & v=-\sqrt{\frac{U_0\nu}{2l}} e^{\frac{Nx}{2l}} N[f(\xi)+\xi f'(\xi)], & \xi=y\sqrt{\frac{U_0}{2\nu l}} e^{\frac{Nx}{2l}},\ v=\frac{\partial\psi}{\partial x}, \\ \psi=\sqrt{2U_0\nu l}\, e^{\frac{Nx}{2l}} f(\xi), & T=T_\infty+T_0 e^{\frac{2Nx}{l}}\theta(\xi), & C=C_\infty+C_0 e^{\frac{2Nx}{l}}\phi(\xi),\ \mathrm{u}=\frac{\partial\psi}{\partial y}, \end{array}\right\} \tag{4.8}$$

where ξ is similarity variable, ψ is stream function, $f\ (\xi)$ is dimensionless stream function, $\theta(\xi)$ dimensionless temperature of the fluid in the boundary layer region and $\phi(\xi)$ dimensionless concentration of the fluid in the boundary layer region.

For the computation of velocity components along the x and y-axes the equations are

$$u = U_0 e^{\frac{Nx}{l}} f'(\xi), \tag{4.9}$$

$$v = -\sqrt{\frac{U_0\nu}{2l}} e^{\frac{Nx}{2l}} N[f(\xi) + \xi f'(\xi)]. \tag{4.10}$$

Using (4.9) and (4.10) in (4.2), the equation of continuity is satisfied identically.

Equation (4.3) into dimensionless form is

$$\left(1+\frac{1}{\beta}\right) f''' + N\left(ff'' - 2f'^2\right) + 2Gr\,\theta + 2Gc\,\phi - Mf' = 0. \tag{4.11}$$

Equation (4.4) becomes

$$u\frac{\partial T}{\partial x} + v\frac{\partial T}{\partial y} = \frac{k}{\rho C_p}\frac{\partial^2 T}{\partial y^2} + \frac{\nu}{C_p}\left(1+\frac{1}{\beta}\right)\left(\frac{\partial u}{\partial y}\right)^2 - \frac{1}{\rho C_p}\ \frac{\partial q_r}{\partial y} - \frac{1}{\rho C_p} Q_0(T - T_\infty).$$

The Rosseland radiative heat flux is represented by q_r also define as

$$q_r = -\frac{4\sigma^*}{3k^*}\frac{\partial T^4}{\partial y},$$

k^* is absorption coefficient, σ^* is Boltzmann constant. If temperature constant is comparatively small, T_4 can be stretched around T_∞ using the Taylor series. The reduced Taylor series takes the form by ignoring the higher order terms as

$$T^4 = 4T_\infty^3 T - 3T_\infty^4,$$

$$T = T_\infty + T_0 e^{\frac{2Nx}{l}}\theta(\xi),$$

$$C = C_\infty + C_0 e^{\frac{2Nx}{l}}\varphi(\xi).$$

Dimensionless form of (4.4) is

$$\left(1+\frac{4}{3}R\right)\theta'' + PrN(\theta' f - 4f'\theta) + \left(1+\frac{1}{\beta}\right)PrEcf''^2 - \Pr Q_T\,\theta = 0. \quad (4.12)$$

Equation (4.5) in dimensionless form is

$$\phi''+ScN(\phi' f - 4f'\phi) - Sc\gamma\,\phi = 0. \quad (4.13)$$

The set of ordinary differential equations obtained is

$$\left.\begin{array}{c} \left(1+\frac{1}{\beta}\right)f''' + N\left(ff'' - 2f'^2\right) + 2Gr\,\theta + 2Gc\,\phi - Mf' = 0, \\ \left(1+\frac{4}{3}R\right)\theta'' + PrN\left(\theta' f - 4f'\theta\right) + \left(1+\frac{1}{\beta}\right)PrEcf'^2 - \Pr Q_T\,\theta = 0, \\ \phi'' + ScN\left(\phi' f - 4f'\phi\right) - Sc\gamma\,\phi = 0, \end{array}\right\} \quad (4.14)$$

with the boundary conditions

$$\left.\begin{array}{ll} f = \mathrm{S}, f' = 1, \theta = 1, \phi = 1, & \text{at } \xi = 0, \\ f' = 0, \theta = 0, \phi = 0, & \text{as } \xi \to \infty. \end{array}\right\} \quad (4.15)$$

In the above equations, N represent the exponential parameter, Gr for the thermal Grashof number, Gc for the concentration Grashof number, R for the radiation parameter, M for magnetic parameter, Prandtl number is represent with Pr, Ec for Eckert number, heat generation parameter is denoted with Q, Scmidt number is denoted with Sc, γ is chemical reaction and S is denoting the suction and injection parameter. Value of these parameters are given as

$$Pr = \frac{\rho C_p \nu}{k}, \quad \mathrm{Gr} = \frac{g\beta_T T_0 L}{U_0^2}, \quad \mathrm{Gc} = \frac{g\beta_c C_0 L}{U_0^2}, \quad \mathrm{Sc} = \frac{\nu}{D_m}, \quad Ec = \frac{U_0^2}{C_p T_0},$$

$$M = \frac{2L\sigma B_0^2}{\rho U_0}, \quad Q_T = \frac{2Q_0 L}{\rho C_p U_0}, \quad \mathrm{R} = \frac{4\sigma^*}{kk^*}T_\infty^3, \quad \mathrm{S} = \frac{v_0}{\sqrt{\frac{\nu U_0}{2L}}}, \quad \gamma = \frac{2k_0 L}{U_0}.$$

4.3 Physical Quantity

Mathematical form of skin friction coefficient is

$$c_f = \left(\frac{\tau_w}{\rho U_w^2}\right). \quad (4.16)$$

Mathematical form of Local Nusselt coefficients is

$$Nu_x = \left(\frac{x q_w}{k(T_\omega - T_\infty)}\right). \quad (4.17)$$

Mathematical form of local Sherwood number is

$$Sh_x = \left(\frac{xq_m}{D_m(C_\omega - C_\infty)}\right), \tag{4.18}$$

where q_w is heat fluxes, q_m is mass fluxes and τ_w represent the shear stress at the surface. These are defined as

$$\tau_w = \mu_B \left(1 + \frac{1}{\beta}\right)\left(\frac{\partial u}{\partial y}\right)_{y=0},\ q_w = \left(-\left(k + \frac{16\sigma^* T_\alpha^3}{3k^*}\right)\left(\frac{\partial T}{\partial y}\right)\right)_{y=0},$$

$$q_m = -D_m \left(\frac{\partial C}{\partial y}\right)_{y=0}. \tag{4.19}$$

The dimensionless quantities obtained are: -

$$\sqrt{Re_x} c_f = \left(1 + \frac{1}{\beta}\right) f''(0),\ (Re_x)^{\frac{-1}{2}} Nu_x = \left(-\left(1 + \frac{4R}{3}\right)\theta'(0)\right),$$

and $(Re_x)^{\frac{-1}{2}} Sh_x = \left(-\phi'(0)\right),$

where Re_x is Reynolds number.

4.4 Solution Methodology

The systems of nonlinear ordinary differential equation (4.14) and appropriate boundary condition (4.15) are first order ODEs that have been transformed. Shooting method is used to solve first order ODEs with proper boundary conditions.

$$f''' = \frac{1}{\left(1+\frac{1}{\beta}\right)}\left(Mf' - N\left(ff'' - 2f'^2\right) - 2Gr\,\theta - 2Gc\,\phi\right), \tag{4.20}$$

$$\theta'' = \frac{1}{\left(1+\frac{4}{3}R\right)}\left(\Pr Q_T\,\theta - PrN(\theta' f - 4f'\theta) - \left(1 + \frac{1}{\beta}\right) PrEcf''^2\right), \tag{4.21}$$

$$\phi'' = \left(Sc\gamma\,\phi - ScN(\phi' f - 4f'\phi)\right). \tag{4.22}$$

Since equations (4.20), (4.21) and (4.22) contain functions of f ,θ and ϕ and its derivatives. The solution of equation (4.20) can be utilized to recognize results in equations (4.21) and (4.22). We are aware of the basic conditions stated at $\xi = 0$ in the above ODEs, equations (4.20), (4.21) and (4.22) give the unidentified condition that is portrayed by W, P and Z respectivly. We have established the symbols for further explanation.

$$y_1 = f, y_2 = y_1' = f', y_3 = y_2' = f'', y_4 = \theta, y_5 = \theta', y_6 = \phi, y_7 = \phi'.$$

The system of ODEs (4.20), (4.21), (4.22) and corresponding initial condition may be represented as:

$$
\begin{aligned}
&y_1 = f, && \\
&y_2 = y_1' = f', && y_1(0) = S, \\
&y_3 = y_2' = f'', && y_2(0) = 1, \\
&y_3' = f''' = \frac{1}{\left(1+\frac{1}{\beta}\right)} \begin{pmatrix} My_2 - N(y_1 y_3 - 2{y_2}^2) - 2Gr\, y_4 \\ -2Gc\, y_6 \end{pmatrix}, && y_3(0) = W, \\
&y_4 = \theta, && \\
&y_5 = \theta', && y_4(0) = 1, \\
&y_5' = \theta'' = \frac{1}{\left(1+\frac{4}{3}R\right)} \begin{pmatrix} \Pr Q_T\, y_4 - PrN(y_1 y_5 - 4y_2 y_4) \\ -\left(1+\frac{1}{\beta}\right) PrEc{y_3}^2 \end{pmatrix}, && y_5(0) = P, \\
&y_6 = \phi, && \\
&y_7 = \phi', && y_6(0) = 1, \\
&y_7' = \phi'' = \left(Sc\gamma\, y_6 - ScN(y_1 y_7 - 4y_2 y_6)\right), && y_7(0) = Z.
\end{aligned}
$$

The RK-4 technique has been used to solve the IVP consisting of the above ODEs for some appropriate substitutes of W, P and Z. The missing condition of velocity profile, temperature profile and concentration profile can be taken at $W = W^{(0)}$, $P = P^{(0)}$ and $Z = Z^{(0)}$ respectively and the Newton's technique may be used to discover the roots.

Domain for approximate numerical results $[0, \xi_\infty]$, where ξ_∞ is chosen in such a way that no discernible modifications are obtained by advancing beyond. The following is the shooting method's stopping condition

$$\max\{|y_2 - 0|, |y_4 - 0|, |y_6 - 0|\} < \varepsilon, \qquad (4.23)$$

where ε is a small positive real number. where $\varepsilon = 10^{-8}$ is the number used in the numerical computation.

4.5 Result and Discussion

The current section presents numerical data in the form of graphs and tables to illustrate the outcomes of the equations discussed in previous sections. These results were obtained by

varying several key factors such as the exponential parameter N, Grashof number Gr, concentration Grashof number Gc, radiation parameter R, magnetic parameter M, Prandtl number Pr, Eckert number Ec, heat generation parameter Q_T, Schmidt number Sc, chemical reaction γ, suction and injection parameter S, skin friction coefficient, Sherwood and Nusselt numbers. The physical characteristics have a direct effect on the temperature, concentration, and velocity profiles.

Tables 4.1 and 4.2 demonstrate how various physical parameters affect the skin friction, Nusselt and Sherwood number for Newtonian and Casson fluids, respectively. When the exponential and suction parameters increase, the Nusselt and Sherwood numbers also increase, despite decrease in skin friction coefficient. Moreover, heat transfer rate increases as the Prandtl number and heat source parameter increase, while skin friction coefficient and mass transfer rate decrease. The Eckert number has an inverse relationship with skin friction, with an increase in the Eckert number resulting in a decrease in the skin friction coefficient, an increase in the mass transfer rate, and a decrease in the rate of heat transmission. Finally, as chemical reaction parameter and Schmidt number increase, skin friction coefficient and rate of heat transmission decrease.

Table 4.1: Variation in $-\left(1+\frac{1}{\beta}\right)f''(0)$,$-\left(1+\frac{4}{3}R\right)\theta'(0)$ and $-\phi'(0)$ for Newtonian fluid.

N	M	Gr	Gc	S	Pr	R	Q	Ec	Sc	γ	$-\left(1+\frac{1}{\beta}\right)f''(0)$	$-\left(1+\frac{4}{3}R\right)\theta'(0)$	$-\phi'(0)$
1.0	0.5	0.1	0.1	0.5	0.7	0.1	0.2	0.2	0.6	0.1	1.56377467	1.65202079	1.46616861
1.5	0.5	0.1	0.1	0.5	0.7	0.1	0.2	0.2	0.6	0.1	1.98090802	2.03184484	1.81881485
2.0	0.5	0.1	0.1	0.5	0.7	0.1	0.2	0.2	0.6	0.1	2.36033938	2.36408617	2.12720864
1.5	0.0	0.1	0.1	0.5	0.7	0.1	0.2	0.2	0.6	0.1	1.82329481	2.08462292	1.85698287
1.5	0.3	0.1	0.1	0.5	0.7	0.1	0.2	0.2	0.6	0.1	1.91969602	2.05222701	1.8335295
1.5	1.0	0.1	0.1	0.5	0.7	0.1	0.2	0.2	0.6	0.1	2.12506942	1.98444449	1.78472990
1.5	0.5	0.2	0.1	0.5	0.7	0.1	0.2	0.2	0.6	0.1	1.91549065	2.05527437	1.83585430
1.5	0.5	0.5	0.1	0.5	0.7	0.1	0.2	0.2	0.6	0.1	1.72910060	2.11513056	1.87908731
1.5	0.5	1.0	0.1	0.5	0.7	0.1	0.2	0.2	0.6	0.1	1.44041467	2.19382611	1.93587483
1.5	0.5	0.1	0.2	0.5	0.7	0.1	0.2	0.2	0.6	0.1	1.91483109	2.05596468	1.83640036
1.5	0.5	0.1	0.5	0.5	0.7	0.1	0.2	0.2	0.6	0.1	1.72715844	2.11688587	1.88044593
1.5	0.5	0.1	1.0	0.5	0.7	0.1	0.2	0.2	0.6	0.1	1.43720882	2.19615511	1.93764130
1.5	0.5	0.1	0.1	0.0	0.7	0.1	0.2	0.2	0.6	0.1	1.59785779	1.85141733	1.64274881
1.5	0.5	0.1	0.1	0.3	0.7	0.1	0.2	0.2	0.6	0.1	1.81676204	1.95645497	1.74468402
1.5	0.5	0.1	0.1	1.0	0.7	0.1	0.2	0.2	0.6	0.1	2.45373881	2.24592580	2.03160714
1.5	0.5	0.1	0.1	0.5	0.3	0.1	0.2	0.2	0.6	0.1	1.95105992	1.14760614	1.83749502
1.5	0.5	0.1	0.1	0.5	0.5	0.1	0.2	0.2	0.6	0.1	1.96950025	1.62081077	1.82558398
1.5	0.5	0.1	0.1	0.5	1.0	0.1	0.2	0.2	0.6	0.1	1.99175673	2.57639940	1.81311254
1.5	0.5	0.1	0.1	0.5	0.7	0.0	0.2	0.2	0.6	0.1	1.98487757	1.94909625	1.81663277
1.5	0.5	0.1	0.1	0.5	0.7	0.5	0.2	0.2	0.6	0.1	1.96776111	2.30576404	1.8266677
1.5	0.5	0.1	0.1	0.5	0.7	1.0	0.2	0.2	0.6	0.1	1.95561081	2.57142407	1.84449001
1.5	0.5	0.1	0.1	0.5	0.7	0.1	0.1	0.2	0.6	0.1	1.97986681	2.00231643	1.81947072
1.5	0.5	0.1	0.1	0.5	0.7	0.1	0.5	0.2	0.6	0.1	1.98353025	2.11475966	1.81722761
1.5	0.5	0.1	0.1	0.5	0.7	0.1	1.0	0.2	0.6	0.1	1.98686925	2.23949006	1.81533374
1.5	0.5	0.1	0.1	0.5	0.7	0.1	0.2	0.1	0.6	0.1	1.98152998	2.08223962	1.81854809
1.5	0.5	0.1	0.1	0.5	0.7	0.1	0.2	0.5	0.6	0.1	1.97904868	1.88108717	1.81961084
1.5	0.5	0.1	0.1	0.5	0.7	0.1	0.2	1.0	0.6	0.1	1.97597126	1.63123159	1.82092344
1.5	0.5	0.1	0.1	0.5	0.7	0.1	0.2	0.2	0.4	0.1	1.96618848	2.04343630	1.37367699
1.5	0.5	0.1	0.1	0.5	0.7	0.1	0.2	0.2	0.7	0.1	1.98956497	2.02565068	2.17740042
1.5	0.5	0.1	0.1	0.5	0.7	0.1	0.2	0.2	1.0	0.1	1.99697252	2.02085708	2.57850407
1.5	0.5	0.1	0.1	0.5	0.7	0.1	0.2	0.2	0.6	0.0	1.97972787	2.03283681	1.79215431
1.5	0.5	0.1	0.1	0.5	0.7	0.1	0.2	0.2	0.6	0.5	1.98460723	2.02887604	1.91604997
1.5	0.5	0.1	0.1	0.5	0.7	0.1	0.2	0.2	0.6	1.0	1.98795513	2.02636482	2.02364856

Table 4.2: Variation in $-\left(1+\frac{1}{\beta}\right)f''(0)$,$-\left(1+\frac{4}{3}R\right)\theta'(0)$ and $-\phi'(0)$ for Casson fluid.

N	M	Gr	Gc	S	Pr	R	Q	Ec	Sc	γ	$-\left(1+\frac{1}{\beta}\right)f''(0)$	$-\left(1+\frac{4R}{3}\right)\theta'(0)$	$-\phi'(0)$
1.0	0.5	0.1	0.1	0.5	0.7	0.1	0.2	0.2	0.6	0.1	1.88596201	1.7094665821	1.52977990
1.5	0.5	0.1	0.1	0.5	0.7	0.1	0.2	0.2	0.6	0.1	2.361132640	2.11450112	1.90574423
2.0	0.5	0.1	0.1	0.5	0.7	0.1	0.2	0.2	0.6	0.1	2.788532733	2.46996675	2.23535769
1.5	0.0	0.1	0.1	0.5	0.7	0.1	0.2	0.2	0.6	0.1	2.170104992	2.16303344	1.9380928
1.5	0.3	0.1	0.1	0.5	0.7	0.1	0.2	0.2	0.6	0.1	2.286960138	2.13329883	1.91825592
1.5	1.0	0.1	0.1	0.5	0.7	0.1	0.2	0.2	0.6	0.1	2.535828616	2.07046650	1.87653047
1.5	0.5	0.2	0.1	0.5	0.7	0.1	0.2	0.2	0.6	0.1	2.294083055	2.13049117	1.91635519
1.5	0.5	0.5	0.1	0.5	0.7	0.1	0.2	0.2	0.6	0.1	2.099917296	2.17351809	1.94491402
1.5	0.5	1.0	0.1	0.5	0.7	0.1	0.2	0.2	0.6	0.1	1.793536548	2.23367278	1.98513015
1.5	0.5	0.1	0.2	0.5	0.7	0.1	0.2	0.2	0.6	0.1	2.294028527	2.13064193	1.91646584
1.5	0.5	0.1	0.5	0.5	0.7	0.1	0.2	0.2	0.6	0.1	2.099887775	2.17386952	1.94516799
1.5	0.5	0.1	1.0	0.5	0.7	0.1	0.2	0.2	0.6	0.1	1.793785331	2.23397833	1.98534593
1.5	0.5	0.1	0.1	0.0	0.7	0.1	0.2	0.2	0.6	0.1	1.977859228	1.90873279	1.70617251
1.5	0.5	0.1	0.1	0.3	0.7	0.1	0.2	0.2	0.6	0.1	2.361132640	2.11450112	1.90574423
1.5	0.5	0.1	0.1	1.0	0.7	0.1	0.2	0.2	0.6	0.1	2.818151662	2.35143189	2.13826361
1.5	0.5	0.1	0.1	0.5	0.3	0.1	0.2	0.2	0.6	0.1	2.328800525	1.21205595	1.91711755
1.5	0.5	0.1	0.1	0.5	0.5	0.1	0.2	0.2	0.6	0.1	2.349207824	1.69825055	1.90968604
1.5	0.5	0.1	0.1	0.5	1.0	0.1	0.2	0.2	0.6	0.1	2.372108815	2.66122315	1.90252489
1.5	0.5	0.1	0.1	0.5	0.7	0.0	0.2	0.2	0.6	0.1	2.365181737	2.02303610	1.90450490
1.5	0.5	0.1	0.1	0.5	0.7	0.5	0.2	0.2	0.6	0.1	2.347346014	2.41815155	1.91033441
1.5	0.5	0.1	0.1	0.5	0.7	1.0	0.2	0.2	0.6	0.1	2.333974942	2.71151683	1.91517824
1.5	0.5	0.1	0.1	0.5	0.7	0.1	0.1	0.2	0.6	0.1	2.360245062	2.08798020	1.90604746
1.5	0.5	0.1	0.1	0.5	0.7	0.1	0.5	0.2	0.6	0.1	2.363433329	2.19004419	1.90498300
1.5	0.5	0.1	0.1	0.5	0.7	0.1	1.0	0.2	0.6	0.1	2.366477279	2.30584778	1.90402761
1.5	0.5	0.1	0.1	0.5	0.7	0.1	0.2	0.1	0.6	0.1	2.362022783	2.17119261	1.90550785
1.5	0.5	0.1	0.1	0.5	0.7	0.1	0.2	0.5	0.6	0.1	2.358471993	1.94498460	1.90644966
1.5	0.5	0.1	0.1	0.5	0.7	0.1	0.2	1.0	0.6	0.1	2.354069697	1.66429653	1.90761328
1.5	0.5	0.1	0.1	0.5	0.7	0.1	0.2	0.2	0.4	0.1	2.345670261	2.12206704	1.45168413
1.5	0.5	0.1	0.1	0.5	0.7	0.1	0.2	0.2	0.7	0.1	2.369888170	2.11063551	2.26790752
1.5	0.5	0.1	0.1	0.5	0.7	0.1	0.2	0.2	1.0	0.1	2.377262985	2.10768290	2.67100444
1.5	0.5	0.1	0.1	0.5	0.7	0.1	0.2	0.2	0.6	0.0	2.360172560	2.11498842	1.88230096
1.5	0.5	0.1	0.1	0.5	0.7	0.1	0.2	0.2	0.6	0.5	2.364274787	2.11296724	1.99314478

The relationship between M and the dimensionless velocity profile $f'(\xi)$ is seen in Fig. 4.1. Typically, increasing M produces the Lorentz force and collision between molecules increases force causing the temperature of fluid to rise and the velocity to fall at boundary layer. The magnetic parameter M is proportional to the magnetic field strength squared and inversely proportional to velocity. Fig. 4.2 analyzes the interaction of the magnetic parameter M with temperature growth. A greater magnetic parameter frequently causes an opposing force known as the Lorentz force. Both the temperature profile and boundary layer viscosity increased because of the force. We realized that when the Casson fluid is used instead of Newtonian fluid, the temperature profiles rise significantly. Fig. 4.3 illustrates the behavior of concentration supply as M increase. It demonstrates that increasing the value of M improves the concentration of fluid supply.

As illustrated in figs 4.4 - 4.6, the exponential parameter has a significant effect on the skin friction coefficient, Nusselt number, and Sherwood number for both Newtonian and Casson fluids. As the exponential parameter increases, the fluid flow's momentum, temperature, and concentration boundary layers decrease. As a result, for both fluids, the velocity, temperature, and concentration decrease as the exponential parameter increases.

The figs 4.7- 4.9 demonstrate the correlation between the suction parameter S and the velocity, temperature and concentration profile. As the suction parameter S increases, the fluid velocity, temperature, and concentration profile decreases. The figures reveal that as the value of S increases, the fluid is drawn closer to the surface.

The effects of Grashof Number Gr on velocity and temperature profiles are depicted in figs 4.10 - 4.11. The Grashof number is defined as the proportion of buoyant to viscous force exerted on a fluid at the boundary layer velocity. From the graphs it is seen rise in Gr begins to increase in velocity profile and reduction in temperature profile. The system is normal to the wall because increasing buoyant body force reduces the value of chemical concentration inside the boundary layer.

Figs 4.12 - 4.13 show how velocity and concentration profiles are affected by concentration Grashof Number Gc. Increasing the concentration Grashof number causes the

momentum flow separation to expand and the concentration boundary layer to contract, according to the graphs.

Fig. 4.14 explore the influence of R on energy circulation. The increasing value of R enhances the fluid's energy circulation. As a result of the increased value of R, the heat energy emitted from the fluid and the energy distribution improved.

Fig. 4.15 depicts the effect of Prandtl Number Pr on energy circulation. The Prandtl Number can be described as a kinematic to thermal diffusivity ratio. The Prandtl number's steady increase enhances fluid density while reducing temperature and improving energy distribution. When the Prandtl number is higher, the diffusion of heat away from the warmed surface is slower than when the Prandtl number is lower.

Fig. 4.16 demonstrates the association between Q_T and temperature profile of the fluid. When compared to the heat source, the flow is independent of external heat. It is investigated that temperature decreases by improving the heat source Q_T .

Fig. 4.17 investigates the impact of Eckert number Ec on temperature profile of the fluid. Eckert number is defined as a ratio of fluid atom kinetic energy to thermal energy. The thermal boundary layers grow as Ec rises. This arises because of the flow's increased thermal conductivity.

Fig. 4.18 investigates the impact of Schmidt number Sc on concentration profile of the fluid. The Schmidt number is defined as the kinematic viscosity to the molecular diffusion coefficient. Increase the intensity of Schmidt number, the mass transfer improves and therefore we examined reduction impact in the concentration profiles.

Fig. 4.19 investigates the impact of chemical reaction parameter γ on concentration profile of the fluid. Increase the intensity of Chemical reaction parameter, the mass transfer improves and therefore we examined reduction impact in the concentration profiles.

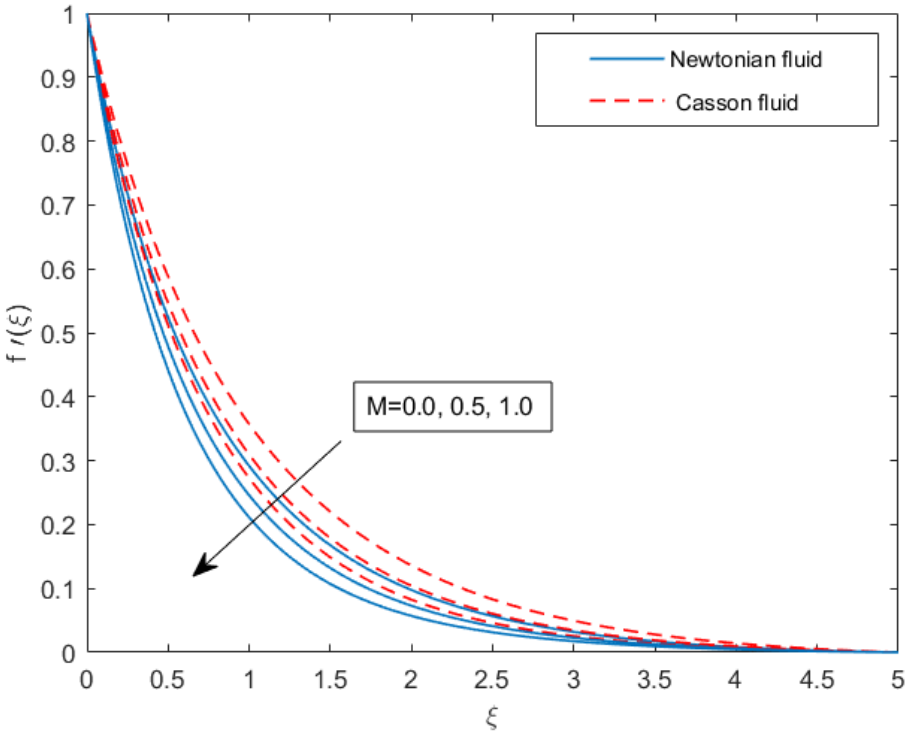

Fig. 4.2: Influence of M on $f'(\xi)$.

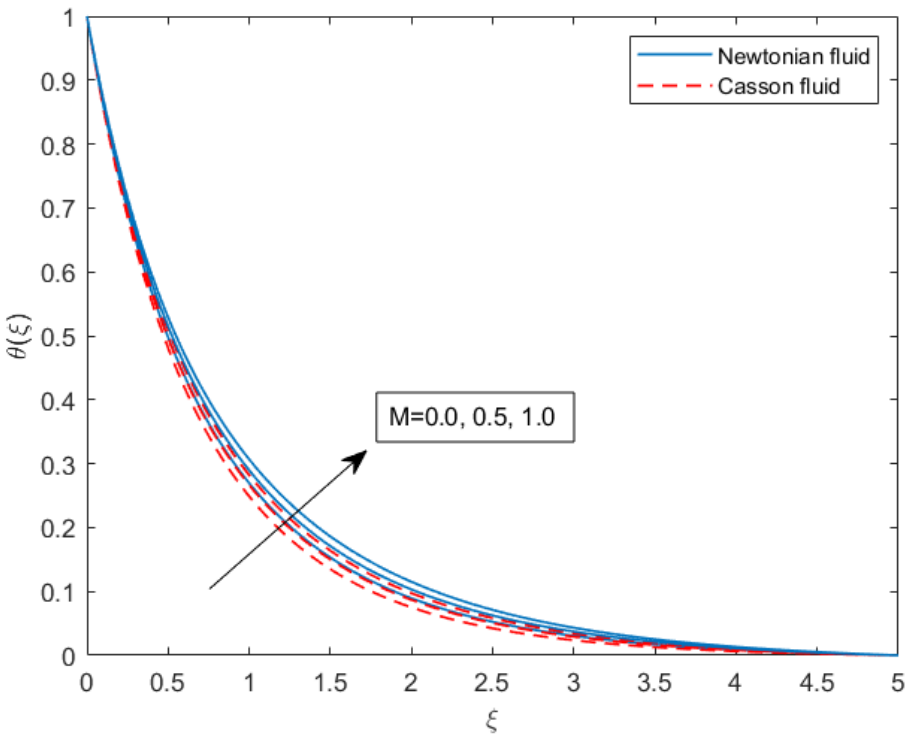

Fig. 4.3: Influence of M on $\theta(\xi)$.

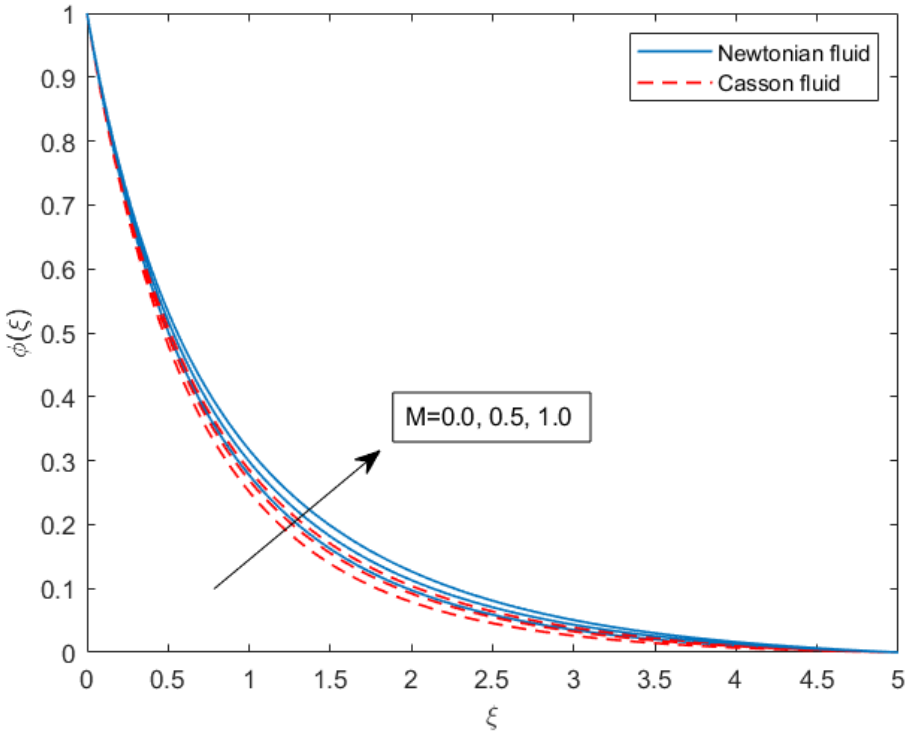

Fig. 4.4: Influence of M on $\phi(\xi)$.

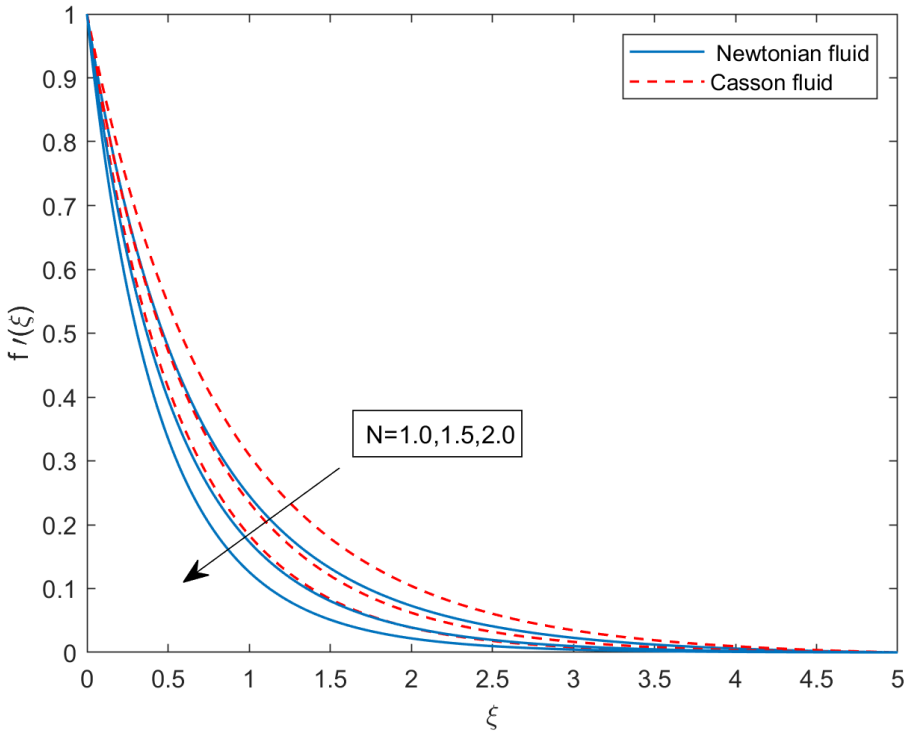

Fig. 4.5: Influence of N on $f'(\xi)$.

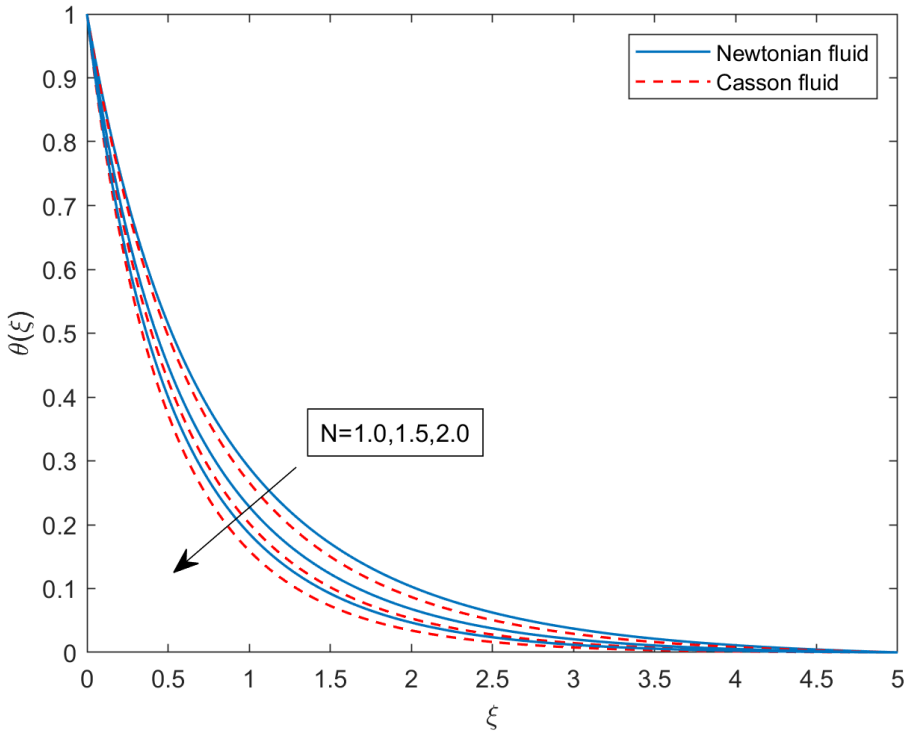

Fig. 4.6: Influence of N on $\theta(\xi)$.

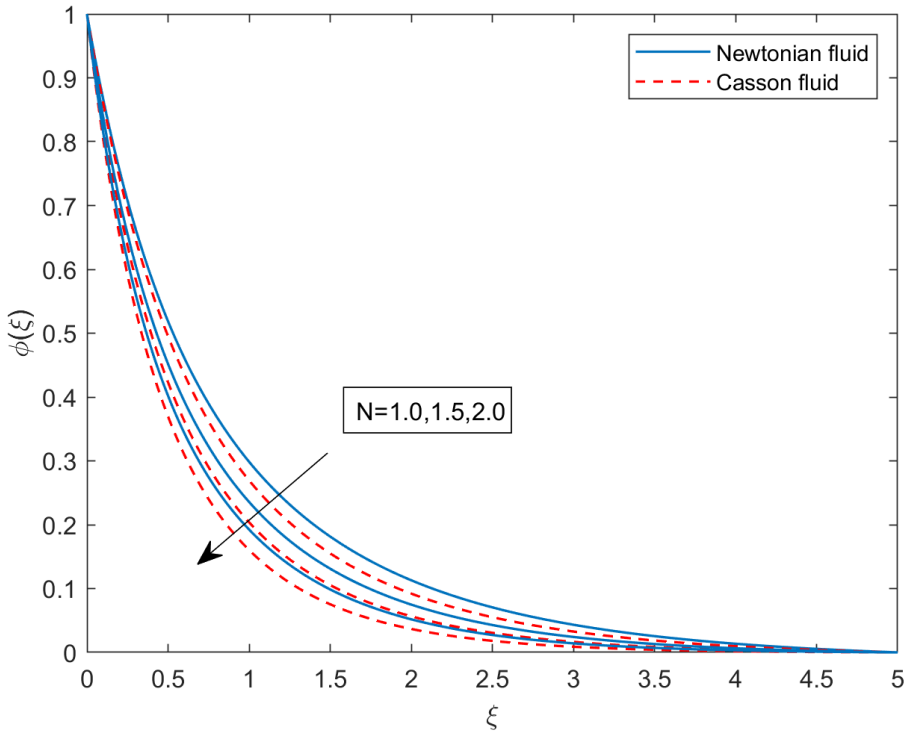

Fig. 4.7: Influence of N on $\phi(\xi)$.

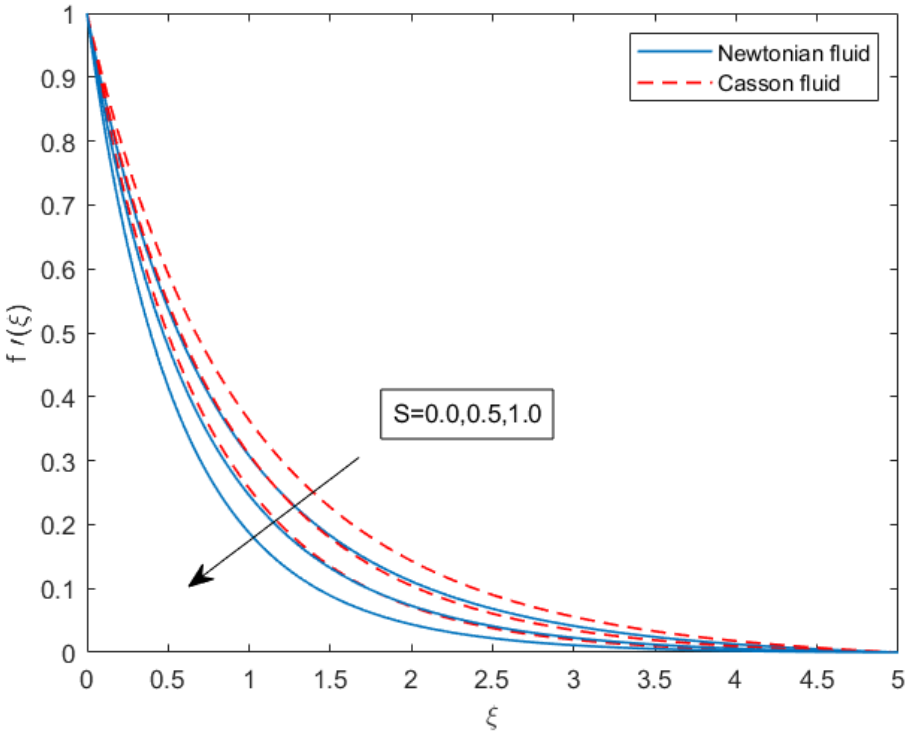

Fig. 4.8: Influence of S on $f'(\xi)$.

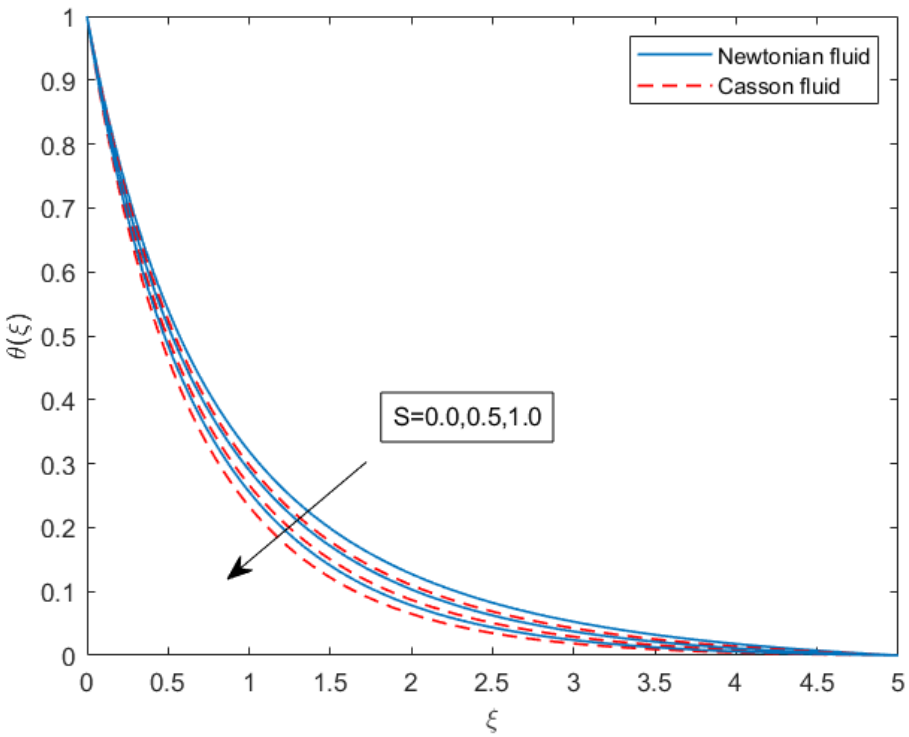

Fig. 4.9: Influence of S on $\theta(\xi)$.

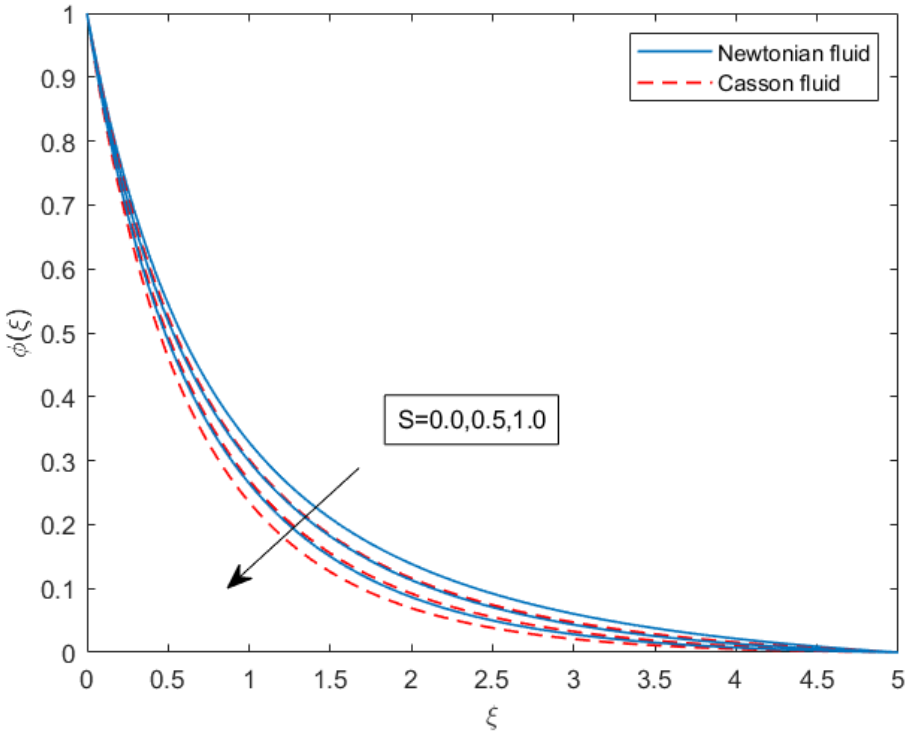

Fig. 4.10: Influence of S on $\phi(\xi)$.

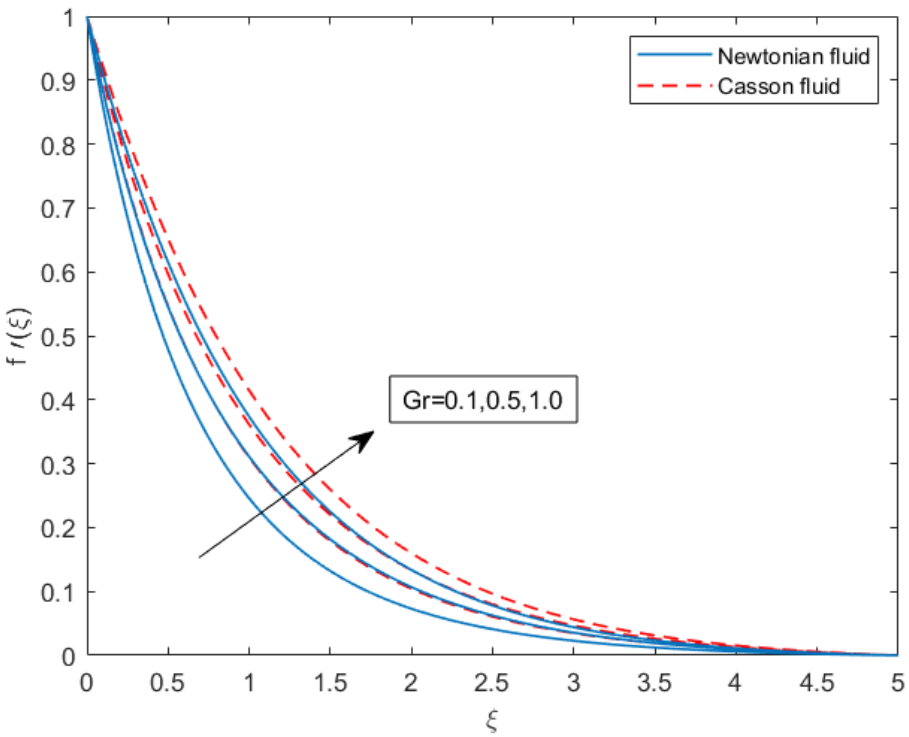

Fig. 4.11: Influence of Gr on $f'(\xi)$.

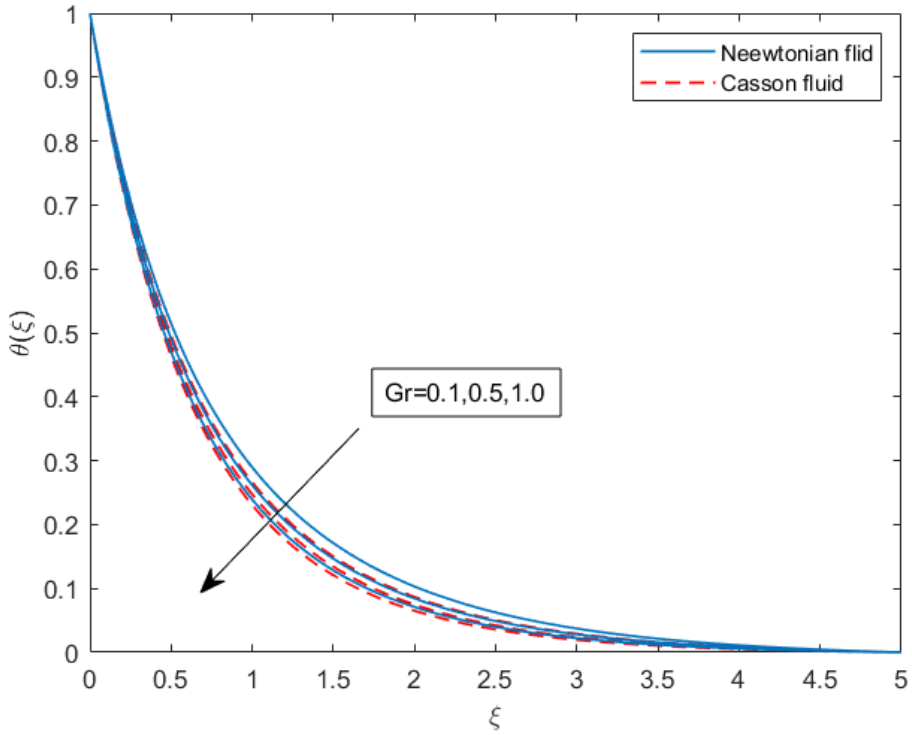

Fig. 4.12: Influence of Gr on $\theta(\xi)$.

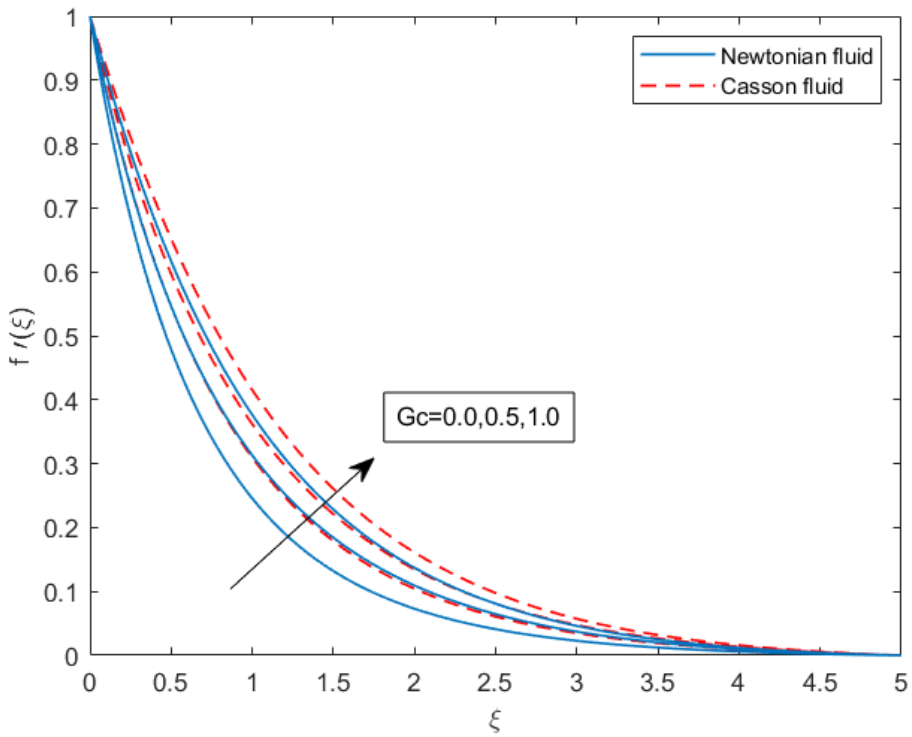

Fig. 4.13: Influence of Gc on $f'(\xi)$.

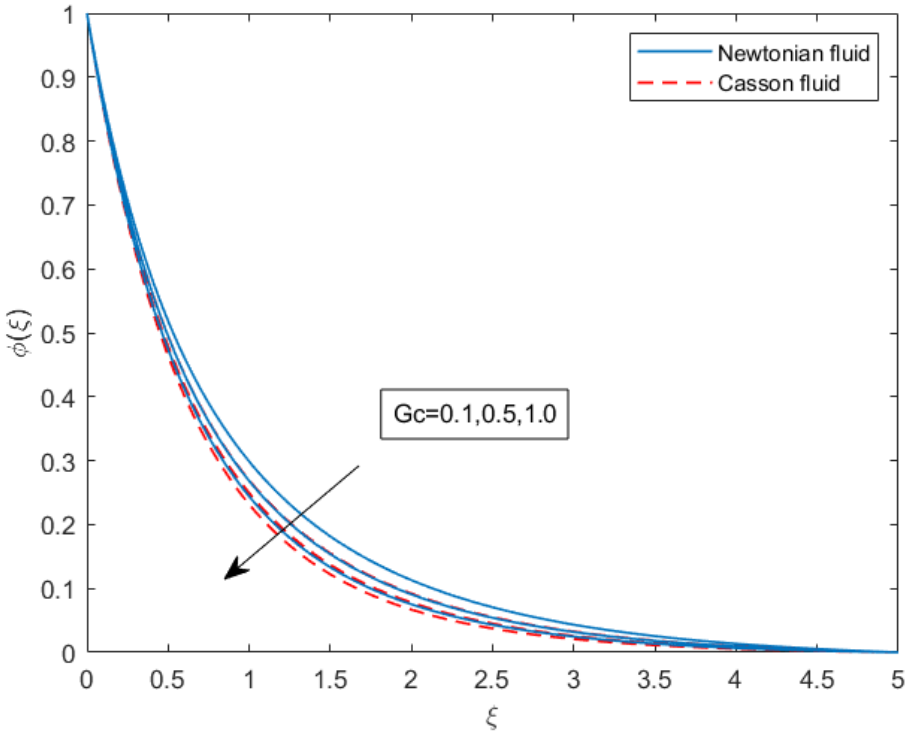

Fig. 4.14: Influence of Gc on $\phi(\xi)$.

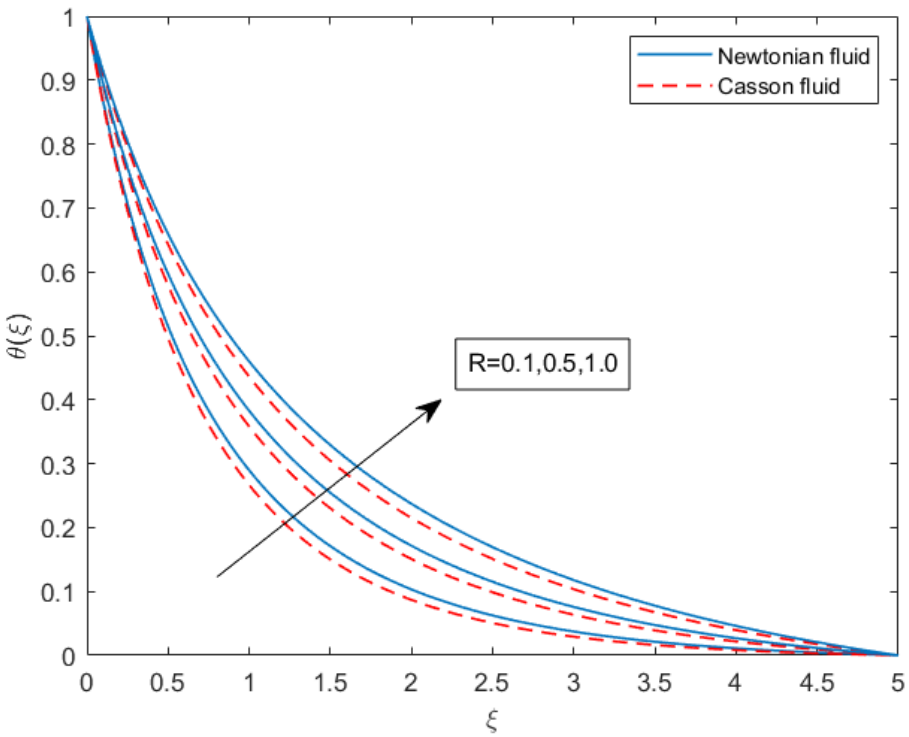

Fig. 4.15: Influence of R on $\theta(\xi)$.

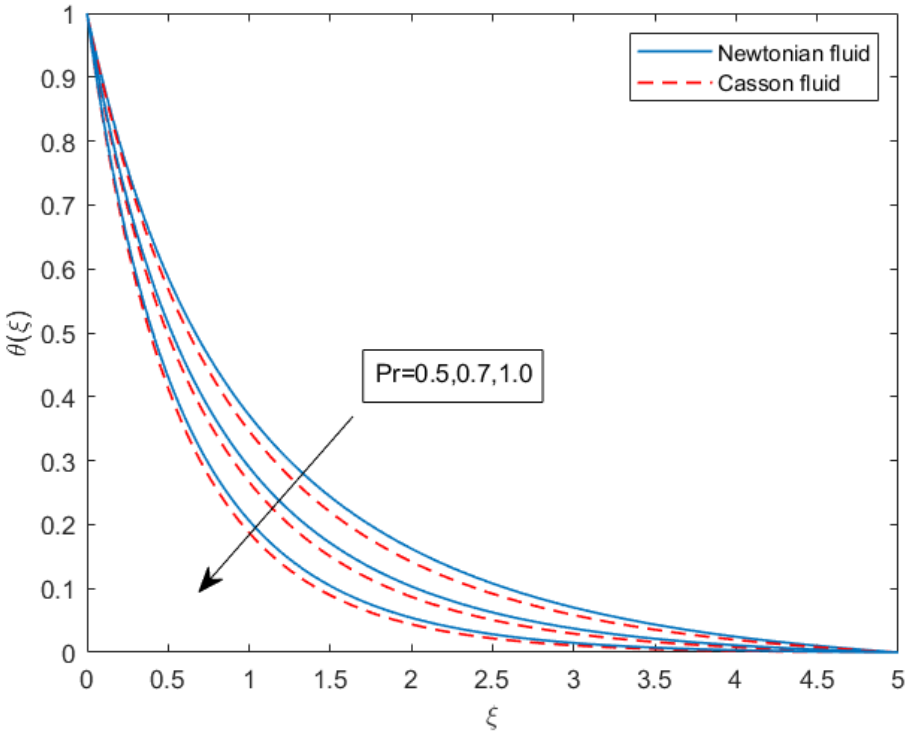

Fig. 4.16: Influence of Pr on $\theta(\xi)$.

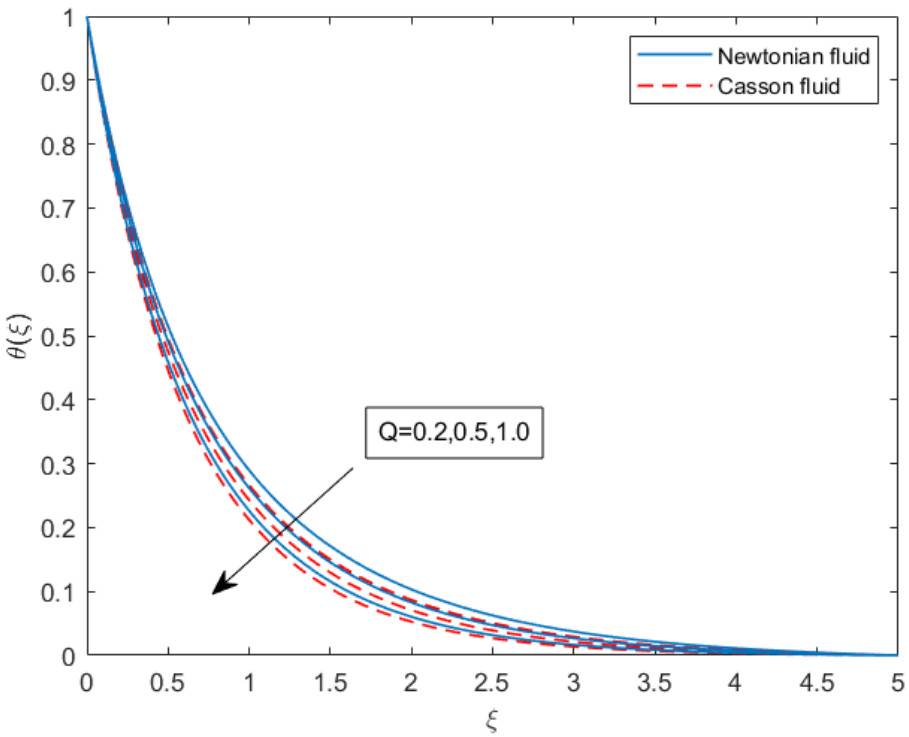

Fig. 4.17: Influence of Q_T on $\theta(\xi)$.

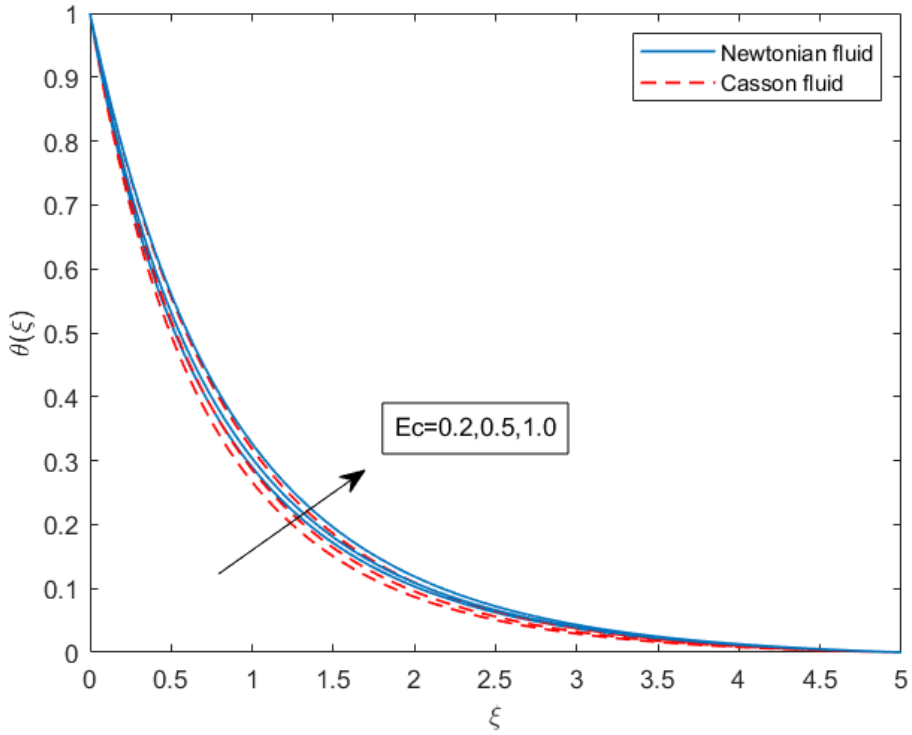

Fig. 4.18: Influence of Ec on $\theta(\xi)$.

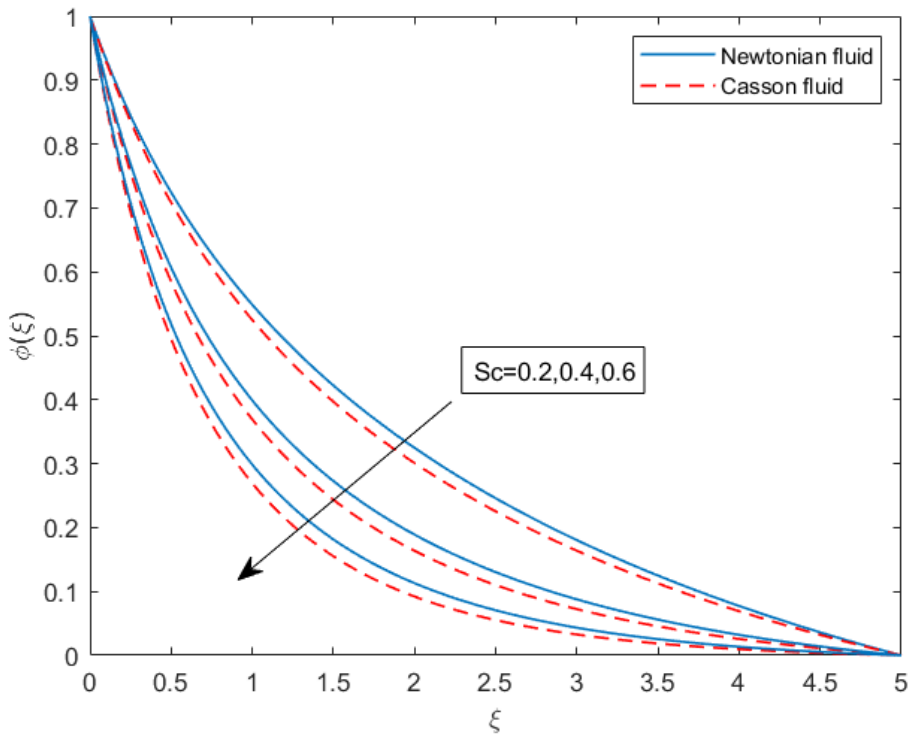

Fig. 4.19: Influence of Sc on $\phi(\xi)$.

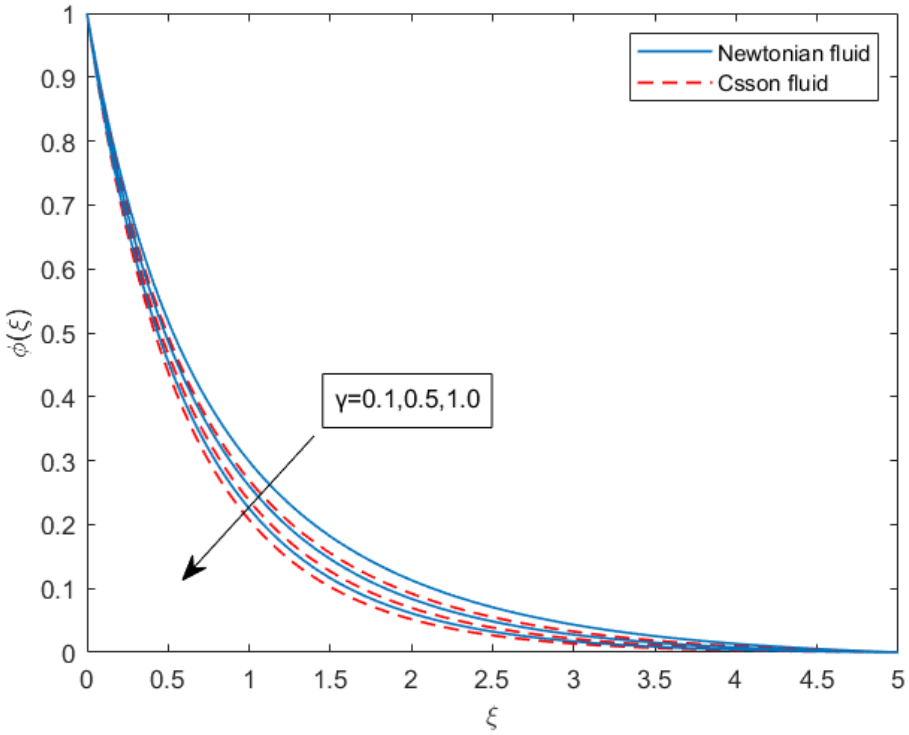

Fig. 4.20: Influence of γ on $\phi(\xi)$.

4.6 Conclusions

The study examined the dissipative and radiative properties of a MHD flow of a Casson fluid on a stretching surface, considering various parameters. Key conclusions of our study are presented below.

- The Casson fluid transfers heat more efficiently than the Newtonian fluid.
- With increasing magnetic parameter values, the thin boundary layer improves.
- We noted an acceleration in the warmness switch rate as the exponential value was increased.
- The mass and heat increase with Gr and Gc.
- Furthermore, when chemical reaction parameter increases, concentration profiles decrease.

CHAPTER 5

INFLUENCE OF THERMALLY RADIATIVE STAGNATION POINT FLOW OF CASSON NANOFLUID WITH MAGNETIC FIELD

5.1 Introduction

In this chapter, the flow model developed by (S. M. Ibrahim, 2020) has been expanded to include the additional effects of inclined thermophoresis and Brownian motion, stagnation point, joule heating, space-based heat source and porosity. The MHD stagnation point flow has been studied using both exponential velocity and boundary conditions. In addition, the similarity transformation is used to generate a set of ODEs by changing the nonlinear PDEs of concentration, momentum, and temperature. We will also use the well-known Shooting method to compute the numerical solution of the transformed PDEs to ODEs. In the result and discussion part, the effect of various model parameters on velocity, temperature, concentration, skin friction coefficient, Nusselt and Sherwood number will be thoroughly discussed.

5.2 Problem Formulation

The flow of Casson nanofluid across an explorational permeable sheet in 2D steady incompressible MHD stagnation point has been taken into consideration. The sheet is positioned so that the y-axis is normal to it in the plane where y = 0 and the flow is limited to $y > 0$. Due to two opposing forces, the surface is stretched along the x axis, the origin is fixed in place, and the sheet forms a thin slit. This sheet is subjected to a normal magnetic field $B = B_0 e^{\frac{Nx}{2L}}$. The flow region has no electric field. Because of the low induced magnetic field, the magnetic Reynolds number is low in the flow zone. The sheet temperature T_s is controlled by using a

convection heating process. C_w represents the concentration of nanoparticles. The nanofluid's temperature and concentration are denoted by T_∞ and C_∞ respectively, for $y \to \infty$.

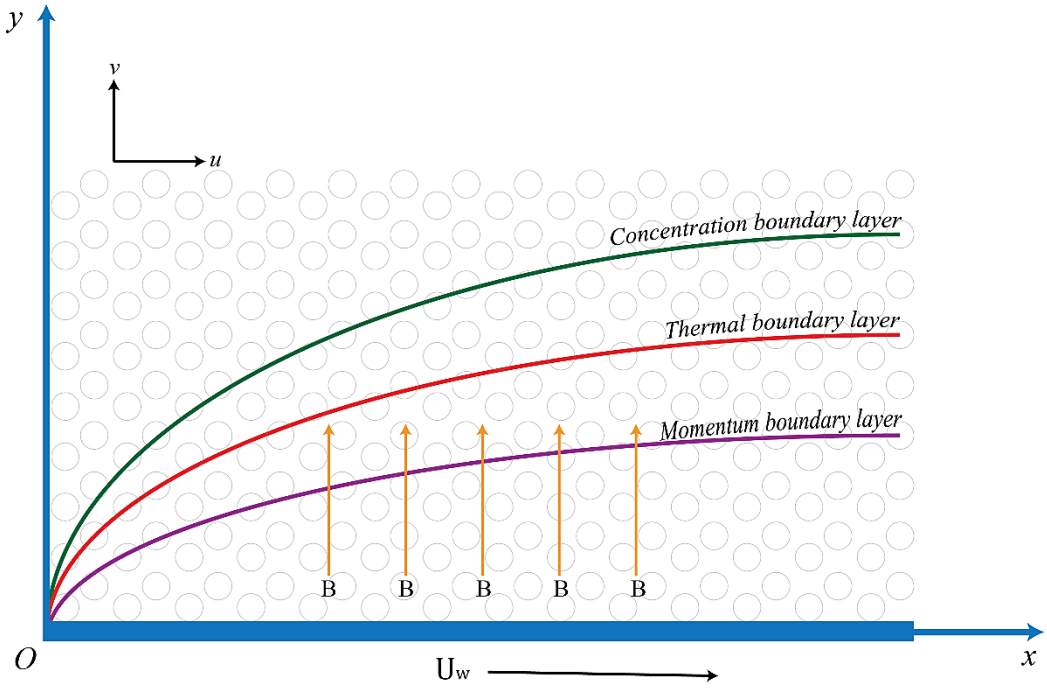

Fig. 5.1: Geometry of physical model.

The governing equation of flow as follows

$$\frac{\partial u}{\partial x}+\frac{\partial v}{\partial y}=0, \tag{5.1}$$

$$u\frac{\partial u}{\partial x}+v\frac{\partial u}{\partial y}=\begin{pmatrix}\nu\left(1+\frac{1}{\beta}\right)\frac{\partial^2 u}{\partial y^2}+U_\infty\frac{\partial U_\infty}{\partial x}+\frac{\sigma B^2(U_\infty-u)}{\rho}+\frac{\nu(U_\infty-u)}{K_p}\\ +g(\lambda_1(T-T_\infty)+\lambda_2(T-T_\infty)^2)\\ +g(\lambda_3(C-C_\infty)+\lambda_3(C-C_\infty)^2)\end{pmatrix}, \tag{5.2}$$

$$u\frac{\partial T}{\partial x}+v\frac{\partial T}{\partial y}=\begin{pmatrix}\frac{k}{\rho C_p}\frac{\partial^2 T}{\partial y^2}+\frac{\nu}{C_p}\left(1+\frac{1}{\beta}\right)\left(\frac{\partial u}{\partial y}\right)^2-\frac{1}{\rho C_p}\frac{\partial q_r}{\partial y}+\frac{1}{\rho C_p}Q_t(T-T_\infty)\\ +\frac{Q_e(T_w-T_\infty)}{\rho C_p}e^{\left(-y\sqrt{\frac{aU_0}{2\nu l}}e^{\frac{Nx}{2l}}\right)}+\tau\left(D_B\frac{\partial c}{\partial y}\frac{\partial T}{\partial y}+\frac{D_T}{T_\infty}\left(\frac{\partial T}{\partial y}\right)^2\right)\\ +\frac{\sigma B^2(U_\infty-u)^2}{\rho C_p}\end{pmatrix}, \tag{5.3}$$

$$u\frac{\partial c}{\partial x}+v\frac{\partial c}{\partial y}=D_B\frac{\partial^2 c}{\partial y^2}+\frac{D_T}{T_\infty}\frac{\partial^2 T}{\partial y^2}-k_1(C-C_\infty)^m, \tag{5.4}$$

with boundary conditions

$$\left.\begin{matrix} u = U_w = aU_0 e^{\frac{Nx}{l}},\ v = v_w = -V(x),\ T = T_w = T_\infty + T_0 e^{\left(\frac{Nx}{L}\right)}, \\ C = C_w = C_\infty + C_0 e^{\left(\frac{Nx}{L}\right)}, \end{matrix}\right), at\ y = 0, \quad (5.5)$$

$$u \to U_\infty = bU_0 e^{\frac{Nx}{l}},\ T \to T_\infty,\ C = C_\infty,\ \ at\ y \to \infty. \quad (5.6)$$

In the previous equations, ν kinematic viscosity, β represents the Casson fluid parameter, T represents Casson fluid nanofluid temperature and T_w represent plate temperature, σ shows the electrical conductivity, U_∞ represents free stream velocity, K_p represents porosity, ρ for fluid density, D_B represents Brownian diffusion coefficient, D_T thermophoresis diffusion coefficient, Q_t shows thermal heat generation, Q_e shows space based exponential heat generation.

Similarity transformations to be taken into account are following

$$\left.\begin{matrix} u=aU_0 e^{\frac{Nx}{l}} f'(\xi), & v=-\sqrt{\frac{aU_0\nu}{2l}} e^{\frac{Nx}{2l}} N[f(\xi)+\xi f'(\xi)], & \xi=y\sqrt{\frac{aU_0}{2\nu l}} e^{\frac{Nx}{2l}}, \\ \psi=\sqrt{2aU_0\nu l}\, e^{\frac{Nx}{2l}} f(\xi), & T=T_\infty+T_0 e^{\frac{2Nx}{l}}\theta(\xi), & C=C_\infty+C_0 e^{\frac{2Nx}{l}}\phi(\xi). \end{matrix}\right\} \quad (5.7)$$

The study used similarity variables ξ, stream function ψ, dimensionless stream function $f(\xi)$, dimensionless temperature of the fluid in the boundary layer region $\theta(\xi)$, and dimensionless concentration of the fluid in the boundary layer region $\phi(\xi)$ to analyze the flow.

Equation (5.1) is satisfied identically.

Equation (5.2) in dimensionless form is

$$\left(1+\frac{1}{\beta}\right) f''' + N\left(ff'' - 2f'^2\right) + \lambda\theta(1+\beta_1\theta) + N^*\lambda\phi(1+\beta_2\phi)$$
$$+M(A-f') + k_p^*(A-f') + 2A^2 = 0. \quad (5.8)$$

Dimensionless form of (5.3) is

$$\left(1+\frac{4}{3}R\right)\theta'' + PrN(\theta' f - 4f'\theta) + \left(1+\frac{1}{\beta}\right) PrEcf''^2 - Pr\,Q\,\theta$$
$$+Pr(N_b\theta'\phi' + N_t(\phi')^2) + PrEcM\left(A - f'(\xi)\right)^2 + PrQ_E e^{(-\xi)} = 0. \quad (5.9)$$

Dimensionless form of equation (5.4) is given as

$$\phi'' + ScN(\phi' f' - 4f'\phi) - Sck_c\,\phi^m + \frac{N_t}{N_b}\theta'' = 0. \quad (5.10)$$

The set of ordinary differential equations (5.8), (5.9) and (5.10) is given below:

$$\left.\begin{array}{c}\left(\left(1+\frac{1}{\beta}\right)f^{'''}+N\left(ff^{''}-2f^{'2}\right)+\lambda\theta(1+\beta_1\theta)+N^{*}\lambda\phi(1+\beta_2\phi)\right)\\ +M\left(A-f^{'}\right)+k_p^{*}\left(A-f^{'}\right)+2A^2=0.\\ \left(\left(1+\frac{4}{3}R\right)\theta^{''}+PrN\left(\theta^{'}f-4f^{'}\theta\right)+\left(1+\frac{1}{\beta}\right)PrEcf^{''2}+Pr\,Q_E e^{(-\xi)}\right)\\ +Pr\,Q_T\,\theta+Pr\left(N_b\theta^{'}\phi^{'}+N_t\left(\phi^{'}\right)^2\right)+PrEcM\left(A-f^{'}(\xi)\right)^2=0.\\ \left(\phi^{''}+ScN\left(\phi^{'}f^{'}-4f^{'}\phi\right)-Sck_c\,\phi^{m}+\frac{N_t}{N_b}\theta^{''}=0.\right)\end{array}\right\} \quad (5.11)$$

the boundary condition are

$$\left.\begin{array}{ll}f=\mathrm{S},f^{'}=1,\theta=1,\phi=1, & \text{at } \xi=0,\\ f^{'}=A,\theta=0,\phi=0, & \text{as } \xi\to\infty.\end{array}\right\} \quad (5.12)$$

In the above equations, β denotes the Casson parameter, N represent the exponential parameter, A for stagnation point, λ for mixed convection variable, N^{*} for buoyancy force ratio, $\beta_1$for nonlinear temperature variable, β_2 for nonlinear convection variable, k_p^{*} for porosity parameter, R for Radiation parameter, M for magnetic parameter, Prandtl number represent with Pr, N_b is equal to Brownian motion parameter, N_t is equal to thermophoresis parameter Ec for Eckert number, Thermal Heat generation parameter denoted with Q_T, Space based heat exponential parameter represent with Q_E, Schmidt number denoted with Sc, m for order of chemical raction, k_c is chemical reaction act on the model and S is denoted by suction and injection parameter.

Value of these parameters are given below

$Pr=\frac{\rho C_p\nu}{k}$, $\mathrm{Gr}=\frac{2lg\lambda_1T_0e^{\frac{2Nx}{l}}}{\nu^2}$, $\mathrm{Gc}=\frac{2lg\lambda_3c_0e^{\frac{2Nx}{l}}}{\nu^2}$, $\mathrm{Sc}=\frac{\nu}{D_B}$, $Ec=\frac{a^2U_0^2}{C_pT_0}$,

$N^{*}=\frac{\lambda_3C_0}{\lambda_1T_0}$, $\beta_1=\frac{\lambda_2}{\lambda_1}(T_w-T_\infty)$, $\beta_2=\frac{\lambda_4}{\lambda_3}(C_w-C_\infty)$, $Re_x=\frac{U_wx}{\nu}$, $A=\frac{b}{a}$,

$M=\frac{2L\sigma B_0^2}{\rho aU_0}$, $Q_T=\frac{2Q_tL}{\rho C_pU_w}$, $\mathrm{R}=\frac{4\sigma^{*}}{kk^{*}}T_\infty^3$, $\mathrm{S}=\frac{v_0}{\sqrt{\frac{\nu U_0}{2L}}}$, $k_c=\frac{2k_1L(C_w-C_\infty)^m}{U_w}$, $Q_E=\frac{2lQ_e}{\rho C_pU_w}$

$k_p^{*}=\frac{2l\nu}{k_pU_0e^{\frac{Nx}{l}}}$, $N_b=\frac{\tau D_B(C_w+C_\infty)}{\nu}$, $N_t=\tau\frac{D_T(T_w-T_\infty)}{T_\infty\nu}$, $\lambda=\frac{G_r}{{Re_x}^2}$.

5.3 Physical Quantity

Mathematical form of skin friction coefficient is

$$c_f = \left(\frac{\tau_w}{\rho U_w^2}\right). \tag{5.13}$$

Local Nusselt coefficients mathematically can be given as

$$Nu_x = \left(\frac{x q_w}{k(T_\omega - T_\infty)}\right). \tag{5.14}$$

Mathematical form of local Sherwood number

$$Sh_x = \left(\frac{x q_m}{D_B(C_\omega - C_\infty)}\right), \tag{5.15}$$

where q_w is heat fluxes, q_m is mass fluxes and τ_w represent the shear stress at the surface. These are defined as

$$\tau_w = \mu_B \left(1 + \frac{1}{\beta}\right)\left(\frac{\partial u}{\partial y}\right)_{y=0},\ q_w = \left(-\left(k + \frac{16\sigma^* T_\alpha^3}{3k^*}\right)\left(\frac{\partial T}{\partial y}\right)\right)_{y=0},$$

$$q_m = -D_B \left(\frac{\partial C}{\partial y}\right)_{y=0}. \tag{5.16}$$

The dimensionless quantities obtained are

$$\sqrt{Re_x} c_f = \left(1 + \frac{1}{\beta}\right) f''(0), \quad (Re_x)^{\frac{-1}{2}} Nu_x = \left(-\left(1 + \frac{4R}{3}\right)\theta'(0)\right),$$

$$(Re_x)^{\frac{-1}{2}} Sh_x = \left(-\phi'(0)\right),$$

where Re_x is Reynold number.

5.4 Solution Methodology

The system of nonlinear ordinary differential equation (5.11) and suitable boundary condition (5.12) are converted into first order ODEs. Shooting method are using to solve first order ODEs with proper boundary conditions. We implement the following procedures:

$$f''' = \frac{-1}{\left(1+\frac{1}{\beta}\right)}\begin{pmatrix} N\left(ff'' - 2f'^2\right) + \lambda\theta(1 + \beta_1\theta) + N^*\lambda\phi(1 + \beta_2\phi) \\ +M(A - f') + k_p^*(A - f') + 2A^2 \end{pmatrix}, \tag{5.17}$$

$$\theta'' = \frac{-1}{\left(1+\frac{4}{3}R\right)}\begin{pmatrix} PrN(\theta' f - 4f'\theta) + \left(1+\frac{1}{\beta}\right)PrEcf''^2 \\ +Pr\,Q_T\,\theta + Pr(N_b\theta'\phi' + N_t(\phi')^2) \\ +PrEcM\left(A - f'(\xi)\right)^2 + Pr\,Q_E e^{(-\xi)} \end{pmatrix}, \tag{5.18}$$

$$\phi'' = Sck_c\,\phi^m - ScN(\phi' f' - 4f'\phi) - \frac{N_t}{N_b}\theta''. \tag{5.19}$$

Since equations (5.17), (5.18) and (5.19) are functions of f , θ and ϕ and their derivatives, the solution of equation (5.17) can be utilized to recognize results in equations (5.18) and (5.19). We are aware of initial conditions given at $\xi = 0$ in the above ODEs, Equations (5.17), (5.18) and (5.19) give the unknown conditions which is represented by W, P and Z respectivly. We have established the symbols for further explanation.

$$y_1 = f, y_2 = y_1' = f', y_3 = y_2' = f'', y_4 = \theta, y_5 = \theta', y_6 = \phi, y_7 = \phi'.$$

The system of ODEs (5.18), (5.19) and (5.20) as well as corresponding initial condition are as follows:

$$\begin{aligned}
&y_1 = f, && \\
&y_2 = y_1' = f', && y_1(0) = S, \\
&y_3 = y_2' = f'', && y_2(0) = 1, \\
&y_3' = f''' = \frac{1}{\left(1+\frac{1}{\beta}\right)}\begin{pmatrix} M(y_2 - A) + k_p^*(y_2 - A) - 2A^2 - \lambda\, y_4(1+\beta_1 y_4) \\ -N^*\lambda\, y_6(1+\beta_2 y_6) - N(y_1 y_3 - 2{y_2}^2) \end{pmatrix}, && \\
& && y_3(0) = W, \\
&y_4 = \theta, && \\
&y_5 = \theta', && y_4(0) = 1, \\
&y_5' = \theta'' = \frac{-1}{\left(1+\frac{4}{3}R\right)}\begin{pmatrix} \Pr Q_T\, y_4 + PrN(y_1 y_5 - 4y_2 y_4) + \left(1+\frac{1}{\beta}\right)PrEc{y_3}^2 \\ +PrQ_E e^{(-\xi)} + PrEcM(A - y_2)^2 + Pr(N_b y_5 y_7 + N_t {y_7}^2) \end{pmatrix}, && \\
& && y_5(0) = P, \\
&y_6 = \phi, && \\
&y_7 = \phi', && y_6(0) = 1, \\
&y_7' = \phi'' = \left(ScKc{y_6}^m - ScN(y_1 y_7 - 4y_2 y_6) - \frac{N_t}{N_b}y_5'\right), && y_7(0) = Z.
\end{aligned}$$

The RK-4 technique has been used to solve the IVP consisting of the above ODEs for some appropriate substitutes of W, P and Z. The missing condition of velocity profile, temperature profile and concentration profile can be taken at $W = W^{(0)}$, $P = P^{(0)}$ and $Z = Z^{(0)}$ respectively and the Newton technique may be used to discover the roots.

Domain for approximate numerical results $[0, \xi_\infty]$. where ξ_∞ is chosen in such a way that no discernible modifications are obtained by advancing beyond. The following are the shooting method's stopping conditions:

$$\max\{|y_2 - A|, |y_4 - 0|, |y_6 - 0|\} < \varepsilon, \tag{5.20}$$

where ε is a small positive real number. where $\varepsilon = 10^{-8}$ is the number used in the numerical computation.

5.5 Result and Discussion

In this segment use of graphs and tables to discuss the numerical conclusions of the equations from the preceding sections. The numerical results are obtained by altering many essential parameters such as exponential parameter N, buoyancy force ratio N^*, β_1 nonlinear temperature variable, β_2 nonlinear convection variable, stagnation parameter A, porosity parameter k_p^*, radiation parameter R, magnetic parameter M, Prandtl number Pr, Eckert number Ec, thermal Heat generation parameter Q_T, space-based exponential heat parameter Q_E, Brownian motion parameter N_b,thermophoresis parameter N_t, Schmidt number Sc, chemical reaction Kc,m order of chemical reaction, Suction and Injection parameter S, Sherwood and Nusselt numbers, as well as the skin friction coefficient. Temperature, concentration and velocity profiles are all affected by these physical characteristics.

Table 5.1: Variation in $-Re_x^{\frac{1}{2}}C_f$, $Re_x^{\frac{-1}{2}}Nu_x$ and $Re_x^{\frac{-1}{2}}Sh_x$ for Newtonian fluid with $S = 0.5, \beta_1 = 0.1, \beta_2 = 0.1, Kc = 0.1, Pr = 0.7, R = 0.1, Q_T = 0.2, Q_E = 0.2, Ec = 0.2, Nb = 1.0, Nt = 1.0, Sc = 0.6, m = 2.$

M	N	A	Kp	λ	N^*	$-Re_x^{\frac{1}{2}}C_f$	$Re_x^{\frac{-1}{2}}Nu_x$	$Re_x^{\frac{-1}{2}}Sh_x$
1.0	1.0	0.1	0.5	0.5	0.1	1.66564608	1.07872527	0.93059855
2.0	1.0	0.1	0.5	0.5	0.1	1.90875542	1.01167559	0.92018953
3.0	1.0	0.1	0.5	0.5	0.1	2.12462982	0.95302841	0.91608539
1.0	2.0	0.1	0.5	0.5	0.1	2.40091331	1.64352878	1.27370957
1.0	3.0	0.1	0.5	0.5	0.1	3.05272328	2.08397469	1.54877173
1.0	1.0	0.2	0.5	0.5	0.1	1.53165058	1.12833212	0.98672424
1.0	1.0	0.3	0.5	0.5	0.1	1.37639717	1.17497537	1.03575974
1.0	1.0	0.1	1.0	0.5	0.1	1.79159182	1.05450143	0.91617348
1.0	1.0	0.1	1.5	0.5	0.1	1.90941404	1.03186910	0.90426872
1.0	1.0	0.1	0.5	1.0	0.1	1.44427662	1.12611214	0.96900473
1.0	1.0	0.1	0.5	1.5	0.1	1.23477938	1.16410599	1.00097025
1.0	1.0	0.1	0.5	0.5	1.5	1.64455506	1.08292012	0.93334738
1.0	1.0	0.1	0.5	0.5	3.0	1.62208173	1.08732241	0.93624972

Table 5.2: Variation in $-\mathrm{Re}_x^{\frac{1}{2}}\mathrm{C_f}$, $\mathrm{Re}_x^{\frac{-1}{2}}\mathrm{Nu_x}$ and $\mathrm{Re}_x^{\frac{-1}{2}}\mathrm{Sh_x}$ for Casson fluid with $S = 0.5, \beta_1 = 0.1, \beta_2 = 0.1, Kc = 0.1, Pr = 0.7, R = 0.1, Q_T = 0.2, Q_E = 0.2, Ec = 0.2, Nb = 1.0, Nt = 1.0, Sc = 0.6, m = 2.$

M	N	A	Kp	λ	N^*	$-Re_x^{\frac{1}{2}}C_f$	$Re_x^{\frac{-1}{2}}Nu_x$	$Re_x^{\frac{-1}{2}}Sh_x$
1.0	1.0	0.1	0.5	0.5	0.1	2.01993124	1.10836292	0.98577682
2.0	1.0	0.1	0.5	0.5	0.1	2.31192891	1.04156179	0.97796808
3.0	1.0	0.1	0.5	0.5	0.1	2.57212733	0.98205232	0.97582509
1.0	2.0	0.1	0.5	0.5	0.1	2.85693628	1.69563672	1.37057386
1.0	3.0	0.1	0.5	0.5	0.1	3.58504627	2.15656259	1.68149293
1.0	1.0	0.2	0.5	0.5	0.1	1.85821478	1.15277191	1.03162474
1.0	1.0	0.3	0.5	0.5	0.1	1.67146801	1.19517972	1.07183121
1.0	1.0	0.1	1.0	0.5	0.1	2.17116542	1.08576081	0.97199746
1.0	1.0	0.1	1.5	0.5	0.1	2.31291451	1.06441947	0.96046118
1.0	1.0	0.1	0.5	1.0	0.1	1.77790597	1.14584033	1.01441317
1.0	1.0	0.1	0.5	1.5	0.1	1.54707057	1.17701878	1.03894085
1.0	1.0	0.1	0.5	0.5	1.5	1.99764978	1.11152496	0.98773001
1.0	1.0	0.1	0.5	0.5	3.0	1.97388287	1.11485759	0.98979770

Table 5.3: Variation in $-\mathrm{Re}_x^{\frac{1}{2}}\mathrm{C_f}$, $\mathrm{Re}_x^{\frac{-1}{2}}\mathrm{Nu_x}$ and $\mathrm{Re}_x^{\frac{-1}{2}}\mathrm{Sh_x}$ for Newtonian fluid with $M = 1.0, N, = 1.0, Kp = 0.5, \lambda = 0.5, S = 0.5, \beta_1 = 0.1, \beta_2 = 0.1, A = 0.1, Kc = 0.1, Q_T = 0.2, Q_E, Sc = 0.6, m = 2, N^* = 0.1.$

Pr	R	Ec	Nb	Nt	$-Re_x^{\frac{1}{2}}C_f$	$Re_x^{\frac{-1}{2}}Nu_x$	$Re_x^{\frac{-1}{2}}Sh_x$
1.0	0.1	0.2	1.0	1.0	1.79999179	1.67815878	0.08841609
1.3	0.1	0.2	1.0	1.0	1.82953957	1.86483452	-0.07540770
0.7	0.2	0.2	1.0	1.0	1.6609628	1.14916972	0.9662006
0.7	0.3	0.2	1.0	1.0	1.65672069	1.21503639	0.99744944
0.7	0.1	1.0	1.0	1.0	1.65250162	0.72449670	1.20854555
0.7	0.1	1.8	1.0	1.0	1.63941351	0.37604157	1.48141511
0.7	0.1	0.2	0.5	1.0	1.66655062	1.19881900	0.21946354
0.7	0.1	0.2	0.7	1.0	1.66706982	1.14877880	0.62675707
0.7	0.1	0.2	1.0	0.5	1.67253005	1.13401919	1.17775945
0.7	0.1	0.2	1.0	0.7	1.66972257	1.11121000	1.07458357

Table 5.4: Variation in $-\mathrm{Re}_x^{\frac{1}{2}}\mathrm{C_f}$, $\mathrm{Re}_x^{\frac{-1}{2}}\mathrm{Nu_x}$ and $\mathrm{Re}_x^{\frac{-1}{2}}\mathrm{Sh_x}$ for Casson fluid with $M = 1.0, N, = 1.0, Kp = 0.5, \lambda = 0.5, S = 0.5, \beta_1 = 0.1, \beta_2 = 0.1, A = 0.1, Kc = 0.1, Q_T = 0.2, Q_E, Sc = 0.6, m = 2, N^* = 0.1.$

Pr	R	Ec	Nb	Nt	$-Re_x^{\frac{1}{2}}C_f$	$Re_x^{\frac{-1}{2}}Nu_x$	$Re_x^{\frac{-1}{2}}Sh_x$
1.0	0.1	0.2	1.0	1.0	2.20980181	1.67101011	0.25291622
1.3	0.1	0.2	1.0	1.0	2.24976403	1.83872273	0.10995609
0.7	0.2	0.2	1.0	1.0	2.01418898	1.18312225	1.01906597
0.7	0.3	0.2	1.0	1.0	2.00893649	1.25301506	1.04847659
0.7	0.1	1.0	1.0	1.0	1.99980599	0.70680757	1.29044266
0.7	0.1	1.8	1.0	1.0	1.97977285	0.31285692	1.58863593
0.7	0.1	0.2	0.5	1.0	2.02083025	1.23352663	0.27112607
0.7	0.1	0.2	0.7	1.0	2.02152789	1.18145685	0.68068243
0.7	0.1	0.2	1.0	0.5	2.02820977	1.16714430	1.23127333
0.7	0.1	0.2	1.0	0.7	2.02484104	1.14287346	1.12860936

Table 5.5: Variation in $-\mathrm{Re}_x^{\frac{1}{2}}\mathrm{C_f}$, $\mathrm{Re}_x^{\frac{-1}{2}}\mathrm{Nu_x}$ and $\mathrm{Re}_x^{\frac{-1}{2}}\mathrm{Sh_x}$ for Newtonian fluid with $M = 1.0, N = 1.0, Nb = 1.0, Nt = 1.0, Kp = 0.5, \lambda = 0.5, S = 0.5, \beta_1 = 0.1, \beta_2 = 0.1, A = 0.1, N^* = 0.1, R = 0.1, Pr = 0.7, Q_T = 0.2, Ec = 0.2, Q_E = 0.2.$

Sc	Kc	m	$-Re_x^{\frac{1}{2}}C_f$	$Re_x^{\frac{-1}{2}}Nu_x$	$Re_x^{\frac{-1}{2}}Sh_x$
0.4	0.1	2.0	1.66374739	1.13098994	0.49592353
0.8	0.1	2.0	1.66722219	1.04168506	1.29907406
0.6	0.5	2.0	1.66612834	1.06798307	1.03501403
0.6	1.0	2.0	1.66663594	1.05687679	1.15019507
0.6	0.1	1.0	1.66573806	1.07554319	0.94841245
0.6	0.1	3.0	1.66561051	1.07994007	0.92267052

Table 5.6: Variation in $-\mathrm{Re}_x^{\frac{1}{2}}\mathrm{C_f}$, $\mathrm{Re}_x^{\frac{-1}{2}}\mathrm{Nu_x}$ and $\mathrm{Re}_x^{\frac{-1}{2}}\mathrm{Sh_x}$ for Casson fluid with $M = 1.0, N = 1.0, Nb = 1.0, Nt = 1.0, Kp = 0.5, \lambda = 0.5, S = 0.5, \beta_1 = 0.1, \beta_2 = 0.1, A = 0.1, N^* = 0.1, R = 0.1, Pr = 0.7, Q_T = 0.2, Ec = 0.2, Q_E = 0.2.$

Sc	Kc	m	$-Re_x^{\frac{1}{2}}C_f$	$Re_x^{\frac{-1}{2}}Nu_x$	$Re_x^{\frac{-1}{2}}Sh_x$
0.4	0.1	2.0	2.01737447	1.16238991	0.53922109
0.8	0.1	2.0	2.02193582	1.07034325	1.36146917
0.6	0.5	2.0	2.02047417	1.09847114	1.08360553
0.6	1.0	2.0	2.02104936	1.08804463	1.19297172
0.6	0.1	1.0	2.02005708	1.10542779	1.00232271
0.6	0.1	3.0	2.01988911	1.10947697	0.97841084

Tables 5.1 - 5.6 illustrate the impact of various physical parameters such as magnetic field, Stagnation point, porosity, exponential parameter, buoyancy force ratio, Thermophoresis and Brownian motion, radiation, Prandtl number, Eckert number, heat generation, Schmidt number, chemical reaction, suction and injection parameter on the skin friction coefficient, Nusselt number and Sherwood number for Newtonian fluid and Casson fluid respectively. The figs. 5.3 - 5.36 are derived from the values presented in the tables.

Fig. 5.2 demonstrates the connection between M and the dimensionless velocity profile $f'(\xi)$.Typically, when M increases, the Lorentz force increases, which causes molecular collisions to increase force and raise fluid temperature while lowering velocity at boundary layer. The square of magnetic field strength is directly proportional to the magnetic parameter M, while velocity is inversely proportional to M. The effect of temperature increase is examined in fig. 5.3 together with the magnetic parameter M. An opposite force known as the Lorentz force is often brought about by a stronger magnetic parameter. Both the temperature profile and boundary layer viscosity increased because of this force. In contrast to Newtonian fluid, we saw that Casson fluid successfully causes the temperature profiles to rise. The behavior of concentration supply for increasing values of M is shown in figure 5.4. It demonstrates that when M values increase, concentration of fluid supply improves. Figure 5.5 shows impact of starching ratio A for different variations on velocity profile $f'(\xi)$. The impact of stagnation points A on the velocity field $f'(\xi)$ is discovered in figure 5.6 for both Newtonian and Casson fluid. Velocity increases in presence of A. The boundary layer thickness and velocity both rise for small values of A. The fact that the free stream velocity gradually grows and as a result, velocity also increases. The velocity rises, and the boundary layer thickness falls as A gets larger. Figure 5.7 and figure 5.8 show the fluctuation in temperature and concentration caused by A.we observed that both are decreases.

The figs. 5.9 - 5.11 demonstrate the influence of an exponential parameter on the skin friction coefficient, Nusselt number, and Sherwood number for both Newtonian fluid and Casson fluid. As the exponential parameter increases, the boundary layers of velocity, temperature, and concentration of the fluid flow decrease for both types of fluids. As a result, for both fluids, the exponential parameter grows while the velocity, temperature, and concentration drop. Fig. 5.12, In the boundary layer, it is seen that decreasing values of the porosity parameter K_p^* result in slower velocity. This is the consequence of the resistance due to porous medium. Additionally, figure illustrates how boundary layer thickness reduces for larger values of K_p^*.

Figs. 5.13 - 5.15 demonstrate the interaction of the suction parameter S with the temperature and concentration profile. The graphs show that as S's mathematical value is increased, the fluid's velocity, temperature, and concentration profile all decrease. The fluid is closer to the surface because of the suction parameter. In fact, density differential in the flow

zone is exacerbated by greater values of S. The density is highly concentrated in the upper section and sparsely concentrated in the bottom. A drop in fluid velocity is seen because of this change in density, it decreases fluid flow between the top and bottom areas. Fig. 5.16 demonstrate how the mixed convection variable λ affects the profile of velocity. The ratio of a fluid's buoyant to viscous forces at the boundary layer is referred to as the mixed convection variable. The velocity profile shows a gain in λ as it begins to rise, whereas the temperature profile shows a decrease. As the buoyant body force of the system, which acts normally to the wall, increases, the chemical concentration within the boundary layer decreases.

Fig. 5.17 demonstrates how the Buoyancy force ratio N^* affects the profile of velocity. The graph shows that when the Buoyancy force ratio rises, the concentration boundary layer thins but the momentum boundary layer thickens. Fig. 5.18 demonstrates the connection between Pr and temperature profile. Since Pr may be stated as a density to thermal diffusivity ratio, increasing Pr's values indicates that the fluid's density is rising while the thermal diffusivity is falling, which lowers the temperature. Fig. 5.19 examine how R affects the flow of energy. The fluid's energy circulation is boosted by R's gradually growing values. As a result of the greater value of R, the fluid releases more heat energy and the distribution of energy get better.

Fig. 5.20 displays the connection between Q_T and the fluid's temperature profile. Because the flow's heat source is not dependent on external heat. We investigated how the thermal heat source Q_T may be enhanced to lower the temperature. The temperature of the fluid steadily rises because of these actions. The effects of Space-based Heat Generation Q_E parameters on temperature distribution are presented in figure 5.21. Temperature rose as a result of a greater value of Q_E.

Fig. 5.22 examines the effect of Eckert number Ec on the fluid's temperature profile. Eckert number is described as a ratio of thermal energy to the kinetic energy of the fluid atom. The thermal boundary layer enlarges with increasing Ec.The increased thermal conductivity of the flow is what causes this process to happen. The dissipation grows as Ec values rise and as a result, the fluid's internal energy grows as well. The fluid's temperature distribution is also improved by this change in internal energy. Rise in Ec causes the concentration distribution to

widen, since the rising values of Ec leads to an increase in the fluid's thermal energy. The link between Nb and temperature profile is shown in fig. 5.23. As the levels of Nb are steadily increased, the temperature profile falls. The mobility of fluid particles is often greatly increased by the amplification of Nb, it enhances the temperature distribution and increases the kinetic energy of the fluid particle. Impact of Nb on concentration distribution is seen in fig. 5.24. The increased values of Nb leads to a rise in the concentration distribution.

Fig. 5.25 demonstrates the connection between Nt and the fluid's temperature distribution. It is demonstrated that raising the numerical values of Nt causes the temperature profile to rise. Physically, when Nt values rise, the nanoparticles are pulled from hotter to cooler regions, raising the temperature profile of the nanofluid. Impact of Nt on concentration distribution is seen in fig. 5.26. The increased values of Nt lead to a rise in the concentration distribution.

Fig. 5.27 examines how the fluid's concentration profile is affected by the Schmidt number Sc. The Schmidt number is the ratio of the molecular diffusion coefficients and kinematic viscosity. Since mass transfer improves as Schmidt number intensity increases, we looked at the influence of lowering on concentration profiles. Fig. 5.28 demonstrate the effect of k_c on the concentration profile. The graph indicates that increased levels of k_c accelerate the temperature distribution while decreasing the concentration profile. Physically, as k_c increases, the molecular diffusion decreases, lowering the concentration and lowering the thickness of the appropriate boundary layer.

Fig. 5.29 demonstrate the order of chemical Reaction m on the concentration profile. Due to rise in m, concentration profile rises. The fluid's velocity decreases as the numerical value β is increased. This indicates that although increasing values of cause fluid viscosity to increase, decreasing values of cause the velocity profile of the nanofluid to drop. Furthermore, as β approaches infinity, the current phenomena transform into Newtonian fluid. Increasing the value of β gradually increases the temperature distribution of the fluid. The volume fraction of nanoparticles increases as β is increased.

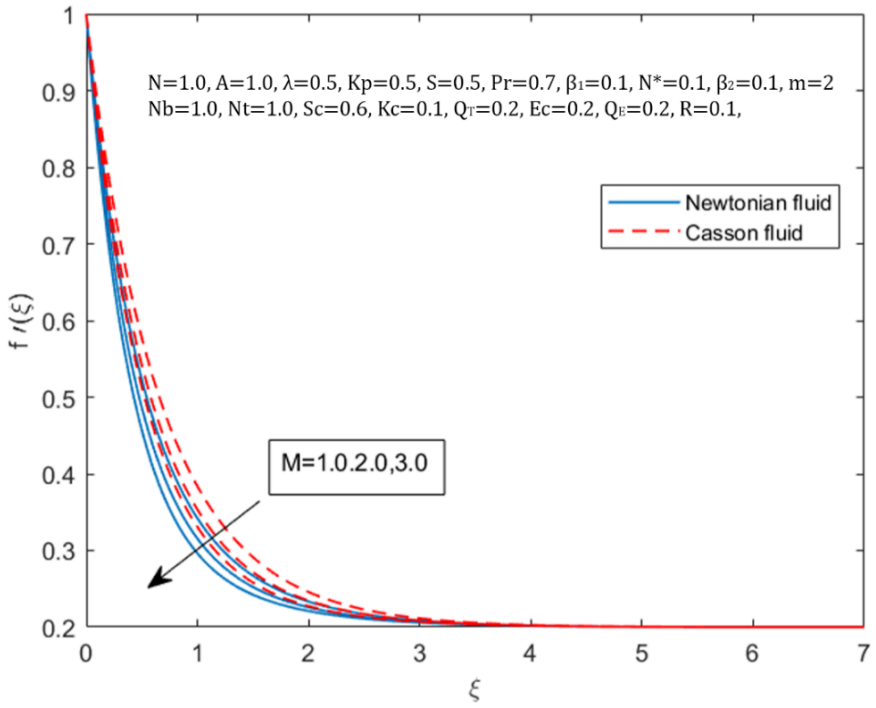

Fig. 5.2: Influence of M on $f'(\xi)$.

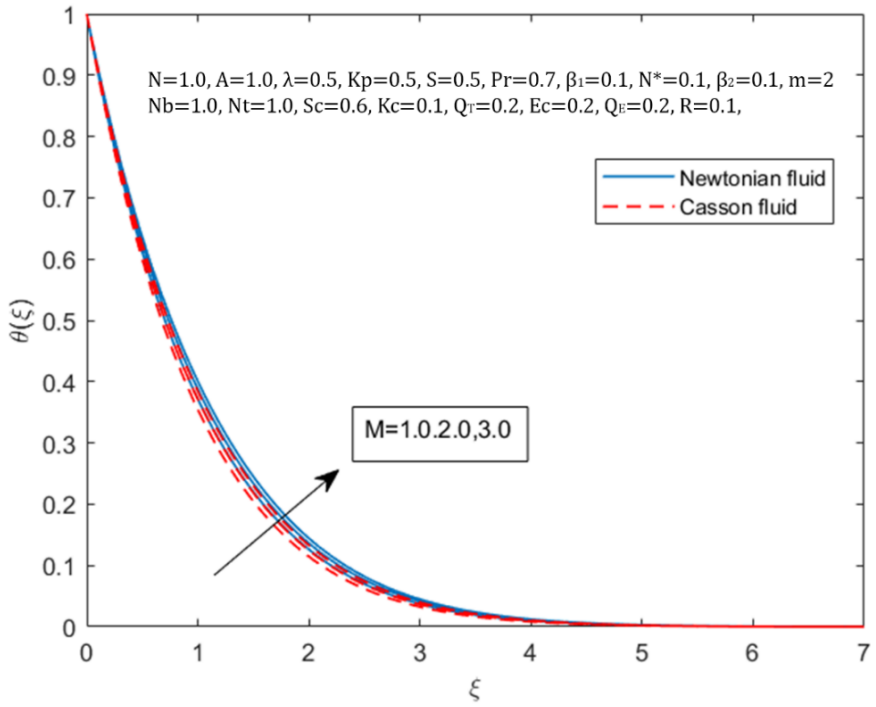

Fig. 5.3: Influence of M on $\theta(\xi)$.

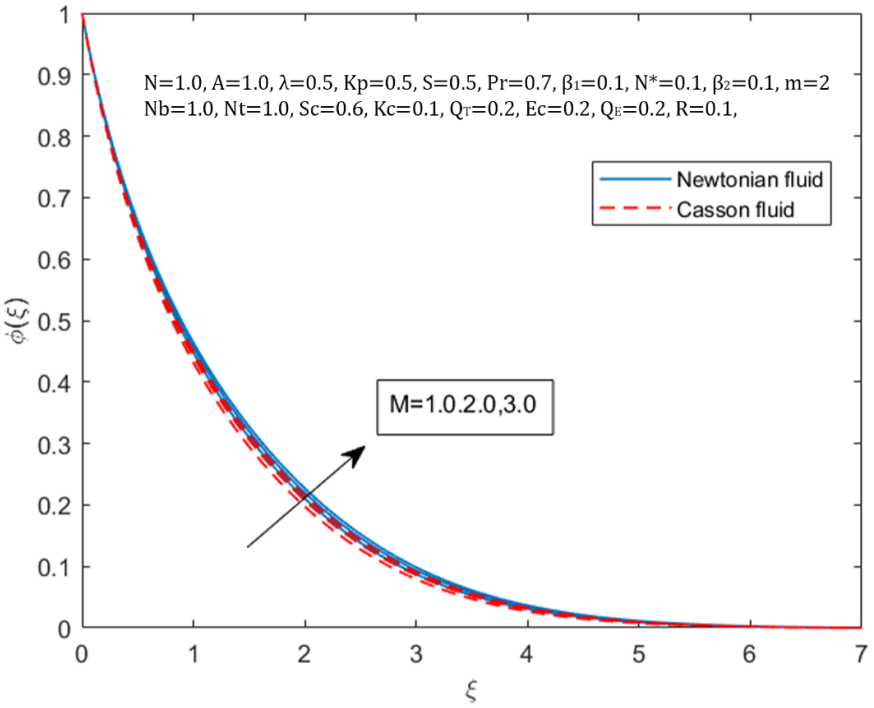

Fig. 5.4: Influence of M on $\phi(\xi)$.

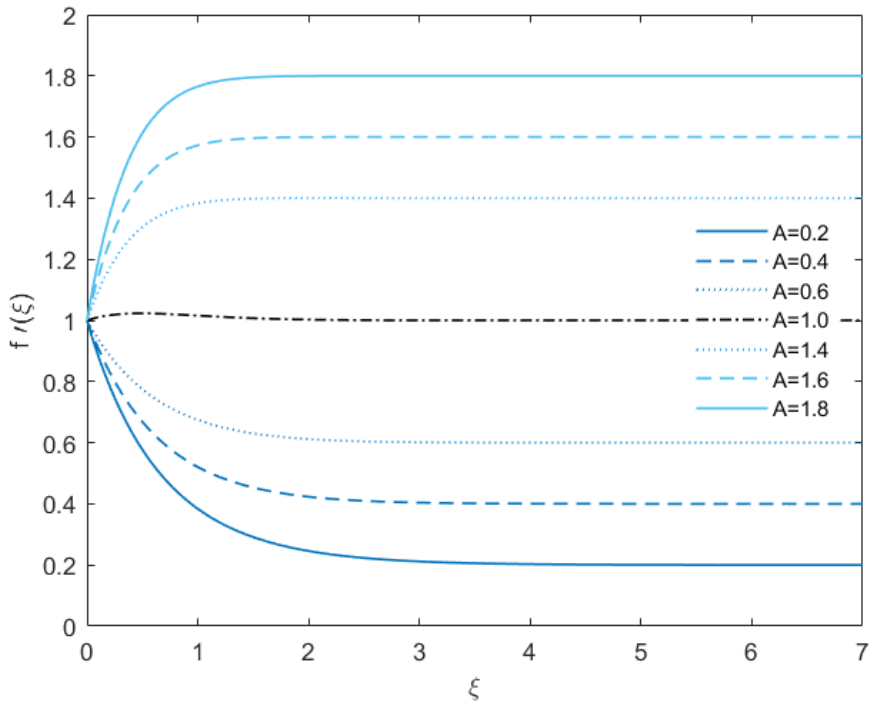

Fig. 5.5: Stagnation point.

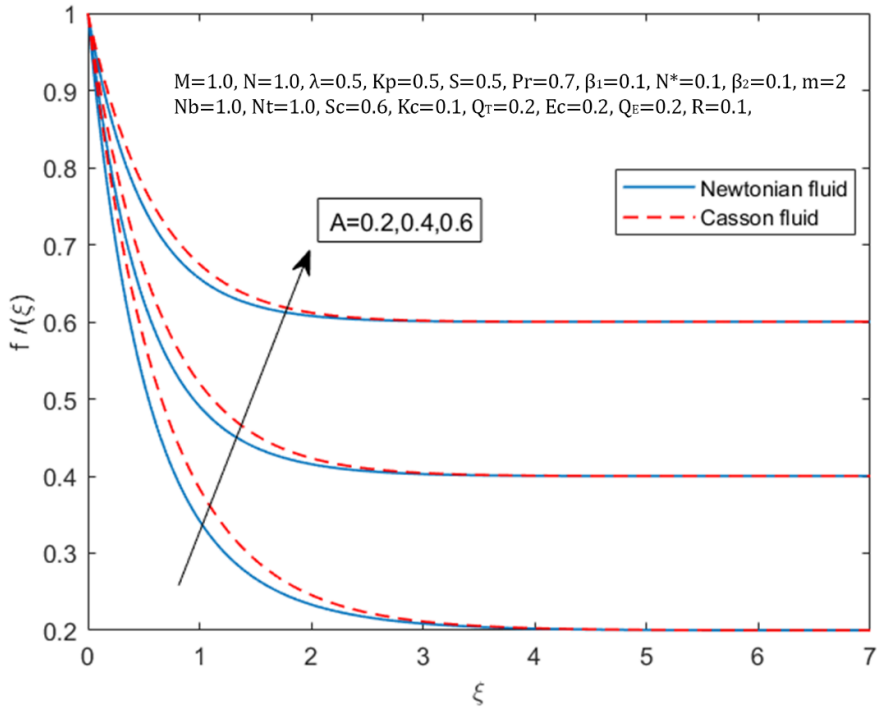

Fig. 5.6: Influence of A on $f'(\xi)$.

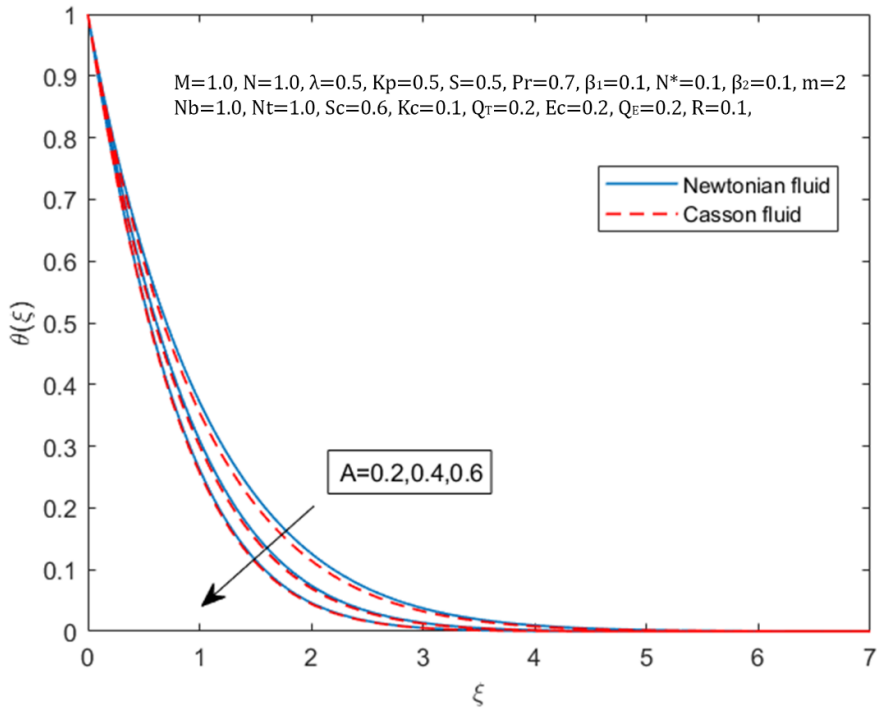

Fig. 5.7: Influence of A on $\theta(\xi)$.

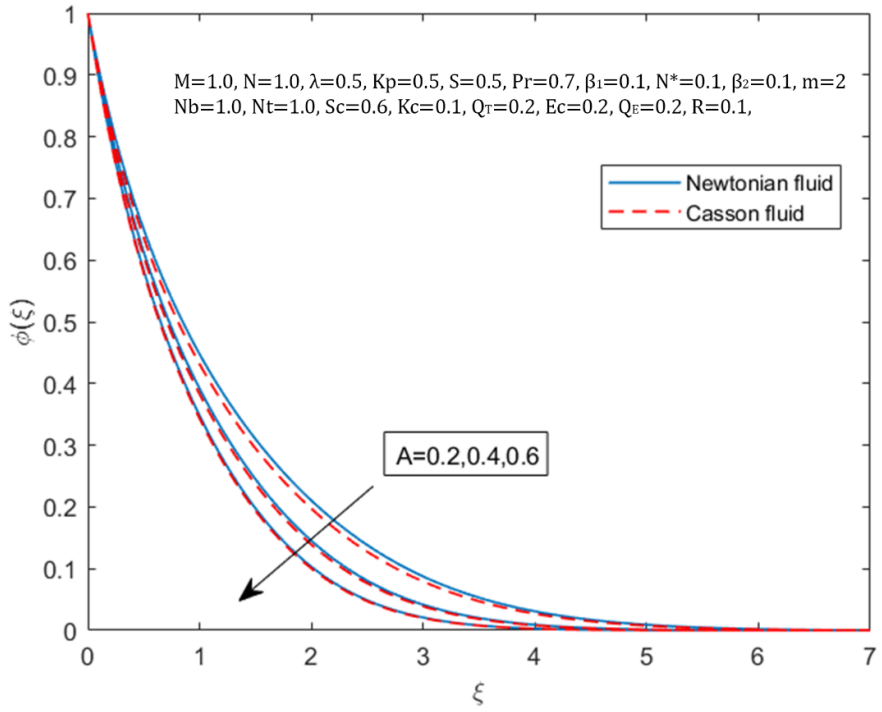

Fig. 5.8: Influence of A on $\phi(\xi)$.

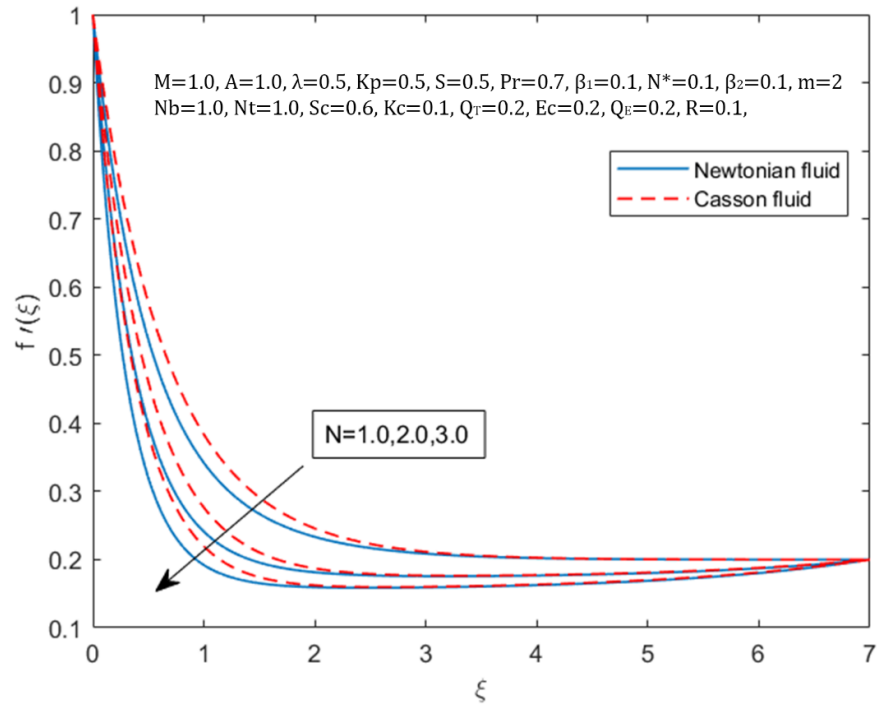

Fig. 5.9: Influence of N on $f'(\xi)$.

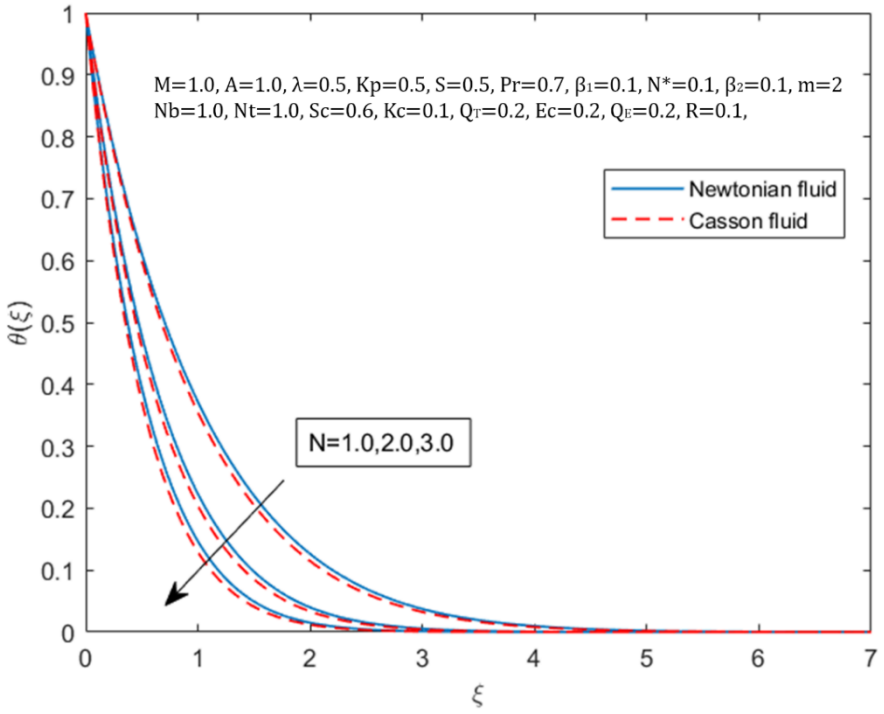

Fig. 5.10: Influence of N on $\theta(\xi)$.

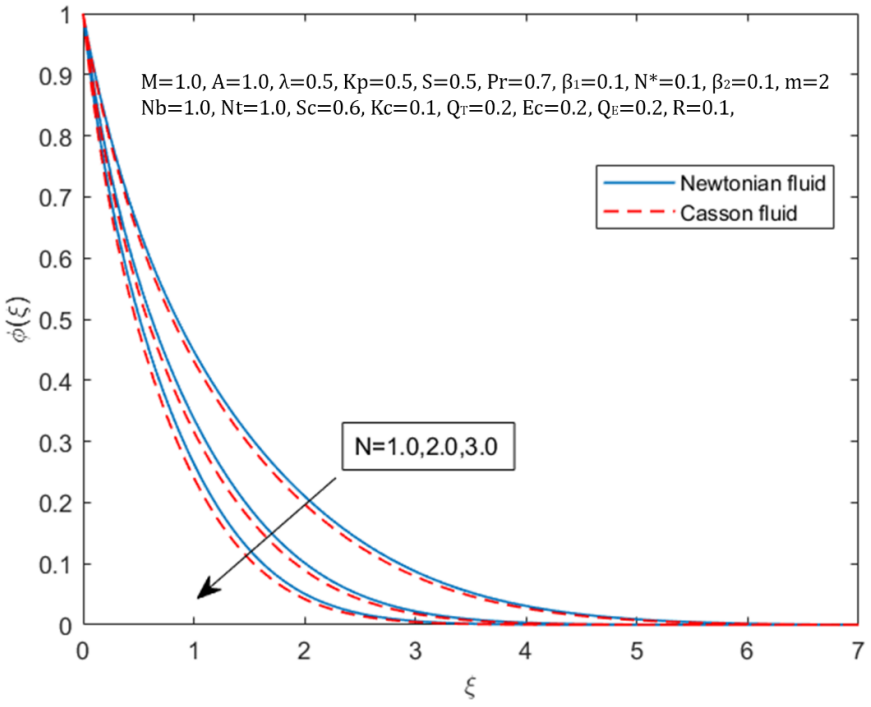

Fig. 5.11: Influence of N on $\phi(\xi)$.

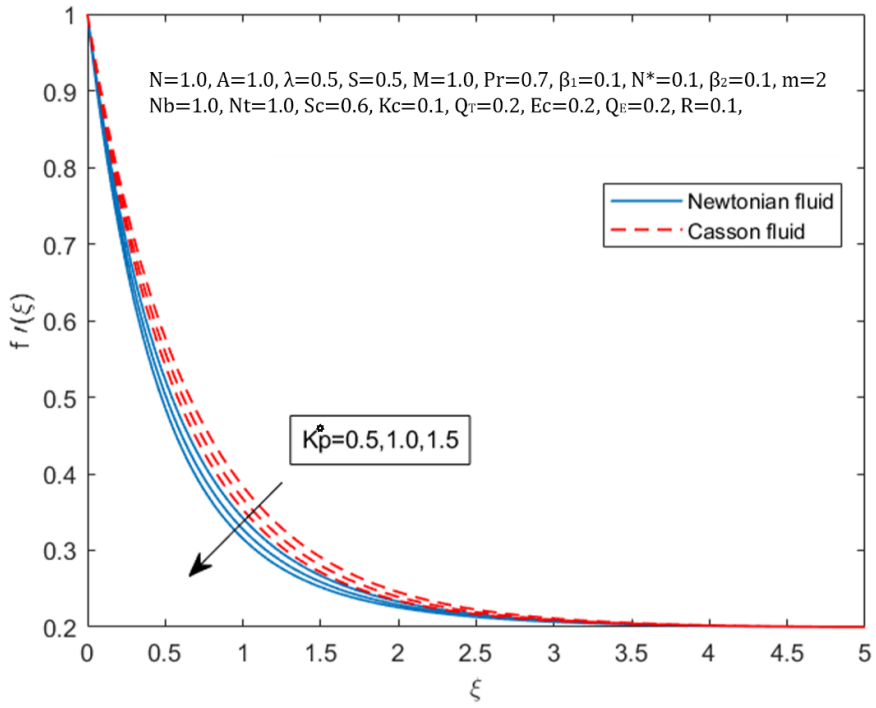

Fig. 5.12: Influence of Kp on $f'(\xi)$.

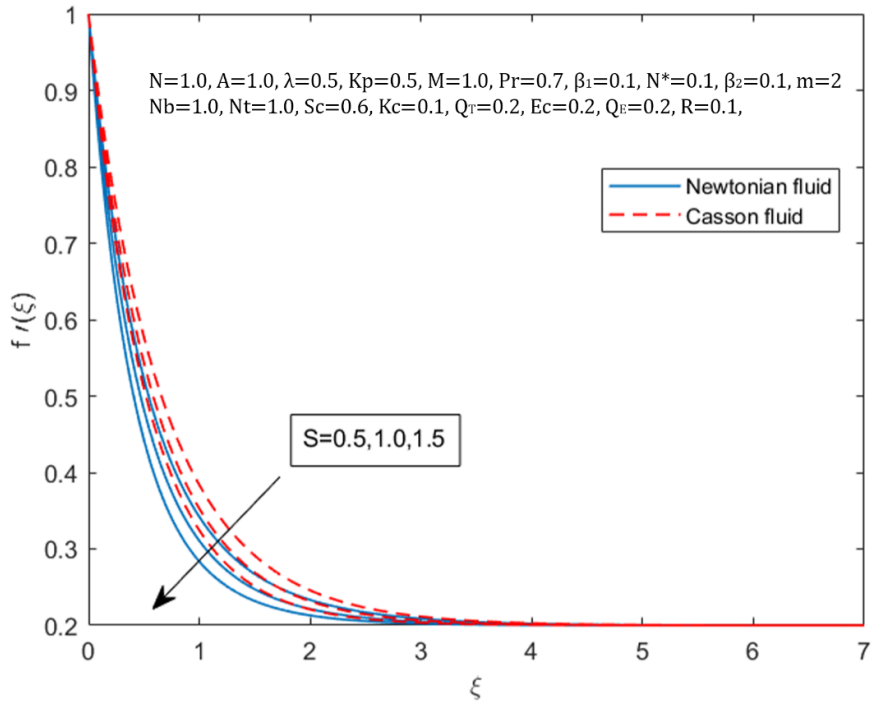

Fig. 5.13: Influence of S on $f'(\xi)$.

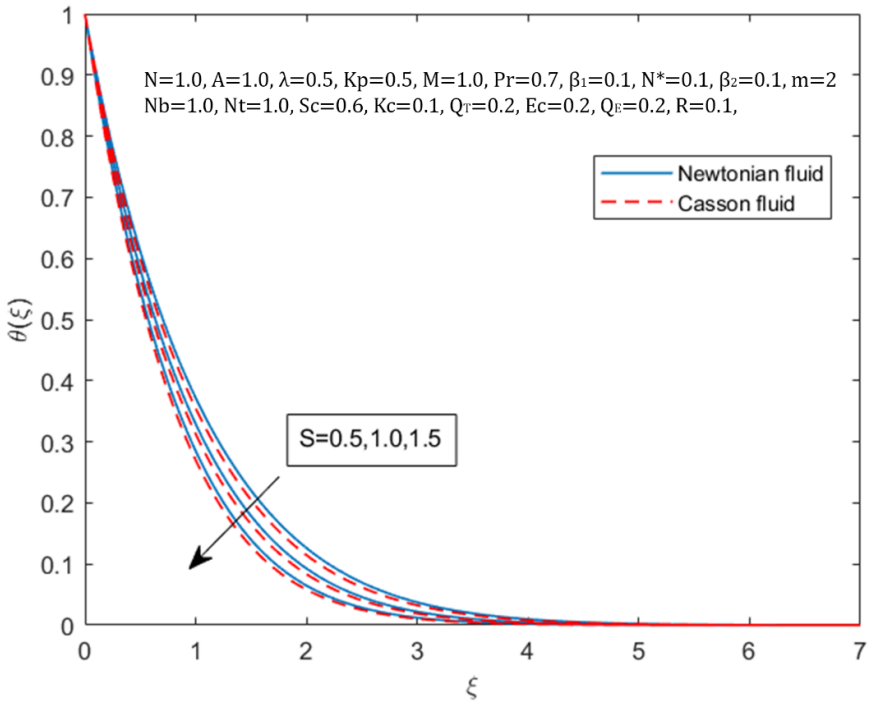

Fig. 5.14: Influence of S on $\theta(\xi)$.

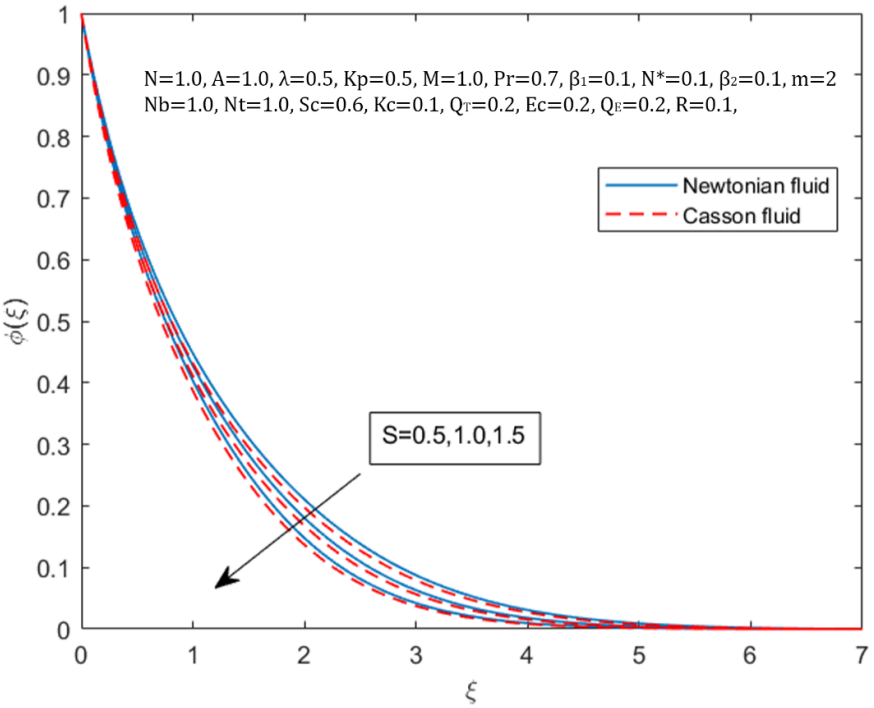

Fig. 5.15: Influence of S on $\phi(\xi)$.

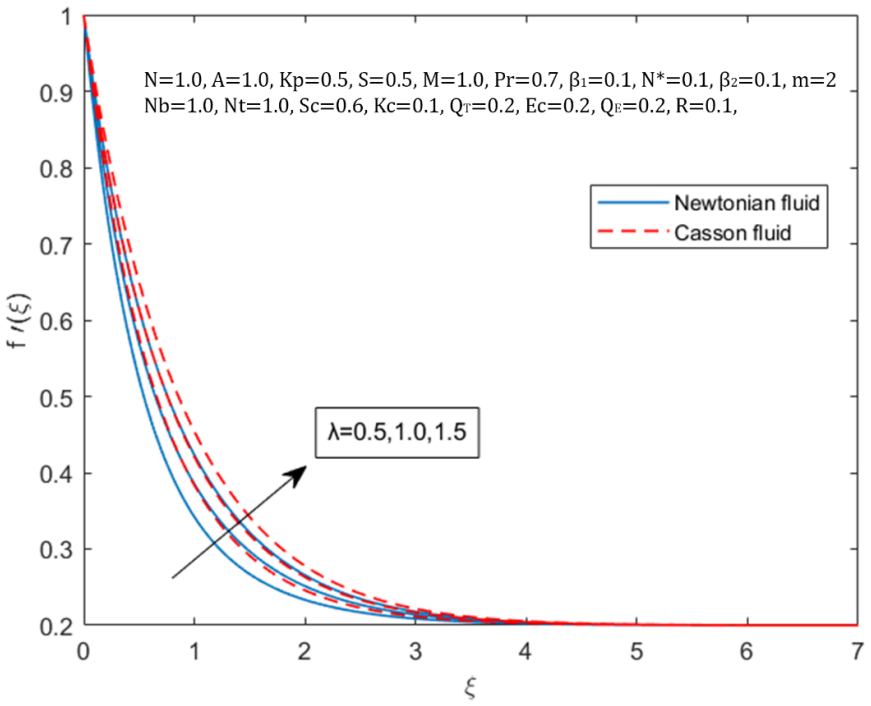

Fig. 5.16: Influence of λ on $f'(\xi)$.

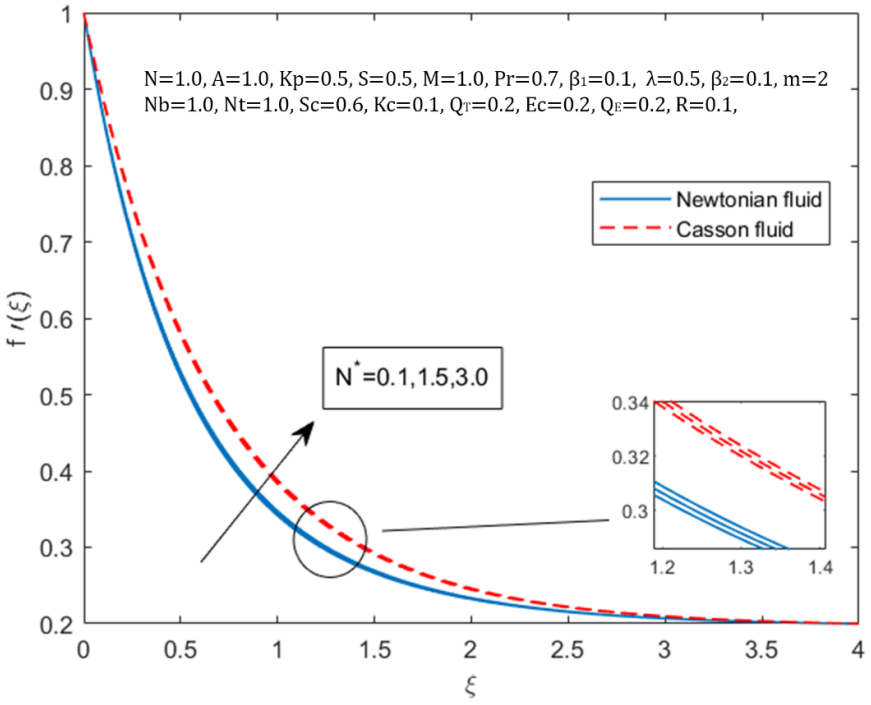

Fig. 5.17: Influence of N^* on $f'(\xi)$.

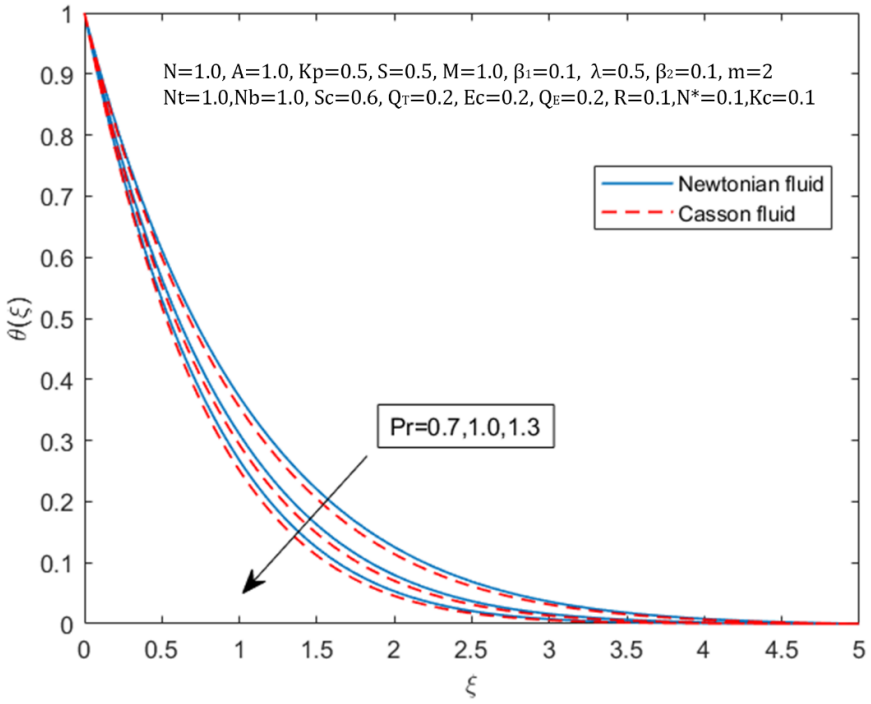

Fig. 5.18: Influence of Pr on $\theta(\xi)$.

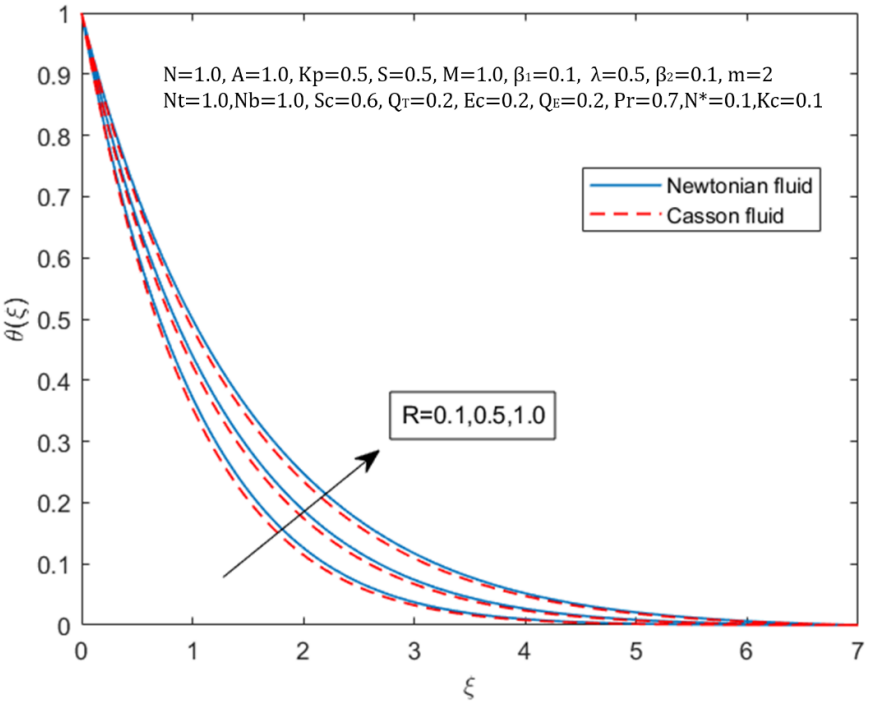

Fig. 5.19: *I*nfluence of R on $\theta(\xi)$.

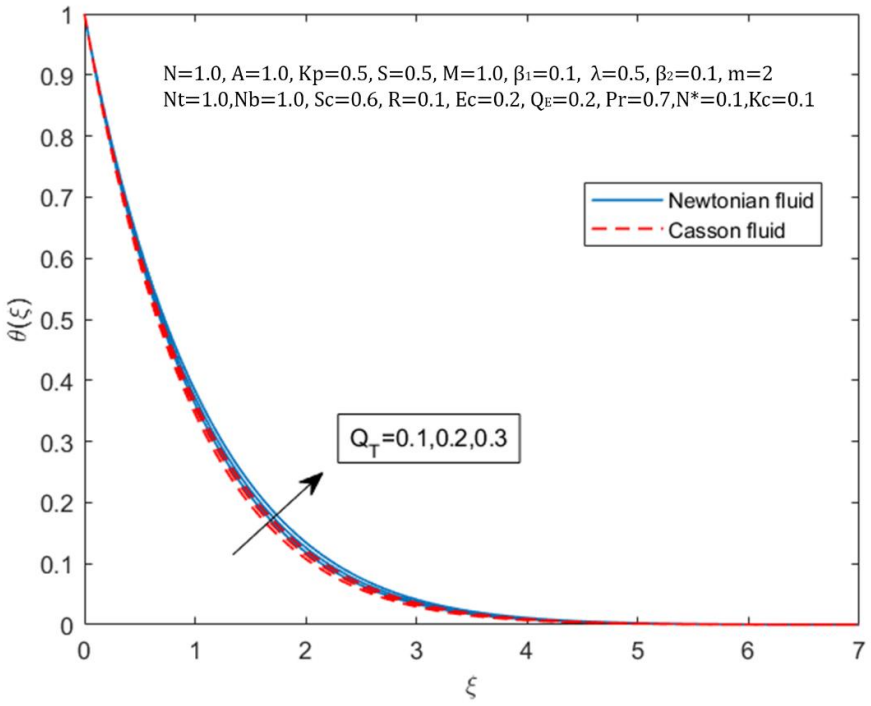

Fig. 5.20: Influence of Q_T on $\theta(\xi)$.

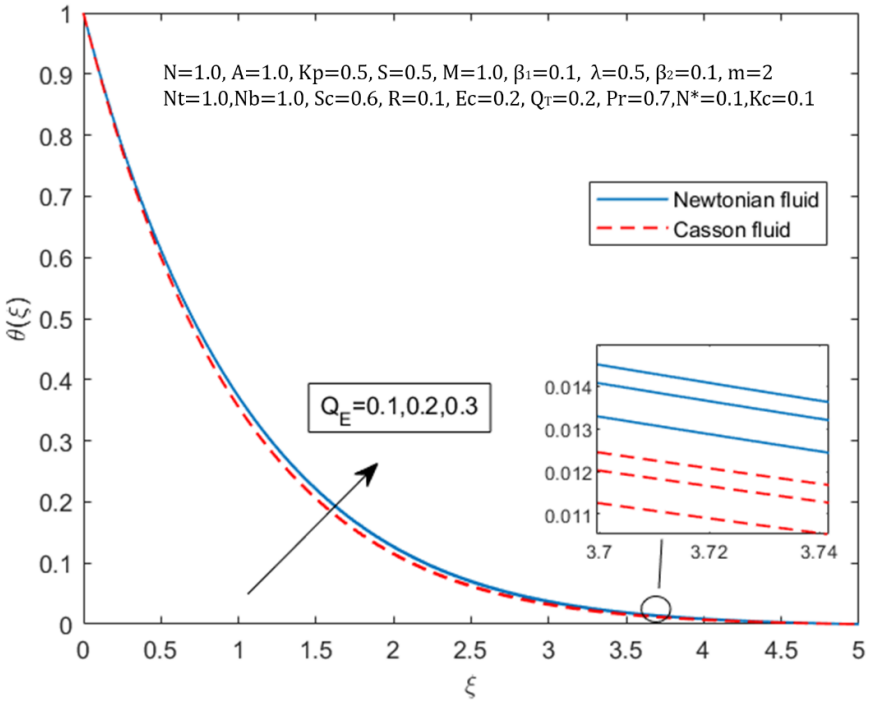

Fig. 5.21: Influence of Q_E on $\theta(\xi)$.

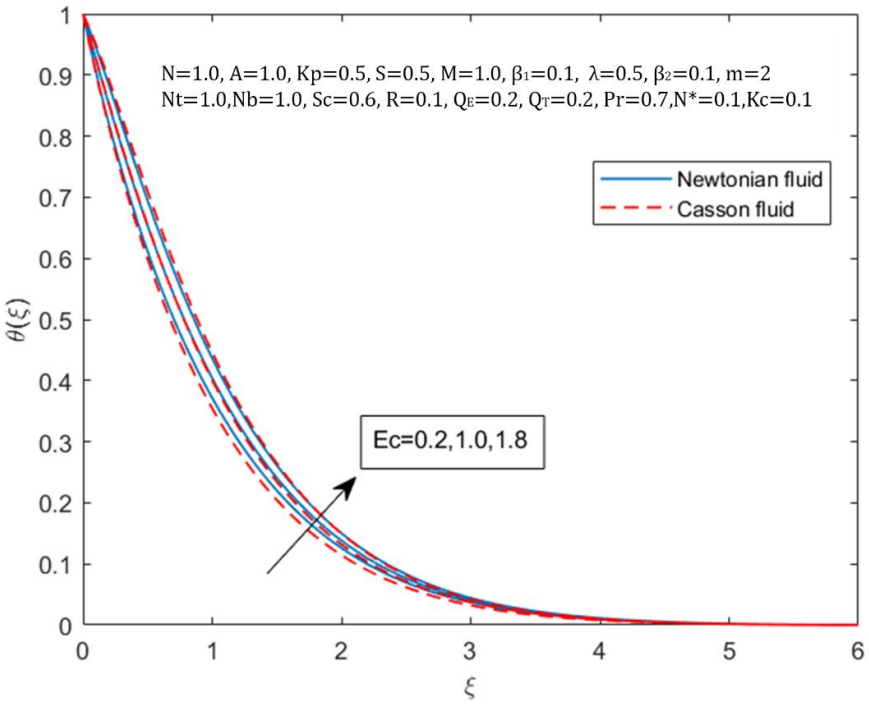

Fig. 5.22: Influence of Ec on $\theta(\xi)$.

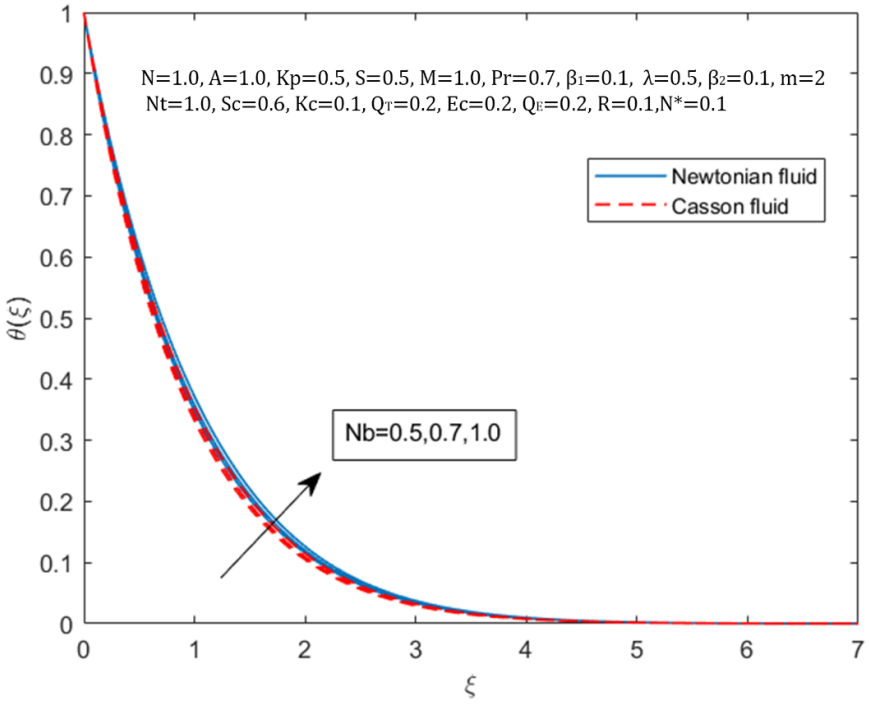

Fig. 5.23: Influence of Nb on $\theta(\xi)$.

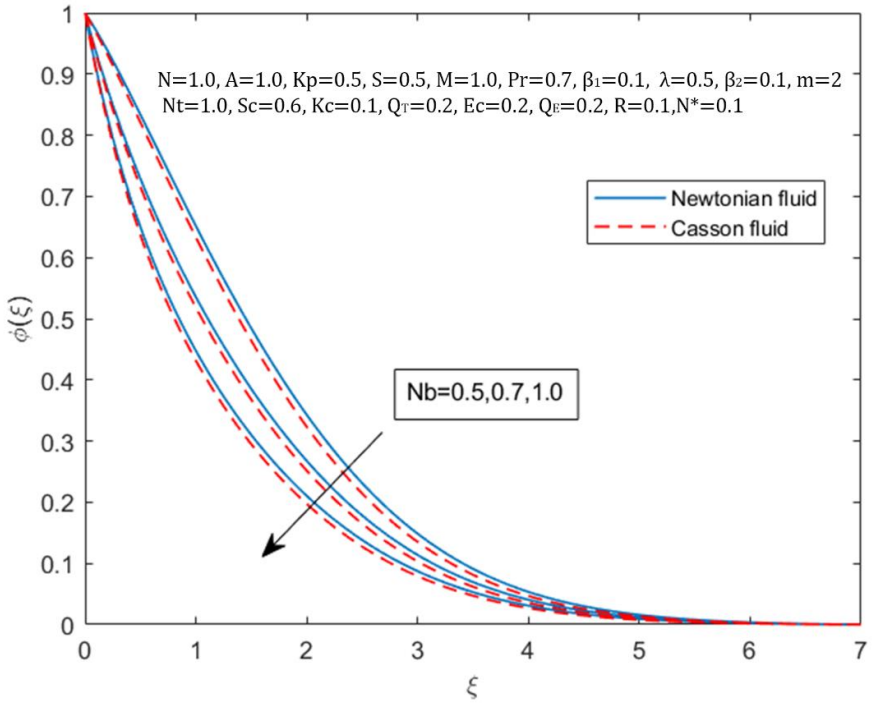

Fig. 5.24: Influence of Nb on $\phi(\xi)$.

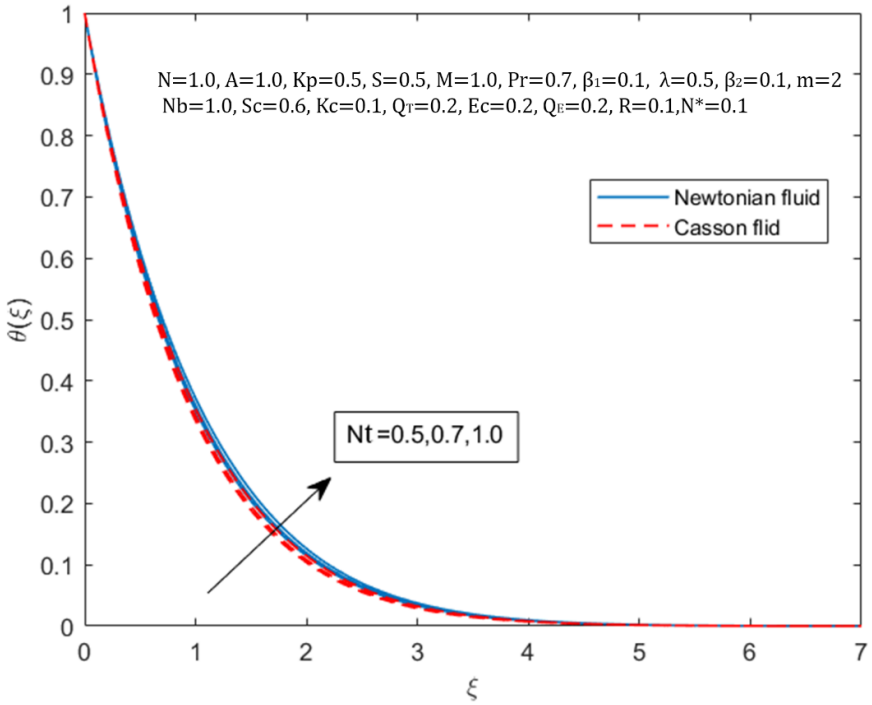

Fig. 5.25: Influence of Nt on $\theta(\xi)$.

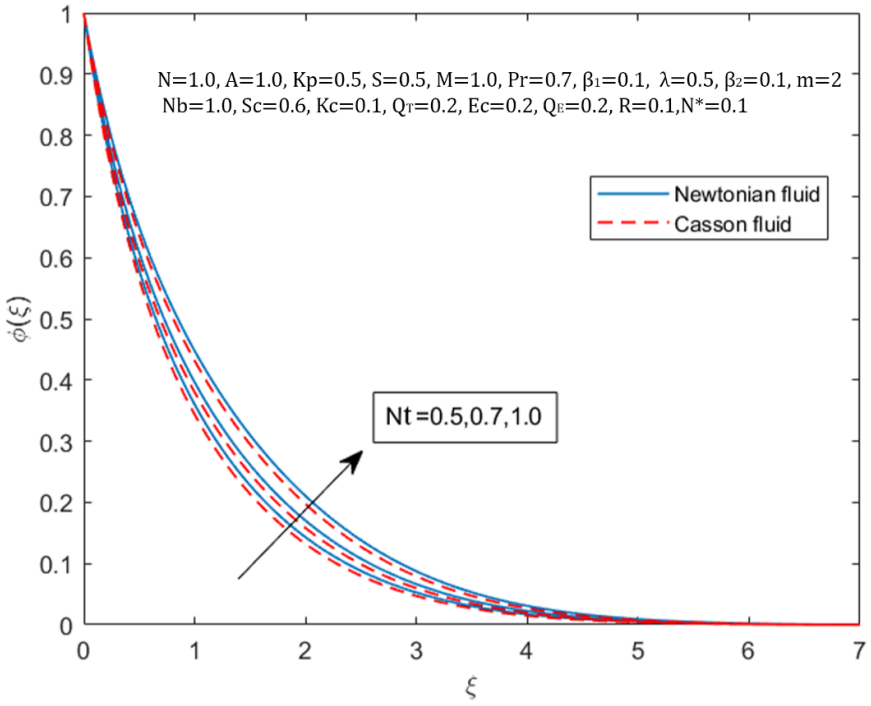

Fig. 5.26: Influence of Nt on $\phi(\xi)$.

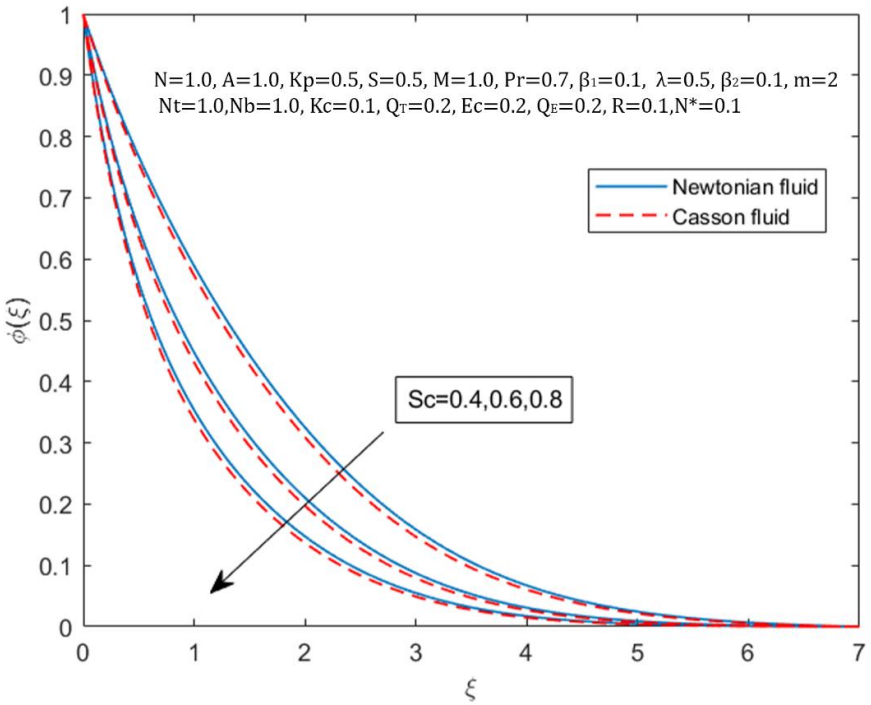

Fig. 5.27: Influence of Sc on $\phi(\xi)$.

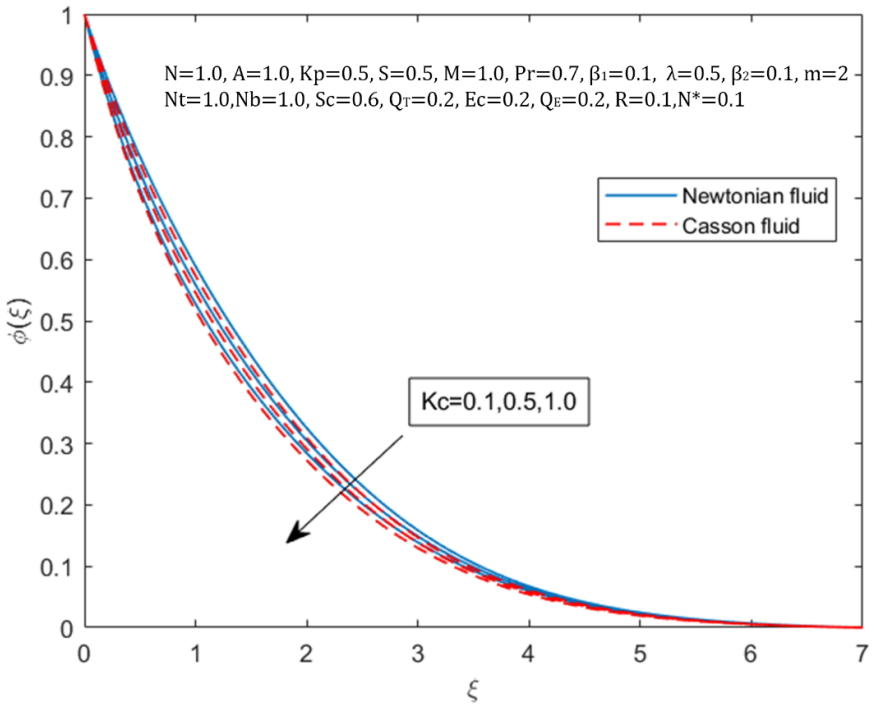

Fig. 5.28: Influence of Kc on $\phi(\xi)$.

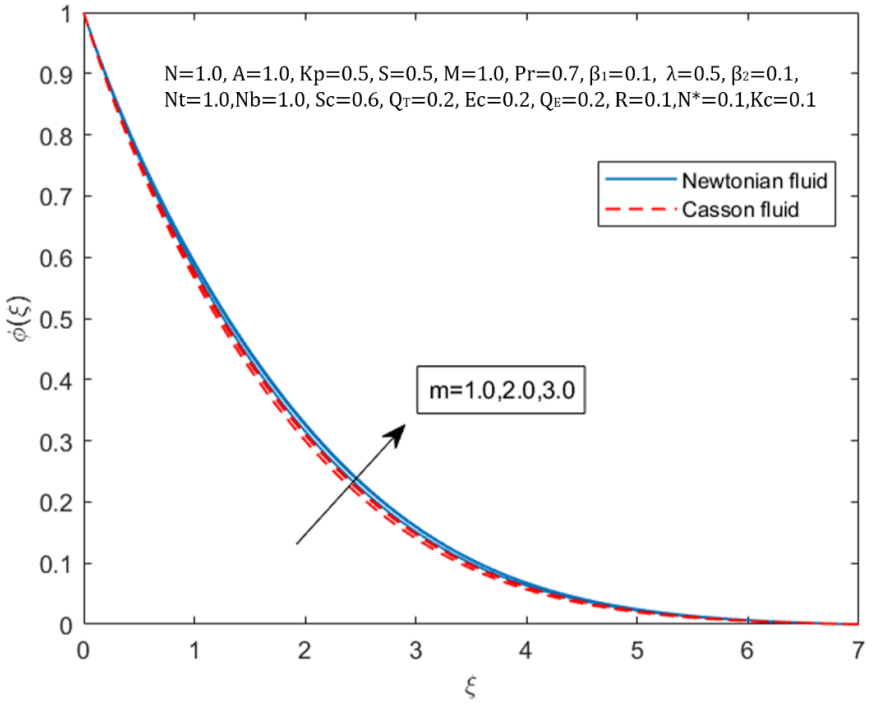

Fig. 5.29: Influence of m on $\phi(\xi)$.

Table 5.7: Comparison of $-\left(1+\frac{1}{\beta}\right)f''(0)$ when $S = 0.5, \beta_1 = 0, \beta_2 = 0, Kc = 0.1, Pr = 0.7, R = 0.1, Q_T = 0.2, Q_E = 0, Ec = 0.2, Nb = 1.0, Nt = 1.0, Sc = 0.6, m = 2, A = 0, Kp = 0, \lambda = 0, N^* = 0, Gc = 0, Gr = 0.$

M	***N***	**(S. M. Ibrahim, 2020)**		**Present work**	
		Newtonian fluid	**Casson fluid**	**Newtonian fluid**	**Casson fluid**
0.0	1.0	1.5403	1.8238	1.5403	1.8237
0.5	1.0	1.7254	2.0509	1.7254	2.0509
1.0	1.0	1.8883	2.2507	1.8883	2.2507
0.5	1.0	1.7254	2.0509	1.7254	2.0509
0.5	1.5	2.1202	2.4999	2.1202	2.4998
0.5	2.0	2.4853	2.9185	2.4852	2.9185

CHAPTER 6

CONCLUSIONS

In this thesis, we have examined influence of thermally radiative stagnation point flow of Casson nanofluid with magnetic field. The physical parameters of the 2D Casson nanofluid have been investigated i.e. exponential parameter N, stagnation parameter A, porosity parameter k_p^*, radiation parameter R, magnetic parameter M, Prandtl number Pr, Eckert number Ec, thermal heat generation parameter Q_T, space-based exponential heat parameter Q_E, Brownian motion parameter N_b, thermophoresis parameter N_t, Scmidt number Sc, chemical reaction Kc, suction and injection parameter S. We derived a set of ODEs by applying the similarity transformation to the nonlinear PDEs of concentration, momentum and temperature. The present model has been combined with $RK4$ to calculate numerical results using the shooting method. Using graphs and tables, it has been thoroughly explored how different acceptable physical characteristics affect the velocity, energy and concentration distribution.

The main conclusion from the current work is outlined below.

- As magnetic field values rose, the velocity profile decreased but temperature and concentration distribution rise.
- Temperature distribution slows as the Prandtl number increases, whereas the concentration distribution accelerates.
- The temperature field exhibits the same behavior as the temperature profile due to the thermophoresis parameter, because of which the temperature profile rises.
- Increase in the exponential and heat source parameters improve the heat transfer rate.
- Brownian motion raises both temperature and concentration in the flow domain due to increased thermal energy transmission.
- Due to stagnation parameter 'A', momentum boundary layer becomes thinner.

- Joule's heating has the effect of raising the temperature at all places.
- The rate of heat and mass transmission increase as λ and N^*increase.
- By boosting the numerical value of Casson parameter, the fluid's velocity drops.
- As chemical reaction parameter increases, concentration profile decreases.

Future work

The problem might possibly be expanded by considering the consideration of several fluid models such as Maxwell, Williamson, Burger, Jeffery and tangent hyperbolic nanofluid. Other effects such as n^{th}-order chemical reaction, activation of energy, inclination magnetic field, viscous dissipation and soil particles can be used to investigate the situation. We may also solve the above-mentioned issue by employing several geometries such as a wedge, channel, cone and cylinder among others.

REFERENCES

[1] Prandtl, L. (1904). On the motion of a fluid with very small viscosity. *In Proceedings of 3rd International Mathematics Congress*, 484-491.

[2] Powell, R. E. (1944). Mechanisms for the relaxation theory of viscosity. *nature*, 154(3909), 427-428.

[3] Casson, N. (1959). A flow equation for pigment-oil suspensions of the printing ink type Rheology of disperse systems.

[4] Platt, J. R. (1961). bioconvection patterns" in cultures of free-swimming organisms. *Science*, 133(3466), 1766-1767.

[5] Gebhart, B. (1962). Effects of viscous dissipation in natural convection. *Journal of fluid Mechanics*, 225-232.

[6] Erickson, L. E. (1966). Heat and mass transfer on moving continuous flat plate with suction or injection. *Industrial & Engineering Chemistry Fundamentals*, 19-25.

[7] Huilgol, R. R. (1968). A second order fluid of the differential type. *International Journal of Non-Linear Mechanics 3(4)*, 471-482.

[8] Ahmadi, G. (1976). Self-similar solution of incompressible micropolar boundary layer flow over a semi-infinite plate. *International Journal of Engineering Science*, 14(7), 639-646.

[9] Soundalgekar, V. M. (1977). Free convection effects on the Stokes problem for an infinite vertical plate, 499-501.

[10] Talbot, L. R. K. R. W. D. R., Cheng, R. K., Schefer, R. W., & Willis, D. R. (1980). Thermophoresis of particles in a heated boundary layer. *Journal of fluid mechanics*, *101*(4), 737-758.

[11] Plumb, O.A. & J. H. (1981). The effect of cross flow and radiation on natural convection from vertical heated surfaces in saturated porous media. *Thermophysics Conference*, June, Palo Alto, California, USA., 23–25.

[12] Rajagopal, K. R. & A. S. Gupta. (1984). An exact solution for the flow of a non-Newtonian fluid past an infinite porous plate. *Meccanica*. 19(2), 158-160.

[13] Hossain, A. & A. C. Mandal. (1985). J. Phys. D: Appl. Phys.

[14] Yoon, H. K. (1987). A note on the Powell-Eyring fluid model. *International communications in heat and mass transfer*, 381-390.

[15] Bestman, A. R. (1990). Natural convection boundary layer with suction and mass transfer in a porous medium. *International journal of energy research*, 14(4), 389-396.

[16] Watanabe, T. (1990). Thermal boundary layers over a wedge with uniform suction or injection in forced flow. *Acta Mechanica*, 119-126.

[17] Pantokratoras, A. (1991). Comment on ‘‘Forced and free mixed convection boundary layer flow with uniform suction or injection on a vertical flat plate” *by T. Watanabe (Acta Mech)*. 123–132.

[18] Das, U. N, Deka, R. K, & Soundalgekar, V. M . (1994). Effect of mass transfer on flow pastan impulsively started infinite vertical plate with constant heat flux and chemical reaction. Forsch. *Ingenieurwes*, 60(10), 284-287.

[19] Kataria, H. & H. Patel. (1996). Effect of magnetic field on unsteady natural convective flow of a micropolar fluid between two vertical walls. *Ain Shams Eng. J*, 1145–1156.

[20] TRIMIS, D. &. (1996). Combustion in a Porous Medium-Advances and Applications. *Combustion Science and Technology*, 153–168.

[21] Choi, S. U.-S. (1998). Nanofluid technology: current status and future research. No. ANL/ET/CP-97466. *Argonne National Lab. (ANL), Argonne, IL (United States)*

[22] Rohsenow, W.M. & J. Y. (1998). Handbook of heat transfer (Vol. 3). New York: McGraw-Hill

[23] Muthucumarswamy, R. (2000). Forschung imIngenieurwesen.

[24] Smits, J. A. (2000). A physical introduction to fluid mechanics. *John Wiley & Sons Incorporated.*

[25] Mahapatra, T. R. (2001). Magnetohydrodynamic stagnation-point flow towards a stretching sheet. *Acta Mechanica*, 152(1), 191-196.

[26] Banerjee, R. & X. Bai, D. Pugh, K. Isaac, D. Klein, J. Edson.L. Oliver. (2002). CFD simulations of critical components in fuel filling systems. *SAE technical paper, Tech*. 324-340.

[27] Xia, B. & D. W. Sun. (2002). Applications of computational fluid dynamics (CFD) in the food industry: a review. *Computers and electronics in agriculture*

[28] Mahapatra, T. R, & Gupta, A. S. (2003). Stagnation-point flow towards a stretching surface. *The Canadian Journal of Chemical Engineering*, 81(2), 258-263.

[29] Afify. (2004). MHD free convective flow and mass transfer over a stretching sheet with chemical reaction. *Heat and Mass Transfer*. 40(6), 495-500.

[30] Lwis, W. R. (2004). Fundamentals of the finite element method for heat and fluid flow, *John Wiley & Sons.*

[31] Nazar, R. & N. Amin, D. Filip, & I. Pop. (2004). Stagnation point flow of a micropolar fluid towards a stretching sheet, *International Journal of Non-Linear Mechanics*, 1227–1235.

[32] Magyari, E. R. (2005). Effect of viscous dissipation on the flow in fluid saturated porous media. *Handbook of porous media*, 391-426.

[33] Q. Wu, S. W. (2005). Stagnation-point flows in a porous medium. *Chemical engineering science*

[34] Alam M. S, R. M. (2006). Dufour and Soret effects on unsteady MHD free convective and mass transfer flow past a vertical porous plate in a porous medium. *Nonlinear Anal Model Control*, 11(3), 217-226.

[35] Buongiorno, J. (2006). Convective transport in nanofluids.

[36] Fox, W. R. (2006). Introduction to Fluid Mechanics.

[37] Kothandaraman, C. P. (2006). Fundamentals of heat and mass transfer. New Age International.

[38] White, M. F. (2006). Viscous fluid flow. Vol. 3. New York: McGraw-Hill.

[39] Layek, G.C, Mukhopadhyay S, & Samad SK. (2007). Heat and mass transfer analysis for boundary layer stagnation point flow towards a heated porous stretching sheet with heat absorption/generation and suction/blowing. *Int Commun Heat Mass Transfer*, 347–356.

[40] Roy, S. D. (2007). Non-similar solution of an unsteady mixed convection flow over a vertical cone with suction or injection. *International Journal of Heat and Mass Transfer*, 181-187.

[41] Hayat, T. A. (2008). MHD flow and mass transfer of an upper-convected Maxwell fluid past a porous shrinking sheet with chemical reaction species. *Physics Letters A*, 372(26), 4698-4704.

[42] Sivagnana Prabhu KK, K. R. (2009). Lie group Analysis for the effect of viscosity and thermophoresis particle deposition on free convective heat and mass transfer in the presence of suction / injection. *Theoret Appl Mech. 36(4)*, 275-298.

[43] Chhabra, R. P. (2010). Non-Newtonian fluids: an introduction In Rheology of complex fluids. *Springer*. 3-34.

[44] Makinde, O. D. (2010). MHD mixed-convection interaction with thermal radiation and nth order chemical reaction past a vertical porous plate embedded in a porous medium. *Chemical Engineering Communications*, 590-608.

[45] Singh, K. D. & R. K. (2010). Indian J. Phys., 84, 93.

[46] Cengel, Y. A. & a. J. (2010). Fundamental of Fluid Mechanics.

[47] Chhabra, R. P., & J. F. (2011). Non-Newtonian flow and applied rheology: *engineering applications.*

[48] Kuznetsov, A. V. (2011). Bio-thermal convection induced by two different species of microorganisms. *International Communications in Heat and Mass Transfer*, 548-553.

[49] Bhattacharyya, K. a. (2012). Stagnation-point flow and heat transfer over an exponentially shrinking sheet. *Communications in Nonlinear Science and Numerical Simulation*. 17(7), 2728-2734.

[50] Kunes, J. (2012). Dimensionless physical quantities in science and engineering. Elsevier.

[51] Kunes. J. (2012). Dimensionless physical quantities in science and engineering first edition. Burlington, *MA: Elsevier*. 658.

[52] Mustafa, M. T. (2012). Stagnation-point flow and heat transfer of a Casson fluid towards a stretching sheet. *Zeitschrift für Naturforschung*. 67(1-2), 70-76.

[53] Pletcher, R. H., Tannehill, J. C., & Anderson, D. (2012). Computational fluid mechanics and heat transfer.

[54] Aman, F. & A. I. (2013). Magnetohydrodynamic stagnation-point flow towards a stretching/shrinking sheet with slip effects. *International commu nications in heat and mass transfer*. 47, 68-72.

[55] Cengel, Yunus, & J. C. (2013). Fluid Mechanics Fundamentals and Applications (SI units). McGraw Hill.

[56] Chakraborty, R. D. (2013). Thermal characteristics of electromagnetohydrodynamic flows in narrow channels with viscous dissipation and Joule heating under constant wall heat flux. International Journal of Heat and Mass *Transfer*, 67, 1151-1162.

[57] GENICK BAR-MEIR, P. H. (2013). Basics of Fluid Mechanics.

[58] Ibrahim, W. a. (2013). MHD boundary layer flow and heat transfer of a nanofluid past a permeable stretching sheet with velocity, thermal and solutal slip boundary conditions. *Computers & Fluids*. 75, 1-10.

[59] Das, K. P. (2014). Nanofluid flow over an unsteady stretching surface in presence of thermal radiation. *Alexandria engineering journal*. 53(3), 737-745.

[60] Nadeem, S. & R. M. (2014). Optimized analytical solution for oblique flow of a Casson-nano fluid with convective boundary conditions. *Int. J. Therm. Sci*, 90-100.

[61] Pramanik, S. (2014). Casson fluid flow and heat transfer past an exponentially porous stretching surface in presence of thermal radiation. *Ain Shams Eng. J.*, 205-212.

[62] Shamey, R. a. (2014). Modelling, simulation and control of the dyeing process. Elsevier.

[63] Yazdi, M. E., Moradi, A., & Dinarvand, S. (2014). MHD mixed convection stagnation-point flow over a stretching vertical plate in porous medium filled with a nanofluid in the presence of thermal radiation. *Arabian journal for cience and engineering*, 2251-2261.

[64] Abolbashari, M. H. (2015). Analytical modeling of entropy generation for Casson nano-fluid flow induced by a stretching surface, *Advanced Powder Technology*. 26(2), 542-552.

[65] Jayachandra Babum, R. G. (2015). Effect of radiation and viscous dissipation on stagnation-point flow of a micropolar fluid over a nonlinearly stretching surface with suction/injection. *J Basic Appl Res Int*, 73–82.

[66] Khalid, A. I. (2015). Unsteady MHD free convection flow of Casson fluid past over an oscillating vertical plate embedded in a porous medium. *Engineering Science and Technology, an International Journal*. 18(3), 309-317.

[67] Mahanta, G. & S. S. (2015). 3D Casson fluid flow past a porous linearly stretching sheet with convective boundary condition. *Alexandria Eng. J.*, 653-659.

[68] Krishnamurthy, M. R. & B. C. (2016). Effect of chemical reaction on MHD boundary layer flow and melting heat transfer of Williamson nanofluid in porous medium. *Engineering Science and Technology, an International Journal*. 19(1), 53-61.

[69] Naramgari, S. a. (2016). MHD flow over a permeable stretching shrinking sheet of a nanofluid with suction/injection. *Alexandria Engineering Journal*. 55(2), 819-827.

[70] Raju, R. S. (2016). Application of finite element method to unsteady magnetohydrodynamic free-convection flow past a vertically inclined porous plate including thermal diffusion and diffusion thermo effects. *Journal of Porous Media*, 19(8).

[71] Sandeep, N. K. (2016). Modified kinematic viscosity model for 3D-Casson fluid flow within boundary layer formed on a surface at absolute zero. *Journal of Molecular Liquids*, 1197-1206.

[72] Jena, S. a. (2017). MHD stagnation-point flow past a stretching sheet through porous media with heat source/sink. *Journal Homepage: http://www. ijesm. co*. 6(8).

[73] Ullah, I. S. (2017). Effects of slip condition and Newtonian heating on MHD flow of Casson fluid over a nonlinearly stretching sheet saturated in a porous medium. *Journal of King Saud University-Science*. 29(2), 250-259.

[74] Afridi, Muhammad Idrees, Muhammad Qasim, & Ilyas Khan. (2018). Entropy generation minimization in MHD boundary layer flow over a slendering stretching sheet in the presence of frictional and Joule heating. *Journal of the Korean Physical Society*. 73(9), 1303-1309.

[75] Ghadikolaei, S. S. & K. H. (2018). Nonlinear thermal radiation effect on magneto Casson nanofluid flow with Joule heating effect over an inclined porous stretching sheet. *Case studies in thermal engineering*. 12, 176-187.

[76] Khan, U. & N. A.-D. (2018). Analysis of magnetohydrody namic flow and heat transfer of Cu-water nanofluid between parallel plates for different shapes of nanoparticles. *Neural Computing and Applications*, 695-703.

[77] Swain, K. S. (2018). Effects of non-uniform heat source/sink and viscous dissipation on MHD boundary layer flow of Williamson nanofluid through porous medium. *In Defect and Diffusion Forum, vol. 389, pp. 110-127*. Trans Tech Publications Ltd.

[78] Asha, S. K. & G. Sunitha. (2019). Effect of joule heating and MHD on peristaltic blood flow of Eyring–Powell nanofluid in a non-uniform channel. *Journal of Taibah University for Science*. 13(1), 155-168.

[79] El-Masry, Y. & Y. Abd Elmaboud, & M. Abdel-Sattar. (2019). The impacts of varying magnetic field and free convection heat transfer on an Eyring–Powell fluid flow with peristalsis. solution. *Journal of Taibah University for Science*. 160, 108299.

[80] Hamid, M. (2019). Heat transfer and flow analysis of Casson fluid enclosed in a partially heated trapezoidal cavity. *International Communications in Heat and Mass Transfer*. 108, 104284.

[81] Kumar, K. A. & V. S. (2019). MHD stagnation point flow of Williamson and Casson fluids past an extended cylinder: anew heat flux model. *SN applied sciences*. 1, 705.

[82] Raza, L. M. , N. Mir, & R. Ellahi. (2019). Effects of different shapes of nanoparticles on peristaltic flow of MHD nanofluids filled in an asymmetric channel. *Journal of Thermal Analysis and Calorimetry*. 140(3), 879-890.

[83] Shahzad, F. & M. S. (2019). MHD tangent hyperbolic nanofluid with chemical reaction, viscous dissipation and Joule heating effects. *AIP advances*. 9(2), 025007.

[84] Abbas, N. M. (2020). Study of three-dimensional stagnation point flow of hybrid nanofluid over an isotropic slip surface. Physica A: *Statistical Mechanics and its Applications*. 554, 124020.

[85] Abubakar, J.U & A D Adeoye. (2020). Effects of radiative heat and magnetic field on blood flow in an inclined tapered stenosed porous artery. *J Taibah Univ Sci*. 14(1), 77-86.

[86] Anantha Kumar, K. & V. Sugunamma, & N. Sandeep. (2020). Effect of thermal radiation on MHD Casson fluid flow over an exponentially stretching curved sheet. *Journal of Thermal Analysis and Calorimetry*. 140(5), 2377-2385.

[87] Ibrahim, S. M. (2020). Analytical modeling of heat and mass transfer of radiative MHD Casson fluid over an exponentially permeable stretching sheet with chemical reaction. *Journal of Engineering Thermophysics*. 29(1), 136-155.

[88] Idowu, A.S & B O Falodun. (2020). Effects of thermophoresis, Soret– Dufour on heat and mass transfer flow of magnetohydrodynamics non-Newtonian nanofluid over an inclined plate. *Arab J Basic Appl Sci.* 27(1), 149-165.

[89] Ijaz Khan, M. a. (2020). Activation energy and binary chemical reaction effect in nonlinear thermal radiative stagnation point flow of Walter-B nanofluid: Numerical computations. *International Journal of Modern Physics* . 34(13), 2050132.

[90] Khan, M. Riaz, Kejia Pan, Arif Ullah Khan, & S. Nadeem. (2020). Dual solutions for mixed convection flow of SiO2− Al2O3/water hybrid nanofluid near the stagnation point over a curved surface. *Physica A: Statistical Mechanics and its Applications*. Khan, 547, 123959.

[91] Mishra, A. & M. Kumar. (2020). Thermal performance of MHD nanofluid flow over a stretching sheet due to viscous dissipation, Joule heating and thermal radiation. *International Journal of Applied and Computing Mathematics*, 1-17.

[92] Thumma, Thirupathi, Abderrahim Wakif, & Isaac Lare Animasaun. (2020). Generalized differential quadrature analysis of unsteady three-dimensional MHD radiating dissipative Casson fluid conveying tiny particles. *Heat Transfer*. 49(5), 2595-2626.

[93] Vaidyaa, H., C. Rajashekharb, B.B. Divyac, G. Manjunathac, Prasada, K., & Animasaund, I. (2020). Influence of transport properties on the peristaltic mhd jeffrey fluid flow through a porous asymmetric tapered channel. *Results in Physics*. 18, 103295.

[94] Vinita, V.poply, R. Goyal, & N. Sharma. (2020). Analysis of the velocity, thermal,and concentration mhd slip flow over a nonlinear stretching cylinder in the presence of outer velocity. 50(2), 1543-1569.

[95] Zainal, N. A. (2020). MHD mixed convection stagnation point flow of a hybrid nanofluid past a vertical flat plate with convective boundary condition. *Chinese Journal of Physics*. 66, 630-644.

[96] Elayarani, M., Shanmugapriya, M., & Kumar, P. S. (2021). Intensification of heat and mass transfer process in MHD carreau nanofluid flow containing gyrotactic microorganisms. Chemical Engineering and Processing-Process Intensification, 160, 108299

[97] Papanastasiou, T. G. (2021). "Viscous fluid flow CRC press.

[98] Abdelmalek, Z. K. (2021). Analysis of generalized micropolar nanofluid with swimming of microorganisms over an accelerated surface with activation energy. Journal of Thermal Analysis and Calorimetry, 144(3). 1051-1063.

[99] Kodi, & Raghunath et al. (2022). Investigation of MHD Casson fluid flow past a vertical porous plate under the influence of thermal diffusion and chemical reaction. 51(1), 377-394.

[100] Warke, A. S.-O. (2022). Numerical investigation of the stagnation point flow of radiative magnetomicropolar liquid past a heated porous stretching sheet. Journal of Thermal Analysis and Calorimetry. 147(12), 6901-6912.